

JAERI-M
92-213

NEUTRONS IN BIOLOGY

January 1993

Satoru FUNAHASHI and Nobuo NIIMURA*

JAERI-M レポートは、日本原子力研究所が不定期に公刊している研究報告書です。

入手の問合わせは、日本原子力研究所技術情報部情報資料課（〒319-11茨城県那珂郡東海村）あて、お申しこしてください。なお、このほかに財団法人原子力弘済会資料センター（〒319-11茨城県那珂郡東海村日本原子力研究所内）で複写による実費頒布をおこなっております。

JAERI-M reports are issued irregularly.

Inquiries about availability of the reports should be addressed to Information Division, Department of Technical Information, Japan Atomic Energy Research Institute, Tokai-mura, Naka-gun, Ibaraki-ken 319-11, Japan.

© Japan Atomic Energy Research Institute, 1993

編集兼発行	日本原子力研究所
印刷	日立高速印刷株式会社

Neutrons in Biology

Satoru FUNAHASHI and Nobuo NIIMURA^{*}

Department of Physics
Tokai Research Establishment
Japan Atomic Energy Research Institute
Tokai-mura, Naka-gun, Ibaraki-ken

(Received December 10, 1992)

The start of JRR-3M in 1990 was a great epoch to the neutron scattering research in Japan. Abundant neutron beam generated by the JRR-3M made it possible to widen the research field of neutron scattering in Japan.

In the early days of neutron scattering, biological materials were too difficult object to be studied by neutrons not only because of their complexity but also because of the strong incoherent scattering by hydrogen. However, the remarkable development of the recent neutron scattering and its related sciences, as well as the availability of higher flux, has made the biological materials one of the most attractive subjects to be studied by neutrons.

In early September 1992, an intensive workshop titled "Neutrons in Biology" was held in Hitachi City by making use of the opportunity of the 4th International Conference on Biophysics and Synchrotron Radiation (BSR92) held in Tsukuba. The workshop was organized by volunteers who are eager to develop the researches in this field in Japan. Numbers of outstanding neutron scattering biologists from U.S., Europe and Asian countries met together and enthusiastic discussions were held all day long.

The editors believe that the presentations at the workshop were so invaluable that it is absolutely adequate to put them on record as an

* Tohoku University

issue of JAERI-M and to make them available for scientists to refer to in order to further promote the research in the future.

Keywords : Neutron Diffraction Biology Structure

中性子散乱構造生物学

日本原子力研究所東海研究所物理部

船橋 達・新村 信雄*

(1992年12月10日受理)

日本の中性子散乱研究は、1990年のJRR-3Mの完成により新しい時代に入り、これまでより一層広い分野の研究が可能になった。従来、生体物質は中性子散乱研究の対象としては、あまりにも複雑であるとともに、水素原子の強い非干渉性散乱のために取り上げにくかったが、最近の中性子散乱とそれに関連した科学の著しい進歩及び中性子束の向上により、中性子散乱の最も魅力的な研究対象の一つとなっている。

1992年9月上旬、つくばで放射光による生物研究の国際会議BSR92が開催されたのを機として、“Neutrons in Biology”と題する国際ワークショップが日立市で開かれた。このワークショップは、この分野の研究を熱心に推進しているボランティアによって組織されたもので、米・欧・亜各国の著名な生体物質中性子散乱研究者が参加し、研究発表と熱心な討論を終日行った。

このワークショップの発表はきわめて重要な内容を持っており、今後の中性子散乱による生物研究の推進に資するところが非常に大きいので、編者は、発表者および組織者の協力を得て、発表資料をJAERI-Mレポートとしてここにまとめた。

Contents

1. Neutrons in Biology at GKSS	1
H.B.STUHRMANN	
2. Small-angle Neutron Scattering Instrument at the Kyoto University Reactor	5
M.SUGIYAMA, S.UEHARA & Y.MAEDA	
3. Polarized Neutron Small-angle Scattering in Biology	12
H.B.STUHRMANN	
4. Small-angle Neutron and X-ray Scattering of Insect Lipophorins	26
C.KATAGIRI, Y.ITO & M.SATO	
5. The Structure of Gelsolin-PIP2 Complex as Studied by Small Angle Neutron Scattering	29
T.ITO, J.FUKUSHIMA, Y.MINEZAKI, I.TANAKA, N.NIIMURA & K.HAYASHI	
6. Small-angle Neutron Scattering Studies of Proteoglycan from Shark Fin Cartilage	30
Y.SANO, N.NIIMURA & I.TANAKA	
7. Small-angle Neutron Scattering Study of Recombinant Yeast- derived Human Hepatitis B Virus Surface Antigen Vaccine Particles	33
Y.ITO, M.SATO, K.KAMEYAMA, N.ISHIKAWA & T.TAKAGI	
8. Inelastic Neutron Scattering from DNA and Water	39
A.AGUI, Y.TOMINAGA & S.IKEDA	
9. Neutron Scattering in Small Biological Molecules and Hydrogen Bonding Studies at Trombay and Future Plans	41
K.K.KANNAN, M.RAMANADHAM, K.R.RAO & P.S.GOYAL	
10. A Large Single Crystal of the Tetragonal Form of Lysozyme Can be Grown in a Concentration Gradient of NiCl_2	61
M.ATAKA & T.KATSURA	
11. Small Angle Neutron Scattering Study of the Initial Stage of Lysozyme Crystallization Process	62
Y.MINEZAKI, I.TANAKA, N.NIIMURA, M.ATAKA & T.KATSURA	
12. Neutron Diffraction Camera Using A Thermo-lumino Sheet	71
M.HIDAKA, T.MORISAKO & M.NISHI	

13.	Low Resolution Neutron Crystallography of Large Macromolecular Assemblies	72
	P.A.TIMMINS	
14.	Diffractometer for Neutron Crystallography in Biology -Japanese Project	80
	N.NIIMURA	
15.	Quast Laue Neutron Protein Crystallography	83
	B.P.SCHOENBORN	
16.	Neutron Scattering Facilities at JRR-3M	84
	S.FUNAHASHI	
Appendix	Program, list and Photograph of participants of "Neutrons in Biology"	89

目 次

1. GKSSでの中性子構造生物研究	1
H.B.Stuhrmann (GKSS,Germany)	
2. 京都大学原子炉実験所の中性子小角散乱装置	5
杉山正明, 上原進一, 前田豊 (京大)	
3. 構造生物研究用偏極中性子小角散乱装置	12
H.B.Stuhrmann (GKSS,Germany)	
4. 昆虫リポフォリンのX線及び中性子小角散乱	26
片桐千仞 ¹ , 伊藤雄而 ² , 佐藤衛 ³ (北大 ¹ , 東大 ² , 阪大 ³)	
5. 中性子小角散乱におけるゲルゾリン-PIP2複合体の構造研究	29
伊藤忠直 ¹ , 福島寿一 ¹ , 峯崎善章 ² , 田中伊知朗 ² , 新村信雄 ² 林浩平 ³ (京大 ¹ , 東北大 ² , 茨大 ³)	
6. フカヒレ軟骨からのプロテオグリカンの中性子小角散乱	30
佐野洋 ¹ , 新村信雄 ² , 田中伊知朗 ² (食総研 ¹ , 東北大 ²)	
7. 中性子小角散乱法における酵母産成B型肝炎ワクチン粒子の構造研究	33
伊藤雄而 ² , 佐藤衛 ³ , 亀山啓一 ² , 石川信義 ² , 高木俊夫 ² (東大 ¹ , 坂大 ²)	
8. DNAとその水の中性子非弾性散乱	39
安宮居あかね ¹ , 富永靖徳 ¹ , 池田進 ² (お茶水大 ¹ , 高工研 ²)	
9. トロムベイでの小さい生体分子と水素結合の中性子散乱と将来計画	41
K.K.Kannan (Bhabha,India)	
10. NiCl ₂ 濃度勾配法によるリゾチームの大きな正方晶系単結晶成長	61
安宅光雄, 曾良達生 (織高研)	
11. 中性子小角散乱によるリゾチーム単結晶成長初期過程の研究	62
峯崎善章 ¹ , 田中伊知朗 ¹ , 新村信雄 ¹ , 安宅光雄 ² , 曾良達生 ² (東北大 ¹ , 織高研 ²)	
12. 熱蛍光板中性子回折カメラ	71
日高昌則 ¹ , 森迫常生 ¹ , 西正和 ² (九大 ¹ , 東大 ²)	
13. 巨大分子複合体の低分解能中性子結晶解析	72
P.Timmins (ILL,France)	
14. 生物結晶構造研究用中性子回折装置-日本の計画-	80
新村信雄 (東北大)	
15. 結晶タンパク質研究用準ラウエ中性子回折法	83
B.P.Schoenborn (BNL,USA)	
16. JRR-3Mの中性子散乱実験装置	84
松橋達 (原研物理部)	
付 録	89
「中性子散乱構造生物学」ワークショップのプログラム, 参加者名簿, 写真	

1. NEUTRONS IN BIOLOGY AT GKSS

H.B. Stuhmann, GKSS Forschungszentrum, Geesthacht, Germany

Although the construction of the GKSS research reactor FRG1 dates back to 1957 it was only in 1989 that this neutron source became attractive for the development of new techniques of neutron scattering and hence for an increasing number of outside users. The FRG1 is a light water, swimming pool type reactor with a thermal power of 5 MW.

Four beam holes of the FRG1 reactor provide neutrons for scattering experiments (Fig. 1) One of them emits cold neutrons. There is an enhancement of the spectral density of cold neutrons with respect to that of the thermal neutrons at wavelengths larger than 2.2 Å. At this very wavelength it does not matter whether the cold source is working or not; the gain factor is 1. At wavelengths near 5 Å the gain factor has already increased to 11 and it reaches 30 at wavelengths larger than 10 Å.

SMALL-ANGLE SCATTERING

The cold neutrons are used in small-angle scattering experiments. There are two small-angle scattering facilities (Fig. 1). SANS1 is mainly used by materials scientists whereas SANS2 is dedicated to biological structure research.

The neutron flux at the velocity selector is 2×10^8 n/cm²/s. A velocity selector with an overall length of 330 mm only cuts out a wavelength band with a relative width $\Delta\lambda/\lambda = 0.1$ (Friedrich et al. 1989). Both instruments have the option of neutron polarization (Schärpf, 1989). The collimator with its movable neutron guide sections is in a long segmented solenoid providing the magnetic guide field for polarized neutrons. The maximum collimation length is 9 m at SANS1 and 15.5 m at SANS2.

The difference between SANS1 and SANS2 becomes apparent at the sample position. SANS1 is almost exclusively used for polarized neutron scattering by dynamic polarized targets. The polarized target station and its use in biological structure research is described elsewhere (Stuhmann, 1992). SANS2, on the other hand, is a multi-purpose small-angle instrument. It is mainly used for studies of materials.

The scattered neutrons are detected by an multiwire chamber filled with a pressurized mixture of 1 atm ^3He , ^4He and CF_4 , 1 bar each. The sensitive area is 55 x 55 cm and the spatial resolution is about 7 mm. The distance between sample and detector may vary from 0.7m to 9m at SANS1 and from 1m to 22m at SANS2. The detector can be displaced in directions orthogonal to the beam axis. All movements of the detector and of the collimating components are controlled by a personal computer.

New technologies make both instruments very efficient. The bent neutron guide section is relatively short (Fig. 1). The gaps between adjacent neutron guide sections including those for insertion devices (velocity selector and polarizer) have been kept as small as possible.

The flux of *polarized* neutrons at SANS1 is characterized by following numbers:

collimation length:	2m
cross section of ^{58}Ni -coated neutron guide	30 x 40 mm
wavelength	$(8.5 \pm 0.4)\text{\AA}$
apparent polarized neutron flux at the sample:	
- from indium activation	$5 \times 10^5 \text{ n/cm}^2/\text{s}$
- deduced from small-angle scattering	$2.8 \times 10^5 \text{ n/cm}^2/\text{s}$
(no correction for detector sensitivity)	

A description of of the small-angle Instrument SANS1 is given by Knop et al. (1991).

REFERENCES

- Friedrich H., V. Wagner, P. Wille (1989) Physica B 156&157, 547-549
- Schärpf O. (1989) Physica B 156&157 639-646
- W. Knop, M. Hirai, G. Olah, W. Meerwinck, H.-J. Schink, H.B. Stuhrmann, R. Wagner, M. Wenkow-EsSouni, J. Zhao, O. Schärpf, R.R. Crichton, M. Krumpolc, K.H. Nierhaus, T.O. Niinikoski, A. Rijllart (1991) Physica B 174, 275-290
- Stuhrmann H.B. (1992) This Conference Proceeding

Fig. 1

New Instruments and novel neutron guides at the FRG-1 research reactor.

SANS: Small-angle neutron scattering facility

SANS1: Study of macromolecules using the interaction of polarized neutrons with polarized targets

SANS2: Study of precipitates, cluster, voids and bubbles in crystalline and amorphous solids

DCD: Double crystal diffractometer

study of large creep, fatigue and sintering cavities in ceramics and high temperature alloys and of other microscopic structures

DENS: Diffuse elastic neutron spectrometer

DENS1: Study of short order and clustering

DENS2: Study of hydrogen content in welds and heat affected zones

FSS: Fourier strain spectrometer

Study of internal stresses in material

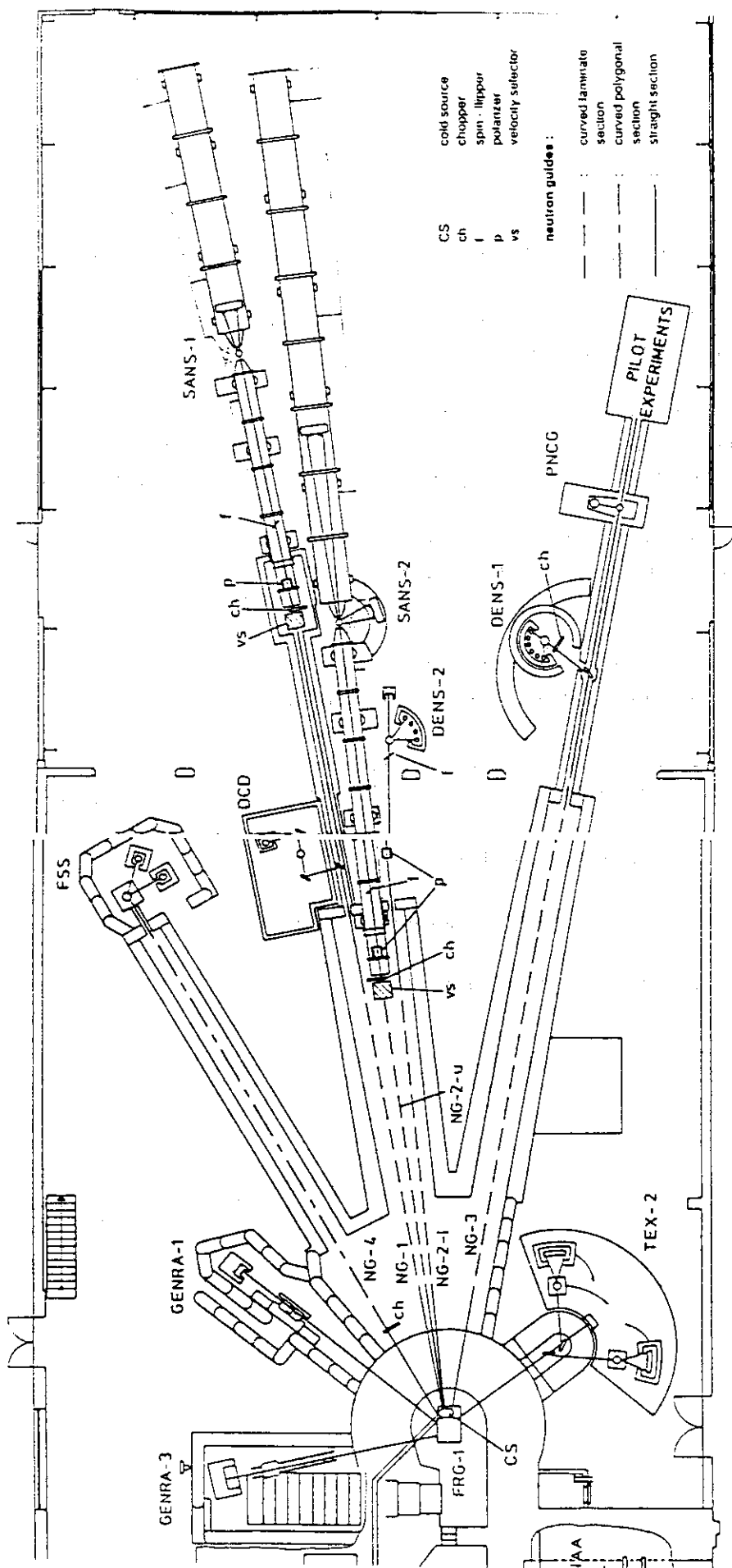
TEX2: Four circle neutron diffractometer

Study of textures in materials, alloys and geological samples

NAA: Neutron activation analysis

PCNG: Prompt neutron capture gamma-ray spectrometer

GENRA1,2: Neutron radiography facilities.



2. SMALL-ANGLE NEUTRON SCATTERING INSTRUMENT AT THE KYOTO UNIVERSITY REACTOR

Masaaki SUGIYAMA, Shin-ichi UEHARA and Yutaka MAEDA
Research Reactor Institute, Kyoto University,
Kumatori, Sennan, Osaka, 590-04, Japan

1. Introduction

A cold neutron source with liquid D₂ at 25 K was installed in the graphite thermal neutron column of Kyoto University Reactor (KUR), which is 5 MW light water moderated, swimming pool type. The cold source is viewed by four neutron guide tubes, supplying cold and very cold neutrons. A neutron guide room is located just outside the original reactor confinement building, and is 9 m wide by 6 m long. From the spatial constraint of the guide room a specially designed small-angle neutron scattering (SANS) instrument has been constructed and its performance has been checked using ferritin as a typical biological sample. In this paper, we describe the components of the instrument and discuss its performance.

2. Construction

The main feature of our SANS instrument is characterized by a double-reflection Ni-Ti multilayer monochromator and two area neutron detectors. The multilayer monochromator is used not only for getting the monochromatic neutron beam, but also for the collimation of the beam. It is built up of two sets of eight multilayer mirrors of a Soller type, each of which is alternative Ni-Ti bilayers with a thickness of 70Å each deposited on both sides of a flat silicon substrate. As shown in Fig. 1, the double reflection monochromator is positioned at the distance of about 1 m from the shutter of the neutron guide, giving rise to monochromatic beams at 5.5 Å with a wavelength band pass $\Delta\lambda/\lambda$ of 15% and a beam divergence of 12 mrad. The beam profile of the double reflected neutrons is given in Fig. 2 with those of the incident and the single reflected neutrons. By replacing Ni-Ti mirrors with Fe,Co-V magnetic mirrors, the double-reflection monochromator is used as a neutron polarizer in addition to a monochromator, a beam bender and a collimator. The details of the double-reflection Ni-Ti multilayer monochromator are given elsewhere [1]. For the beam collimation at the vertical direction ⁶LiF tiles are used making converging slits.

The SANS spectrometer has two area detectors. The larger one is a multi-wire proportional chamber (MWPC) of 51x51 cm² sensi-

tive area, and is fixed at a sample-to-detector distance of 1.5 - 3 m. The smaller one is also a MWPC of $21 \times 21 \text{ cm}^2$ sensitive area, and can be moved over scattering angles of up to 90° at the distance of 0.8 m. The characteristics of both detectors are given in Table 1. In principle there is no differences in both detectors, but the large counter is built in a large aluminum case and has a poor spatial resolution. By filling $^3\text{He-Ar-CO}_2$ (50-47.5-2.5%) counter gas mixture, both are working well with a delay-line position encoding. The linearity and the resolution in position decoding are given in Fig. 3 for the small detector. To maintain these performance of the detectors, a gas purifier containing Ca metal shots is mounted and the counter gas is circulated by convection by heating the purifier. The details of our two-dimensional position detectors are given elsewhere [2].

3. Performance

To check the total performance of our SANS instrument, we performed a preliminary experiment with an iron storage protein, ferritin. Ferritin consists of protein shell and iron core. The shell of proteins consists of 24 subunits, and it contains iron micelle ranging from 0 to 4500 iron atoms per one molecule. The reversible iron storage process is very interesting from the viewpoint of biomineralization. The core is supposed to be iron oxy-hydroxide. At the early stage of neutron scattering experiments Stuhmann *et al.* have investigated this biomolecule in details [3]. In our preliminary test ferritin and apoferritin were used. The apoferritin was obtained by using thioglycolic acid as a chelating agent. A typical scattering curve is shown in Fig. 4. In Table 2 we summarize the characteristics of our SANS instrument.

References

- [1] T.Ebisawa, S.Tasaki, T.Akiyoshi and N.Achiwa, "Proceedings of ICANS-XI(KEK Report 91-25)", Vol.2, (KEK,1990) p.899.
- [2] Y.Maeda, M.Sugiyama and S.Uehara, *ibid.*, Vol.2, (KEK,1990) p.932.
- [3] H.B.Stuhmann, J.Haas, K.Ibel, M.H.J.Koch and R.R.Crichton, J. Mol. Biol., 100, 399 (1976).

Table 1. Characteristics of two PSDs.

	Type A	Type D
Active area[cm ²]	21x21	51x51
Vessel material	10[mm](flat plane)	14[mm] (4[mm] dome plus 10[mm] diaphragm)
Active depth[mm]	26	26
Anodes	20 μ Au-coated W wires spacing 2.5[mm]	20 μ Au-coated W wires spacing 4.0[mm]
Grids (for position readout)	50 μ Au-coated W wires spacing 1.25[mm]	50 μ Au-coated W wires spacing 2.0[mm]
Cathodes	50 μ Au-coated W wires and Alminized mylar sheet	50 μ Au-coated W wires and Alminized mylar sheet
Wire plane spacing[mm]	6.5	6.5
Filled gas	³ He-Ar-CO ₂ (50-47.5-2.5%)	³ He-Ar-CO ₂ (50-47.5-2.5%)
Gas pressure[Pa]	3.0x10 ⁵	3.0x10 ⁵
Gas purifier	150°C heated Ca shots	400°C heated Ca shots
Applied voltage		
anode [V]	+2500	+2000
cathode [V]	-250	-250
Position encoding	Delay line method	Delay line method
Spatial resolution[mm]	3x3 (for X and Y axes)	8x8 (for X and Y axes)

Table 2. Characteristics of KUR SANS.

Cold Neutron Bent Guide Tube	Ni-mirror
Characteristic Wavelength	2.6 [Å]
Total Length	11 [m]
Beam Cross Section	1×7.5 [cm ²]
Monochromator	Double Reflection Ni-Ti Multilayer Monochromator
Wavelength	5.5 [Å]
Wavelength Resolution	$\Delta\lambda/\lambda=15\%$
Reflectivity	0.9×0.9=0.81
Collimator	
Horizontal	Double Reflection Ni-Ti Multilayer Monochromator
Vertical	Convergent ⁶ Li Slits
Angular Resolution	$\Delta\theta/\theta=15\%$
Sample-to-Detector Distance	0.8~3 [m]
Q-range	
Fixed Large Detector	0.004~0.1 [Å ⁻¹]
Movable Small Detector	0.01~1.2 [Å ⁻¹]
Maximum Flux at Sample	
CNS-ON	3.9×10 ⁴ [n/cm ² ·s]
CNS-OFF	2.4×10 ³ [n/cm ² ·s]
Detector	
Large Detector	
Counter Gas	³ He-Ar-CO ₂ (50%-47.5%-2.5%)
Active Area	51×51 [cm ²]
Spatial Resolution	8mm×8mm
Position Readout	Delay Line
Small Detector	
Counter Gas	³ He-Ar-CO ₂ (50%-47.5%-2.5%)
Active Area	21×21 [cm ²]
Spatial Resolution	3mm×3mm
Position Readout	Delay Line
Auxiliary Equipment	
Polarizer	(Fe,Co)-V Magnetic Mirror

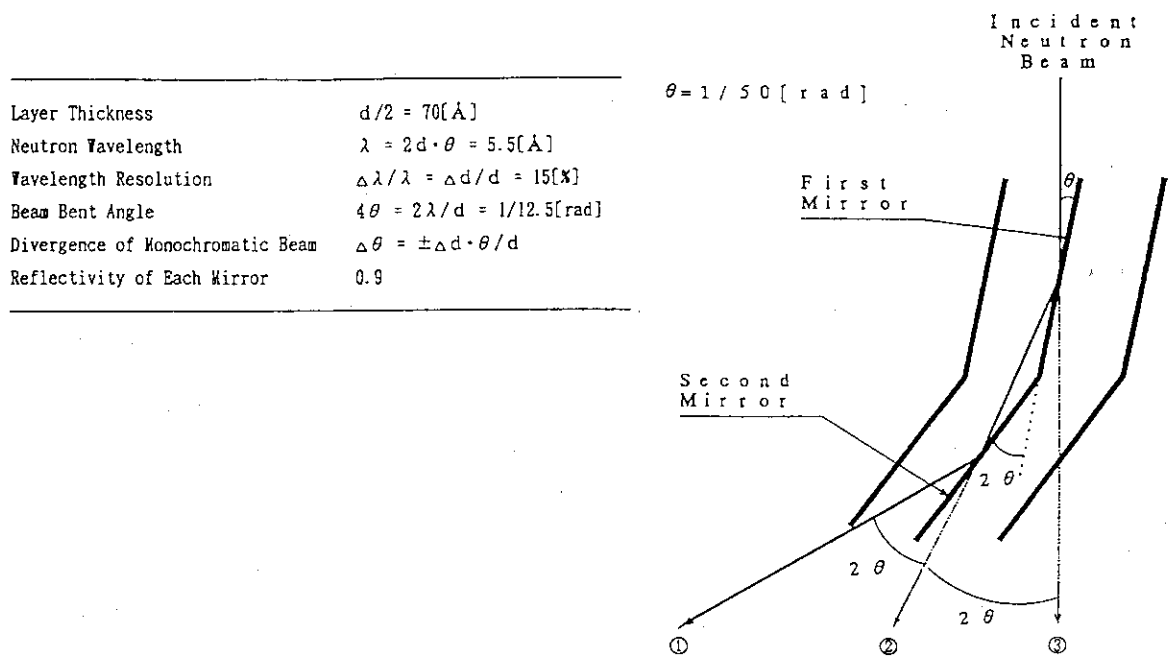


Fig. 1. Schematic drawing of the double-reflection multilayer monochromator.
 ①, ② and ③ represent the double-reflected, the single-reflected and the incident beams, respectively.

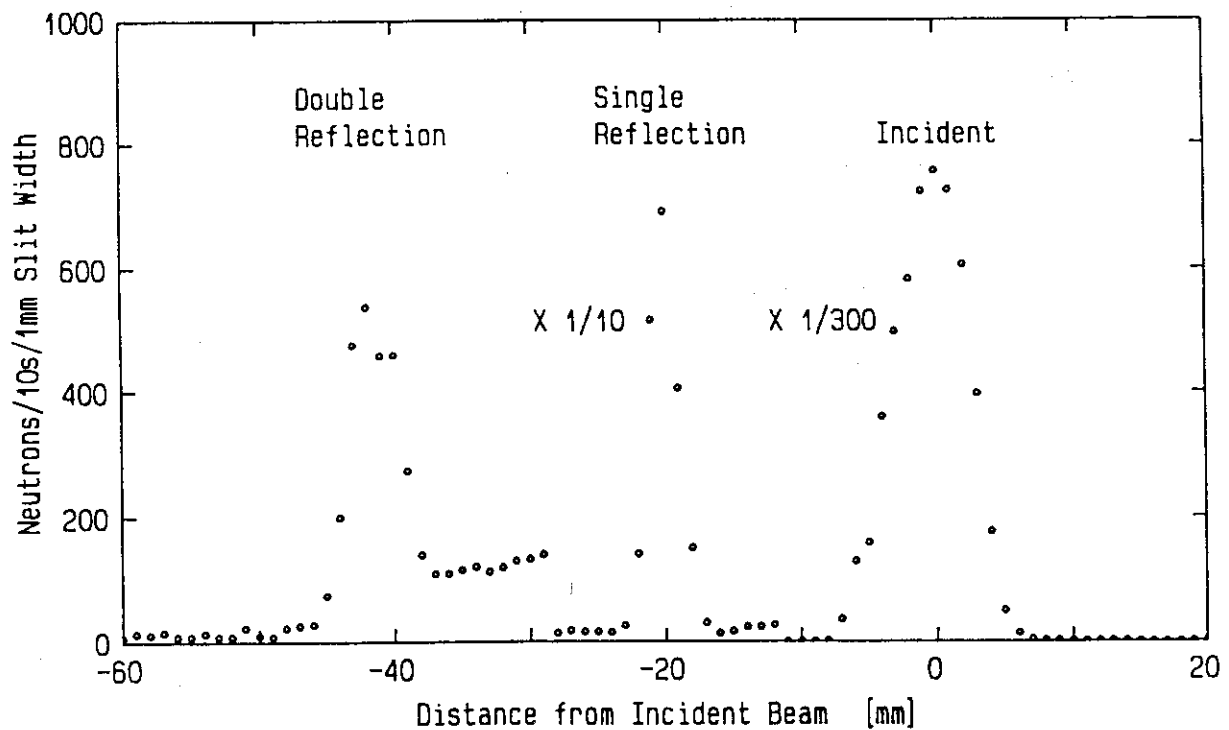


Fig. 2. Beam profile at a distance of 50 cm from the monochromator.

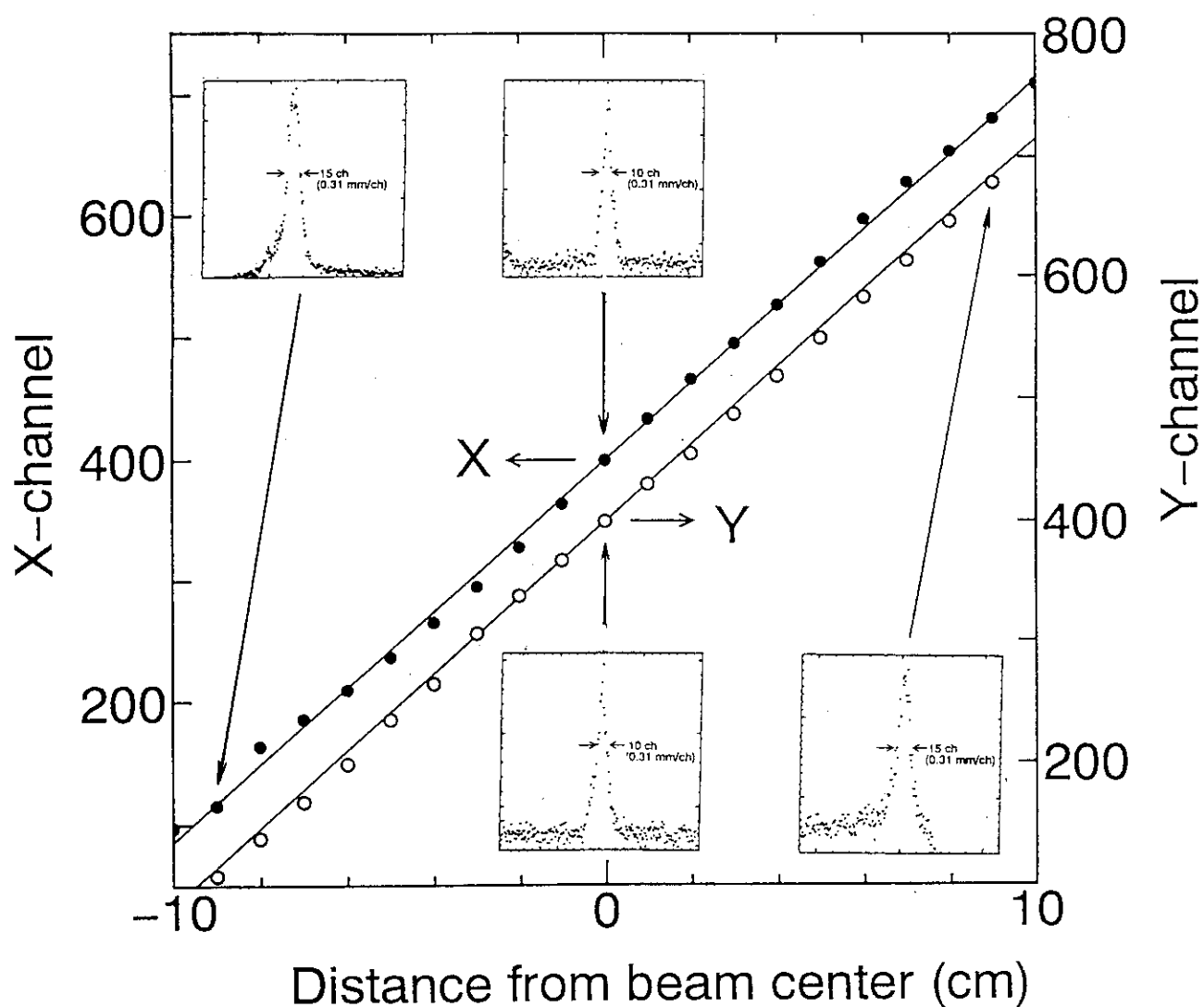


Fig. 3. Relation between neutron impact position and two-dimensional channel assignment. 1 channel = 0.31 mm. The inserts show the response to a pinhole beam giving the spatial resolution.

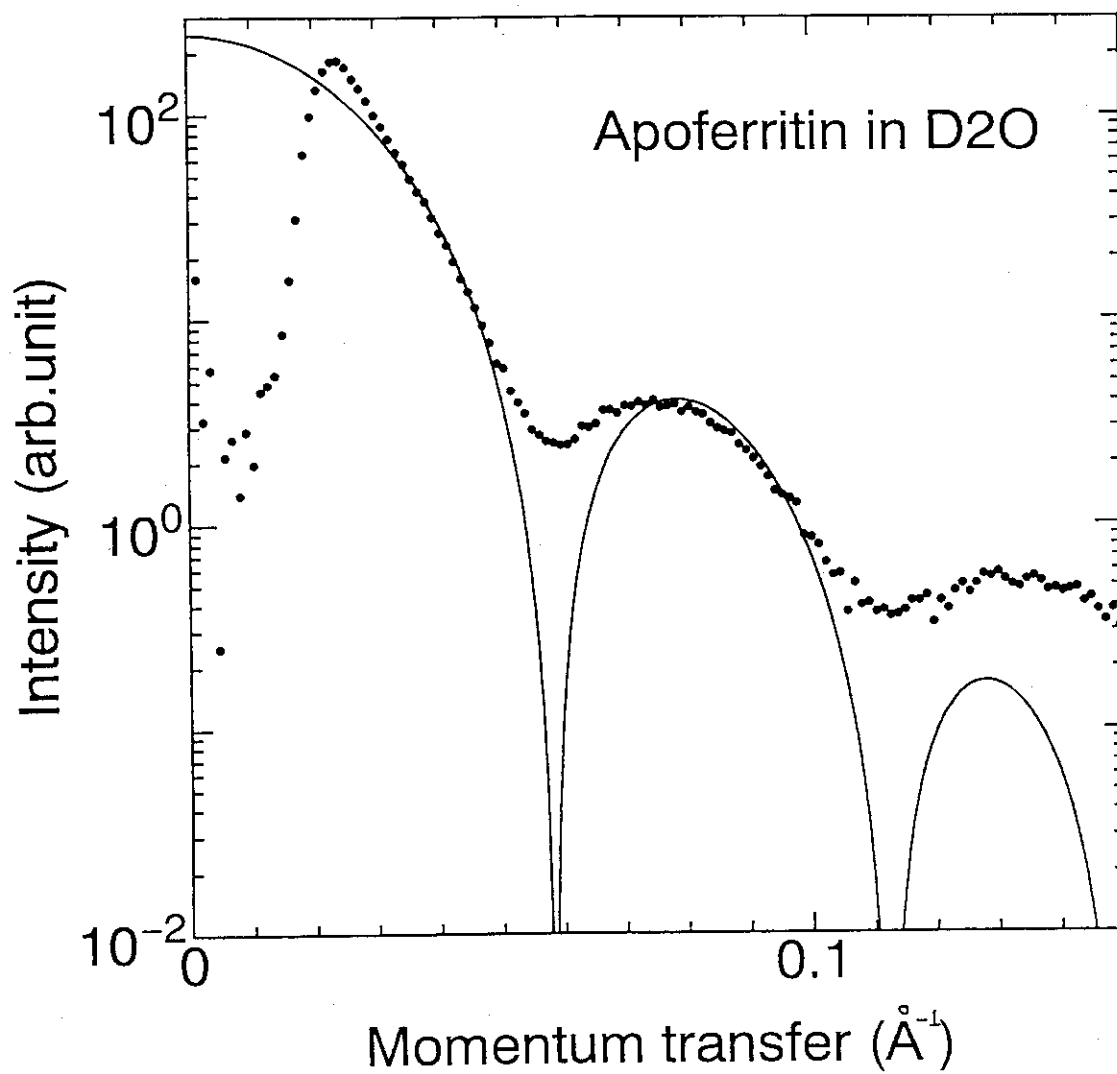


Fig. 4. Neutron small-angle scattering of apoferritin in D_2O .

The full line is a calculated scattering curve, assuming that the inner and outer diameters of the protein shell are 60 \AA and 140 \AA , respectively.

3. POLARIZED NEUTRON SMALL-ANGLE SCATTERING IN BIOLOGY

H.B. Stuhrmann, GKSS Forschungszentrum, 2054 Geesthacht

Experiments of polarized neutron scattering from polarized proton spin targets have first been tried at the Institute Laue-Langevin at Grenoble (Hayter, Jenkin, White, 1974). The target material was lanthanum magnesium nitrate hydrate, $(\text{La}_2\text{Mg}_3(\text{NO}_3)_{12} \cdot 24\text{H}_2\text{O})$, abbreviated as LMN. It also served as a proton spin target in nuclear physic experiments (Schmugge, Jeffries, 1965). Looking for proton spin targets with higher proton content high energy physicists started using hydrogenous organic compounds, like frozen alcohols, diols etc. the proton spins of which could be almost completely polarized (Glättli, 1971; de Boer et al. 1974, Niinikoski, Udo, 1976). These materials are excellent glass formers at very low temperatures and hence ideal solvents of polymers and biological macromolecules. It is therefore not surprising that this very fact was recognized by different groups who succesfully tried neutron scattering from polarized frozen solutions of proteins (Knop et al. 1986), of dicyclohexyl-18-crown-6 (Koghi et al. 1987) and of polymers (Glättli et al. 1989). A method of neutron scattering more powerful than isotopic substitution has become available (Stuhrmann, 1989).

THE INTERACTION OF NEUTRON SPINS WITH NUCLEAR SPINS

The interaction of a neutron spin s with a nuclear spin I is described by a scattering amplitude operator :

$$A = b + B \mathbf{I} \cdot \mathbf{s} \quad (1)$$

The formal treatment of this equation yields the intensity S of coherent neutron scattering from a many body system (Abragam and Goldman, 1982):

$$S = |U|^2 + 2 n \text{Re}[UV^*] + |V|^2 \quad (2)$$

U = amplitude of the unpolarized sample.

V = amplitude of the polarized sample

n = polarisation of the neutrons, $(-1 < n \leq 1)$

In biological samples the most prominent non-spinless nucleus is the proton ($^1\text{H} = \text{H}$). The deuterons ($^2\text{H} = \text{D}$) will have to be considered in deuterated samples only. The effect of nitrogen nuclear spins on the intensity is small.

Thus we write

$$V = P_H V_H + P_D V_D + P_N V_N \quad (3)$$

P_H , P_D and P_N are nuclear spin polarizations referring to protons, deuterons and nitrogen nuclei, respectively. Considering protons and deuterons only, the ideal experiment determines the following basic scattering functions:

$$|U|^2, |V_H|^2, |V_D|^2, |V_H+V_D|^2, \text{Re}[UV_H], \text{Re}[UV_D], \text{Re}[U(V_H+V_D)]$$

For this purpose it is required that the polarisation of the incident neutrons and that of the target nuclei are known. Moreover, it is necessary that the polarization of each isotope can be varied separately.

In practice, pure polarized nuclear targets are preferred, i.e. only one isotopic spin is significantly polarized. Small-angle scattering then can be written in the following form:

$$I(Q) = \int_{\Omega} S(Q) d\Omega = I_U(Q) + nP I_{UV}(Q) + P^2 I_V(Q) \quad (4)$$

$Q = 4\pi/\lambda \sin\theta$, where λ and 2θ are the mean wavelength of the neutrons and the scattering angle respectively. The basic scattering functions of nuclear spin contrast variation I_U , I_{UV} , and I_V can be obtained from a couple of measurements with the neutron spin polarizations $n=1$ and $n=-1$. The difference between the scattering curves yields I_{UV} , whereas the sum diminished by I_U leaves I_V .

Coherent scattering as discussed above is non-spinflip scattering, i.e. the neutron maintains its spin state. Spin flip processes give rise to incoherent scattering. The elimination of the later could be achieved by spin analysis of the scattered neutrons. In practice, approximative methods are used to separate coherent scattering from incoherent scattering (de Cloizeau, Jannink, 1986). There is strictly no spin incoherent neutron scattering when $nP = 1$.

The influence of nuclear polarization on the intensity of polarized neutron scattering varies with the isotope. Among the nuclei occurring in polymers and biomolecules the proton contributes most strongly to spin dependent neutron scattering (Tab. 1). The effect of deuterons though weaker is significant in deuterated samples. The influence of ^{13}C and ^{14}N can be neglected in most cases.

Tab. 1. Nuclear magnetic moments μ (in units of nuclear magnetons) and spin dependent scattering lengths (abstracted from Glättli & Goldman, 1987)

	natural abundance [%]	I	μ/μ_N	ν (NMR) at 2.5 T [MHz]	b [10^{-12} cm]	IB
^1H	99.98	1/2	2.7927	106.45	-0.374	1.456
^2H	0.014	1	0.8573	16.34	0.667	0.285
C					0.665	-
^{13}C	1.108	1/2	0.7022	26.77	0.60	-0.03
^{14}N	99.63	1	0.4036	7.69	± 0.04	
O					0.580	-
P	100	1/2	1.1305	43.09	0.51	?
S					0.28	
Fe					0.95	

ISOTOPIC AND NUCLEAR SPIN CONTRAST VARIATION

The well-known technique of contrast variation by isotopic substitution is extended to nuclear spin contrast variation by allowing for nuclear spin polarization. Assuming that the incident neutrons are completely polarized parallel ($n = +1$) or antiparallel ($n = -1$) to the direction of the external magnetic field, the effective nuclear scattering lengths in units of 10^{-12} cm are

$$\begin{aligned} \text{for protons:} & \quad -0.374 \pm 1.456 P_H \\ \text{for deuterons:} & \quad +0.665 \pm 0.285 P_D \end{aligned}$$

These and other scattering lengths are used to calculate the scattering density which is defined by

$$\rho = \frac{\sum_{j=1}^N b_j + P_j I_j B_j}{V} \quad (5)$$

This expression is extended by a polarization dependent term called nuclear spin density. Nuclear spin contrast is the change in nuclear spin density as it may occur at a phase boundary, for instance.

The polarization dependent amplitudes look very similar to those used in isotopic substitution. In the case of H/D exchange we write:

$$\begin{aligned} \text{for hydrogen: } b &= b_H + (0.665 - (-0.374)) X \\ &= b_H + 1.039 X \end{aligned}$$

where X is the degree of substitution of H by D. Note that range of scattering lengths achieved by proton spin polarization is nearly three times larger than that obtained from isotopic substitution of H by D.

POLARIZATION OF NEUTRONS AND NUCLEAR SPINS

Neutrons

As the wavelength distribution of neutrons beams used in small-angle scattering is fairly broad ($\Delta\lambda/\lambda = 0.1$) beam bender neutron polarizers using supermirrors are a good choice (Schärpf, 1989). The polarization of the emerging beam is very close to $n=1$.

The polarization direction of a polarized neutron beam is inverted to $n=-1$ by a Mezei type, flat coil spin flipper (Schärpf, 1980). As there is a spread in wavelengths a slight depolarization occurs (typically $n = -0.96$). This is taken into account properly by Eq. 2.

Nuclei.

Nuclear spins are polarized by a magnetic field. The nuclear polarization reaches appreciable amounts at very low temperatures only. At $T = 10$ mK and in a magnetic field of 10 T the proton spins in thermal equilibrium would have a polarization of 0.77. The time needed to reach the thermal equilibrium would be very long in biological systems, i.e. the lattice and the nuclear spin system don't know of each other.

This very fact is the necessary prerequisite of dynamic nuclear spin polarization (DNP) (Abragam and Goldman, 1982; Glättli and Goldman, 1987). In this case, an unequal population of the nuclear magnetic substates is attained by induced transitions between electron-nucleus spin states. Paramagnetic centres are added to the sample. Usually these are organic radicals. At temperatures below 1 K and in a magnetic field of 2.5 T, their unpaired electronic spins are almost completely polarized. By 4 mm microwave irradiation, at a frequency slightly off the center of the ESR peak, all nuclear spins get gradually polarized. The sign of the nuclear spin polarization is determined by the frequency of the microwaves: At frequencies

slightly below the ESR-peak the nuclear spins will get oriented parallel to the external field, whereas the opposite direction of nuclear spin polarization is achieved at frequencies slightly above that of the ESR peak.

After a few hours of microwave irradiation the proton spin polarization reaches final values between 0.6 to 0.9 (Knop et al. 1992). The deuteron will be less polarized because of their lower nuclear magnetic moment (Tab. 1). - The microwaves are switched off. The absence of heating by microwaves makes the temperature drop to about 100 mK. The relaxation time of the nuclear spin system is of the order of weeks (frozen spin target).

The nuclear polarization is measured by continuous wave NMR. The same circuit operated at a higher power level is used for selective nuclear spin depolarization of the frozen spin target. After proton spin depolarization only the spins of the deuterons and of those of the nitrogen nuclei remain polarized. Thereafter the deuterons may be depolarized as well and we are left with a sample of nitrogen nuclei polarized only, if there are any. The contribution of nitrogen spin dependent neutron scattering from dilute protein or RNA solutions is extremely small. It is comparable to magnetic scattering from the paramagnetic centres.

In deuterated samples selective polarization of the hydrogen isotopes is used in order to prepare pure proton spin targets or pure deuteron spin targets. The selectively depolarized targets are quite stable. Their lifetime is of the order of weeks at temperatures below 200 mK. This time is long enough for polarized neutron small-angle scattering studies. A schematic presentation of the nuclear polarization facility is given in Fig. 1.

THE SAMPLE AND ITS ENVIRONMENT

Any sample to be dynamically polarized needs a certain amount of paramagnetic centres, typically some 10^{19} cm^{-3} . These are organic radicals. A very popular one is sodium bis(2-ethyl-2-hydroxybutyrate)oxochromate, $\text{Na}[\text{Cr}(\text{C}_6\text{H}_7\text{O}_5)_2\text{O}]\cdot\text{H}_2\text{O}$, or abbreviated as EHBA-Cr(V). About 1 wt.% of this compound is added to strongly deuterated samples in order to achieve a good nuclear spin polarization by DNP. Protonated samples (= neutron spin filters) need a higher concentration of EHBA-Cr(V).

EHBA-Cr(V) is fairly stable in acid solution but decomposes quickly at $p_{\text{H}} > 6$. The halftime of dissolved EHBA-Cr(V) at $p\text{H} = 7$ is about 10 minutes. Crystalline EHBA-Cr(V) can be stored at 4°C in the dark for years without significant decomposition.

Solutions at room temperature need to be frozen in such a way that their small-angle scattering will not change. There are solvents which can be transformed into a frozen glassy state, at least when freezing occurs rapidly, say in a few seconds. A glycerol-water mixture (1:1) has this property. It is a good solvent for biological macromolecules. Among the solvents for polymers ortho-terphenyl is a good glass-former (Glättli et al. 1989).

There are various ways which may be used to freeze the sample. The simplest one is to produce frozen beads in liquid nitrogen. This method is used in the large scale production of target material for high energy physics experiments. The solution should be transformed into beads within 1 hour. - This time may be too long for EHBA-Cr(V) at pH = 7. In this case it is mandatory to freeze the whole sample (about 1 ml) in a single shot. After having added the (acid) EHBA-Cr(V) solution to the buffered solution of biomolecules the components are mixed rapidly and injected into a precooled copper mould at liquid nitrogen temperature. The whole procedure takes 40 seconds. Within this time about 10% of EHBA-Cr(V) will have decayed.

The way how a frozen sample is introduced into the refrigerator varies strongly with its construction. Frozen beads may be transferred through the microwave guide into the cavity (Glättli et al. 1989). For a compact sample with dimensions of 17 x 17 x 3 mm the sample chamber of the refrigerator has to be opened (Stuhrmann, 1991).

Frozen spin targets require temperatures well below 200 mK. Only dilution refrigerators will reach this range of temperatures. The cooling power is due to the continuous dilution of liquid ^3He in ^4He . As thermal neutrons are strongly absorbed by ^3He the sample will not be cooled directly by the ^3He - ^4He mixture. It will be put into a separate cell filled with liquid ^4He which is coupled to mixing chamber by a heat exchanger (Knop et al. 1992).

SPIN CONTRAST VARIATION EXPERIMENTS

The scattering length of protons varies with nuclear spin polarization over a much wider range than can be achieved by isotopic substitution of H by D (Tab. 1). Thus, contrasts became accessible which could not be reached before (Glättli et al. 1989). As the contrast is varied by nuclear spin polarization this method is ideally suited for the *in situ* structure determination of labelled parts of a larger particle. Furthermore, hydrogen is the most abundant element in polymers and biomolecules. Hence, hydrogen labels are powerful, and they can be tailored to any size.

As the incoherent scattering of hydrogen may obscure diffraction all hydrogens of the sample will be substituted by deuterium except those which belong to the label. Proton spin polarization then will create a strong spin contrast giving rise to additional neutron scattering due to the polarization dependent terms $I_{yy}(Q)$ and $I_y(Q)$. These basic scattering functions allow the determination of the site of label with respect to the host particle and the structure of the label, respectively. It is this idea which has lead to the construction of a polarized target facility at the GKSS Research Centre at Geesthacht in collaboration with CERN, Geneva (W. Knop et al. 1992).

Several proteins and tRNA in a deuterated solvent were studied in order to confirm the expected nuclear spin contrast. The experiments on myoglobin, bovine serum albumin (Knop et al. 1989) and apoferritin (Knop et al. 1992) showed that the polarization added contrast equals the contrast of the unpolarized target at $P_H = 0.67 \pm 0.03$. The uncertainty mainly comes from the determination of the proton spin polarization by NMR. The minimum of polarized neutron small-angle scattering of tRNA is at $P_H = 0.69 \pm 0.03$. The results are summarized in Fig. 2.

When the intensity of polarized neutron scattering varies nuclear spin polarization in the same way at any Q , then the contrast of the dissolved particle is similar to its nuclear spin contrast. Both contrasts may be uniform inside the volume of the dissolved particle, for instance. The basic scattering functions then will look quite similar. This has been observed with the proteins mentioned above and also with tRNA. It appears that nuclear polarization is homogeneous in proteins and ribonucleic acids, at least at a structural resolution of 40Å.

This finding is of considerable interest, when we are going to investigate the *in situ* structure of components of larger particles. Let the host particle be completely deuterated and the labelled region be protonated. Polarized neutron scattering from the proton spin target shows $I_p(Q)$ of the label only. From the basic scattering function $I_p(Q)$ the shape of the label can be deduced, provided the nuclear spin polarisation is uniform.

In practice, the deuterated solvents and the dissolved biomolecules will contain a small fraction of normal hydrogen. Nuclear spin contrast then will develop with polarization not only in the labelled region but also elsewhere. If the volume of the label is not too small (> 0.1) compared to that of the host particle then a modest nuclear spin contrast of the latter will not obscure the scattering from the strong spin contrast of the label.

Small labels in large heterogeneous particles are less easily identified by

polarized neutron scattering. Long range density fluctuations of both the contrast and the proton spin contrast may give rise to amplitudes comparable in size to that of the well-contrasted label. The contrast of the unlabelled particle should be kept low in order to let it appear fairly transparent to the incident thermal neutrons. A transparent matrix is also used by Nierhaus (1983) to study the *in situ* structure of ribosomal proteins of the large subunit of E.coli ribosomes. This method which relies on isotopic substitution only starts from perfect transparency of the unlabelled ribosome. Although the determination of the *in situ* structure of small labels by proton spin contrast variation is not bound to this strict requirement the strategy of the 'glassy' ribosome proposed by Nierhaus remains useful in polarized neutron scattering.

In a first try the transparent ribosomes were studied by proton spin contrast variation. The deuteration of the ribosomal proteins and that of the rRNA has been chosen in such a way that their scattering densities match that of a H_2O/D_2O mixture containing 92% D_2O (* in Fig.2). This solvent cannot be used in nuclear spin contrast variation as water is not a glass former. The scattering density of a mixture of deuterated glycerol and heavy water is considerably higher (Fig. 2). In order to decrease the contrast of the solute the degree of deuteration of the solvent was lowered to 0.85 and in another experiment to 0.74. Polarized neutron scattering from these samples was dominated by the scattering of the large ribosomal subunit because the scattering density of the solute turned out to be the average of the solvent densities.

The protonated label - the ribosomal protein L3 - gave rise to a change of the small-angle scattering intensity by about 0.15 which was almost entirely due to an interference of the amplitude of the label with that of the large ribosomal subunit. The scattering intensity from the L3-protein of about 0.005 of the total forward scattering could not be determined. Moreover, the large proton content of the solvent gave rise to strong polarization dependent, incoherent scattering and absorption of small-angle scattering. The only result which could be obtained from the interference term is the distance between the L3-protein and the center of mass of the large ribosomal subunit: it amounts to $(50 \pm 20) \text{ \AA}$.

The degree of deuteration of the ribosomal subunit was increased from 0.55 (the experiment mentioned above) to more than 0.9. Polarized small-angle scattering from the almost perdeuterated ribosomal subunit dissolved in a deuterated solvent (glycerol/water, 45 wt% D_2O) gave rise to a very low small-angle scattering (Fig.3). There is even a zero of $I_{VV}(Q)$ at $Q = 0.025 \text{ \AA}^{-1}$ which may be due to the intramolecular structure of the ribosomal subunit. Polarized small-angle scattering of the derivatives with protonated ribosomal proteins L3, L4, and L3+L4 is significantly larger than the scattering from the

unlabelled particle. The zero in $I_{yy}(Q)$ has dissappeared. The added intensities appear to be due to the scattering from the protonated labels, and to a smaller(?) extent to that from the interference of the label with the particle to which it is bound. Now, the conditions are met which allow *in situ* structure determination of small labels by nuclear spin contrast variation. The data are presently analyzed.

The results presented in this paper are due to a collaboration between high energy physicists at CERN, Geneva, neutron physicists from the Institut Laue - Langevin, Grenoble, and Molecular Geneticists of the Max-Planck Institute at Berlin. I am very much indebted to my coworkers at GKSS Geesthacht who ran the experiments of dynamic nuclear polarization and to the technical staff of GKSS who prepared the infrastructure to accept the polarized target station from CERN. The project is supported by the Bundesministerium für Forschung und Technologie, Bonn (grant No. I21E05 and 03ST2GEE).

REFERENCES

- Abragam A., M. Goldman (1982) Nuclear Magnetism: Order and Disorder. Clarendon Press, Oxford
- Des Cloizeau J., G. Jannink (1987) Les Polymères en Solution: leur Modélisation at leur Structure. Les éditions de Physique, Paris
- De Boer W., M. Borghini, K.Morimoto, T.O. Niinikoski (1974) Low Temp. Phys. 15, 249
- Glättli H. (1971) Proc. 2nd Int, Conf. on Polarized Targets, Ed. G.Shapiro, Berkeley, LBL 500, p.281
- Glättli H., M. Goldman (1987) Methods of Experimental Physics, Vol. 23, Part C, edited by K. Sköld and D.L. Price, pp 241-286, Academic Press, London
- Glättli H., C. Fermon, M. Eisenkremer (1989) J. Phys. (Paris) 50, 2375-2388
- Hayter J.B., G.T. Jenkin, J.W. White (1974) Phys. Rev. Lett. 33, 696
- Knop W., K.H. Nierhaus, V. Novotny, T.O. Niinikoski, M. Krumpolc, M. Rieubland, A. Rijllart, O. Schärpf, H.-J. Schink, H.B. Stuhmann, R. Wagner (1988) Helv. Phys. Acta, 50, 741-746

- Knop W., H.-J. Schink, H.B. Stuhmann, R. Wagner, M. Wenkow-Essouni, O. Schärpf, M. Krumpolz, T.O. Niinikoski, M. Rieubland, A. Rijllart (1989) J. Appl. Cryst. 22, 352-362
- Knop W., M. Hirai, H.-J. Schink, H.B. Stuhmann, R. Wagner, J. Zhao, O. Schärpf, R.R. Crichton, M. Krumpolz, K.H. Nierhaus, A. Rijllart, T.O. Niinikoski (1992) J. Appl. Cryst. 25, 155-165
- Koghi M., M. Ishida, Y. Ishikawa, S. Ishimoto, Y. Kanno, A. Masaike, Y. Masuda, K. Morimoto (1987) J. of the Phys. Soc. of Japan, 96, 2681-2688
- Nierhaus K.H., R. Lietzke, R.P. May, V. Novotny, H. Schulze, K. Simpson, F. Wurmbach, H.B. Stuhmann (1983) Proc. Nat. Acad. Sci. USA 80, 2889
- Niinikoski T.O, F. Udo (1976) Nucl. Instr. and Methods 134, 219
- Schärpf O. (1980) Proc. ILL workshop, F. Mezei, editor, Lecture Notes in Physics No. 128, pp. 27-52, Springer Verlag
- Schärpf O. (1989) Physica B, 156&157, 639-646
- Schmugge T.J., C.D. Jeffries (1965), Phys. Rev. 138, A1785
- Stuhmann H.B. (1989) Physica B, 156&157, 444-451
- Stuhmann H.B. (1991), Biochimie, 73, 899-910

Figures

Fig. 1. Schematic presentation of the polarized target station.

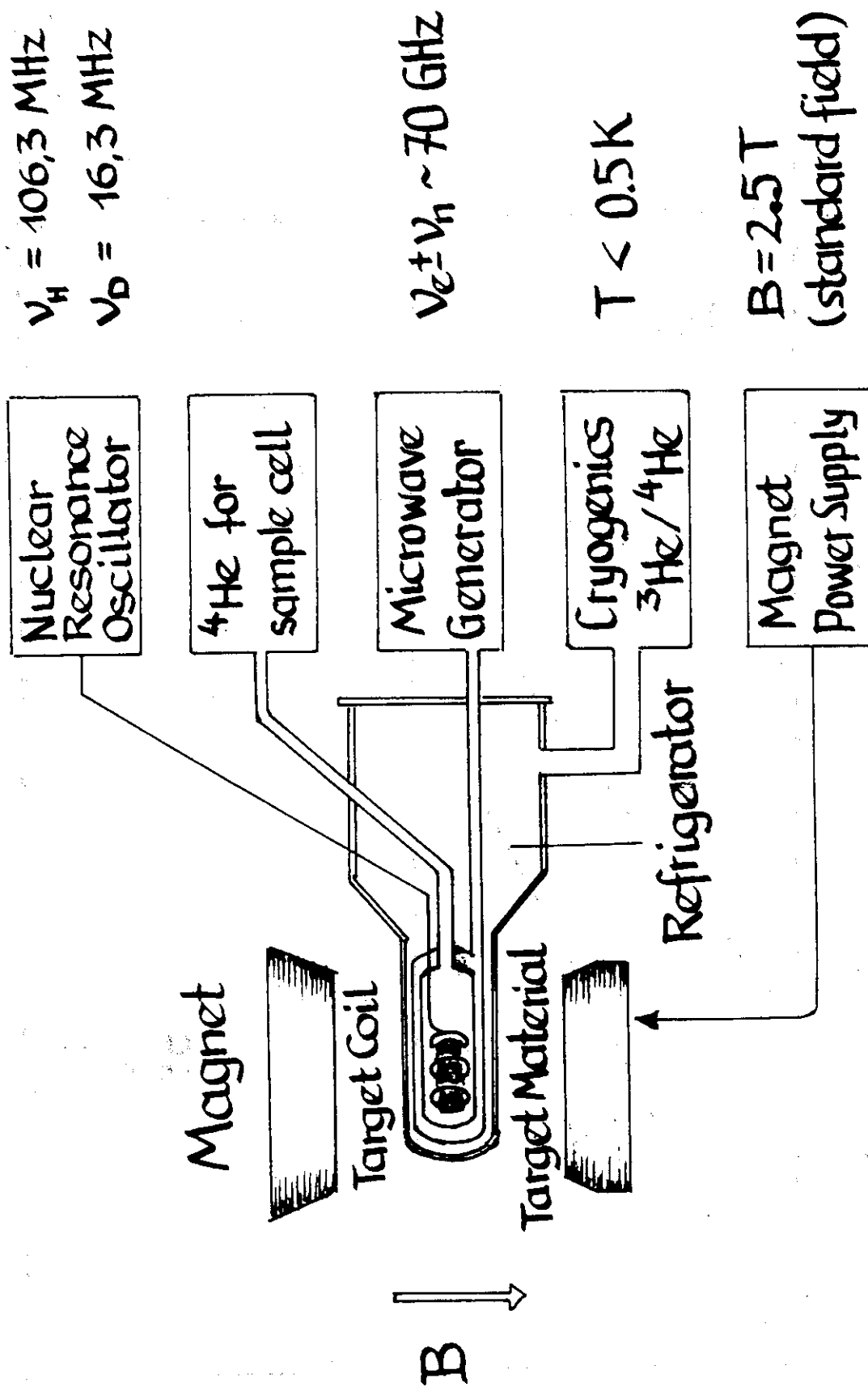
Fig. 2. Scattering densities in units of 10^{10} cm^{-2} as a function of proton spin polarization P_H .

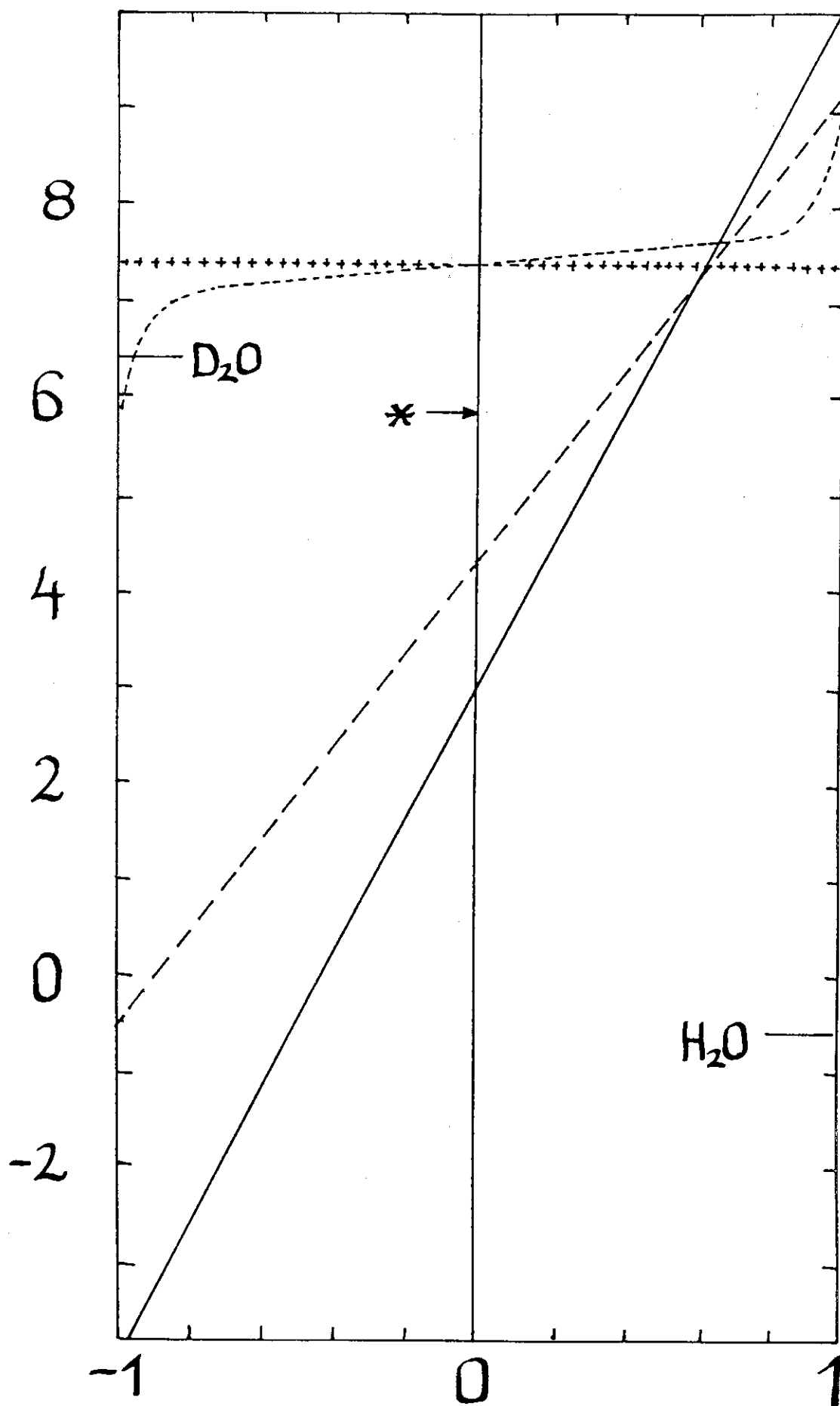
-----	proteins
- - - - -	ribonuclei acids (tRNA)
+++++	deuterated glycerol / heavy water (45 wt.% D_2O) (protons polarized only)
.....	the same solvent, proton spins and deuteron spins polarized.

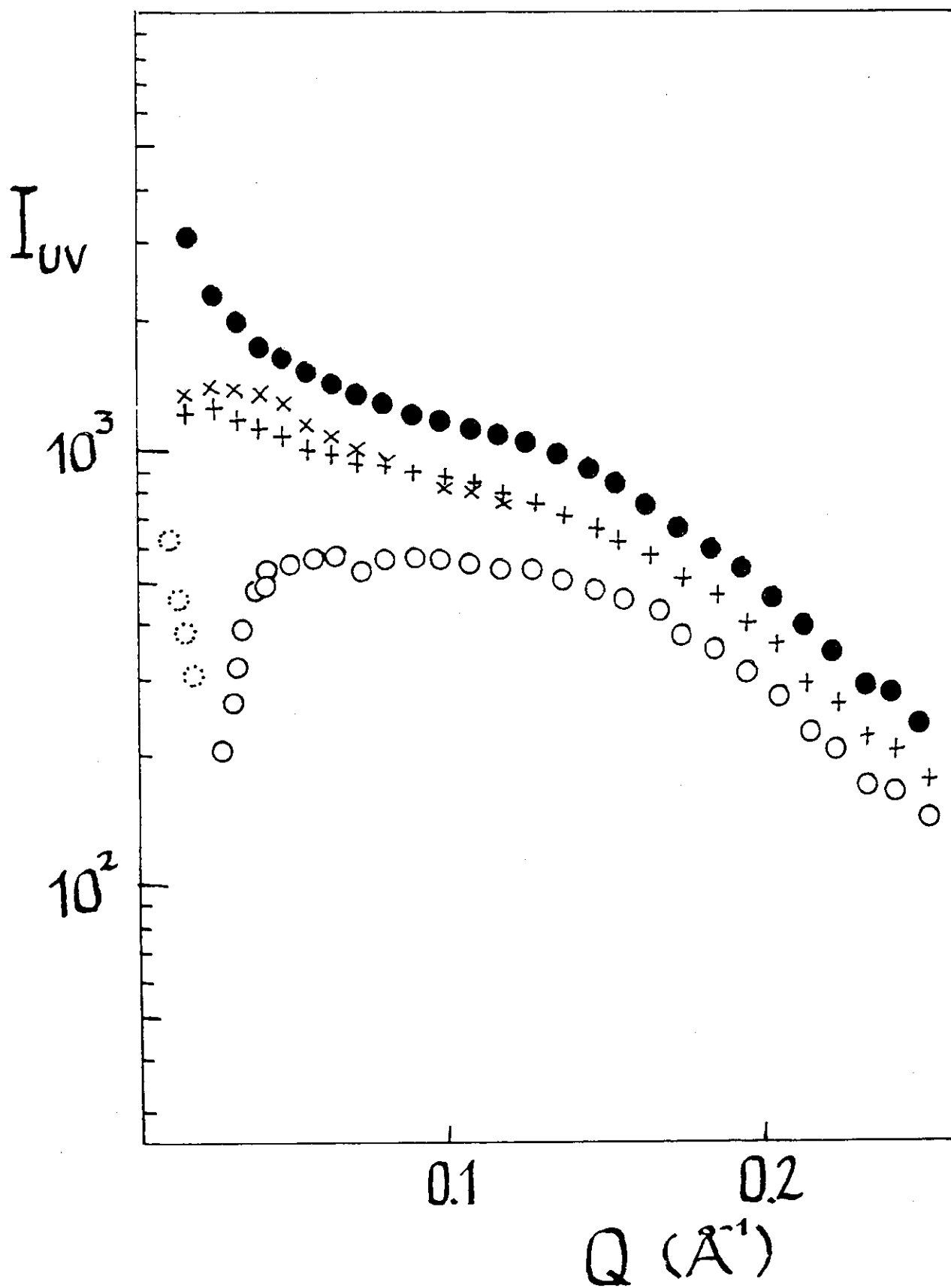
Fig. 3. Polarized neutron scattering from the deuterated large ribosomal subunit ($M = 1.4 \times 10^6$) of E.coli ribosomes and its derivatives. The molecular weight of the labelled proteins is 2.3×10^4 . The solvent is the same as described in Fig. 2.

- the deuterated large subunit
- × the deuterated subunit + protonated protein L3
- ⊕ the deuterated subunit + protonated protein L4
- the deuterated subunit + protonated proteins L3 and L4

These scattering curves are of the type $I_{\vec{q}\vec{q}}$, i.e. they are cross terms. As the contrast is low, it is not surprising that one of the scattering curves changes its sign at low Q (dotted circles denote opposite sign of $I_{\vec{q}\vec{q}}$). Only proton spins were polarized, i.e. the deuteron spins had been selectively depolarized.







4. SMALL-ANGLE NEUTRON AND X-RAY SCATTERING OF INSECT LIPOPHORINS

Katagiri, C.*, Ito, Y.† and Sato, M.§

*Biochemistry Laboratory, Institute of Low Temperature Science, Hokkaido University, Sapporo, †Institute for Solid State Physics, The University of Tokyo, Tokyo and §Institute for Protein Research, Osaka University, Suita, Japan.

Lipophorin is a circulating lipoprotein in insects and serves as a reusable shuttle to transport various lipids such as diacylglycerol and hydrocarbons between tissues (1). Lipophorin has been identified in all insect species that have been examined to date and is present in all life stages. Lipophorin isolated from the hemolymph (blood) of larvae, pupae and resting adults ($M_r = 6 \times 10^6$) comprises 50-60% protein and 40-50% lipids. The protein moiety is composed of two nonexchangeable, integral apoproteins, apolipophorin I (apoLp-I, $M_r = 2.5 \times 10^5$) and apolipophorin II (apoLp-II, $M_r = 8.5 \times 10^4$).

The structure of lipophorin was investigated by a small-angle X-ray scattering method over the temperature range 0-45°C. The small-angle X-ray scattering profile of lipophorin exhibited a symmetrical sphere with heterogeneous internal electron density. Cockroach and locust lipophorins, which contain hydrocarbons, demonstrated radially symmetrical distribution of electron density inside the particles. Previous studies using differential scanning calorimetry suggested that the hydrocarbon-rich region is located in the core of lipophorin particle (2). Distance distribution functions, $P(r)$, calculated for a simulated three-layer model (electron-rich shell, middle layer, and electron-deficient core) with radial electron density distribution, show good agreement with those observed experimentally for cockroach and locust lipophorins. The dimensions and electron density obtained for the middle layer revealed that this layer is occupied mainly by diacylglycerol and apoLp-II. Since phospholipid and apoLp-I were reported to be located in the outer shell (3,4), we proposed a spherical lipophorin model composed of three radially symmetrical layers; 24 Å thick surface layer with phospholipid and apoLp-I, a 23 Å thick middle layer with diacylglycerol and apoLp-II and an inner core of 37 Å radius with hydrocarbons (5). The three-layer model was also supported by hydrocarbon-rich diacylglycerol-poor lipophorin, although the dimensions of the model for this lipophorin differs from those of the previous model in the small size of the middle layer which correlates well with the low diacylglycerol content of this lipophorin (6).

Further detailed information on the internal structure of the lipophorin was obtained from the small-angle X-ray

scattering experiments with the contrast variation method. Cockroach lipophorin was investigated by raising the electron density of the solvent by addition of sucrose. The linear dependence of the square root of the zero intensity on the scattering density of the solvent yields the average scattering density ($0.355e/\text{\AA}^3$) of the particles at zero contrast. The dependence of the squared radius of gyration on the inverse of the contrast yields the radius of gyration (49.1\AA) of the particles at infinite contrast and the parameters a (38.4) and b (0.3). The sign of a is an indicator for the internal distribution of scattering density; a positive value for a , as found for cockroach lipophorin, signals that a less dense core is surrounded by a dense shell. A positive and small value for b indicates that the centers of the different electron density regions within the particles coincide. Simulated three-layer model was obtained according to the above mentioned methods using $P(r)$. Thus, the three-layer model was supported again.

A small-angle neutron scattering contrast variation on this lipophorin was also performed. The scattering profile at zero contrast demonstrated the second maximum smaller than that obtained by X-ray scattering (Fig. 1 a and b). The radius of gyration of the particles at infinite contrast was the same as obtained by X-ray scattering (Fig. 2). Since D_2O increases the contrast in the different way from that which sucrose does, the neutron scattering study will give us the more detailed information upon the internal structure of the lipophorin particle. Further analyses are now in progress.

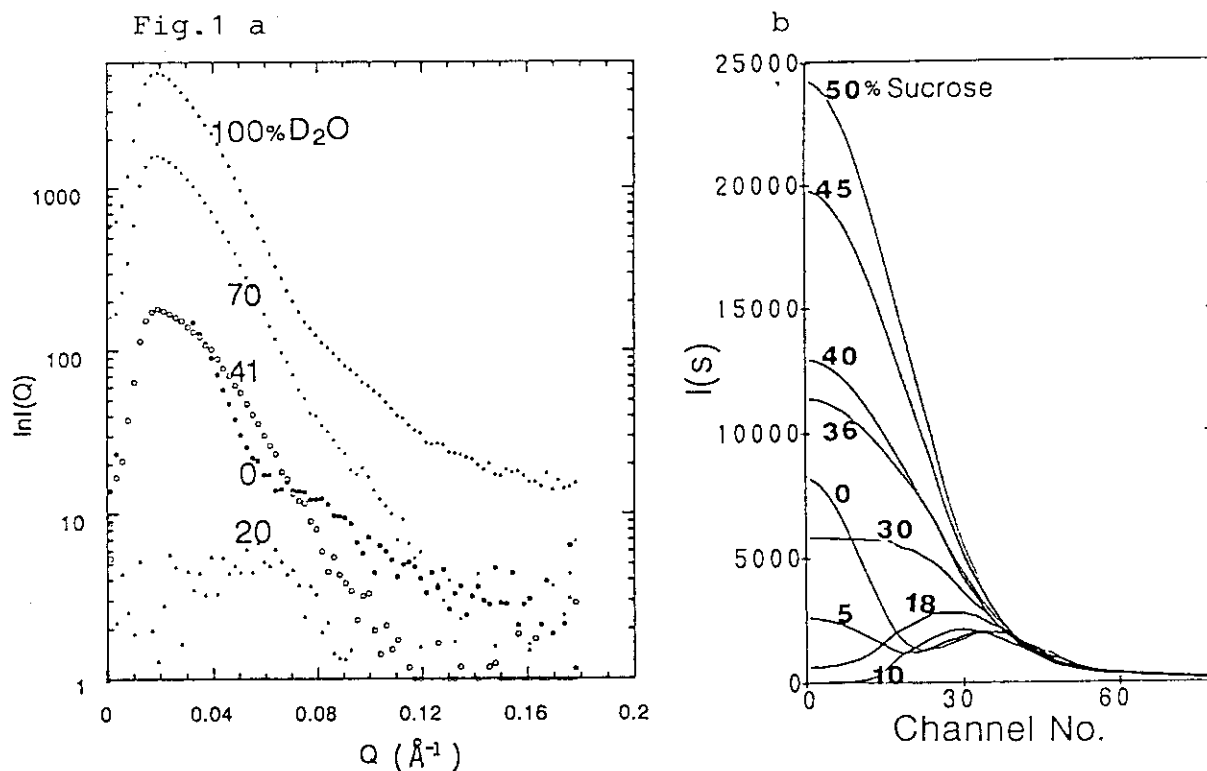
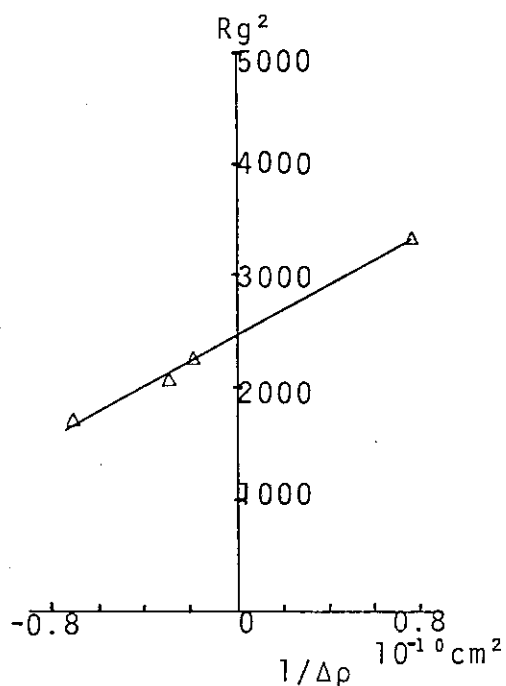


Fig.2



REFERENCES

1. Chino, H. (1985) in Comp. Insect Physiol. Biochem. Pharmacol. (Kerkut, G.A. and Gilbert, L.I. eds) vol.10, pp.115-135, Pergamon Press, Oxford
2. Katagiri, C., Kimura, J. and Murase, N. (1985) J. Biol. Chem. 260, 13490-13495
3. Katagiri, C. (1985) Biochim. Biophys. Acta 834, 139-143
4. Kashiwazaki, Y. and Ikai, A. (1985) Arch. Biochem. Biophys. 237, 160-169
5. Katagiri, C., Sato, M. and Tanaka, N. (1987) J. Biol. Chem. 262, 15857-15861
6. Katagiri, C., Sato, M., de Kort, C. A. D. and Katsube, Y. (1991) Biochemistry 30, 9675-9681

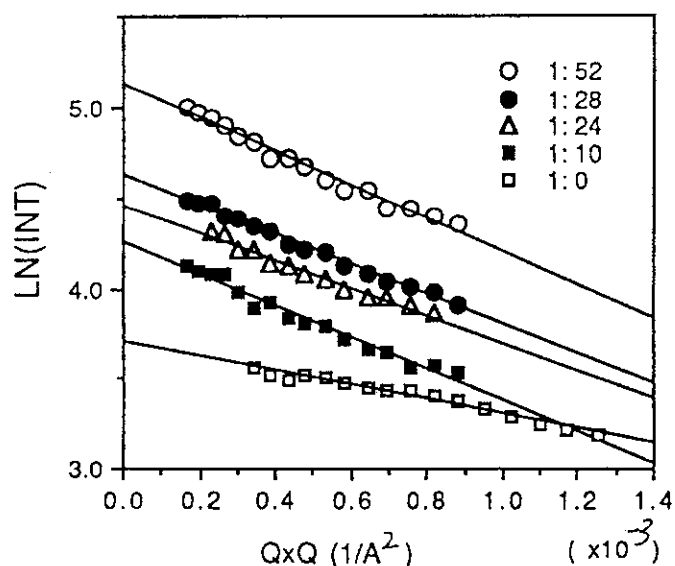
5. THE STRUCTURE OF GELSOLIN-PIP2 COMPLEX AS STUDIED BY SMALL ANGLE NEUTRON SCATTERING

I. ITO*, J. FUKUSHIMA*, Y. MINEZAKI**, I. TANAKA**, N. NIIMURA** and K. HAYASHI*** *Faculty of Science, Kyoto Univ., Kyoto 606, **Laboratory of Nuclear Science, Tohoku Univ. Sendai 982 and ***Department of Physiology, Ibaraki Univ., Mito 310, Japan

The mechanical structure of F-actin and actin polymerization are regulated by so-called actin binding proteins which specifically interact with actin. Recently it is demonstrated *in vitro* that some of actin binding proteins such as gelsolin and profilin interact with phosphatidylinositol diphosphate (PIP2) which is one of intermediate products of phosphatidylinositol (PI)-transmembrane signal transduction system. These results suggest the interaction of these proteins with PIP2 may play an essential role in the transmembrane signal transduction system.

Here we studied the interaction of gelsolin with PIP2 by small angle neutron scattering method. The scattering measurements were made using SANS-U in Japan Atomic Energy Research Institute. Figure 1 shows Guinier plots of the scattering of gelsolin solutions (22 μ M) in the presence of various molar ratios of PIP2 to gelsolin (0, 10, 24, 28, 52, respectively). The scattering intensity increases with an increase in the molar ratio of PIP2, and a linear region was observed in respective Guinier plots. These results show gelsolin and PIP2 form an complex, and the stoichiometry of PIP2 to gelsolin depends on the molar ratio of PIP2. Using contrast variation technique, we are doing more detail analysis of the binding mode of PIP2 in the complex.

Figure 1: Guinier plots



6. SMALL-ANGLE NEUTRON SCATTERING STUDIES OF PROTEOGLYCAN FROM SHARK FIN CARTILAGE

Yoh SANO¹, Nobuo NIIMURA², Ichiro TANAKA²

1. National Food Research Institute, Tsukuba City, Ibaraki 305, Japan
2. Laboratory of Nuclear Science, Tohoku University, Sendai 982, Japan

Introduction

Chondroitin sulfate, one of natural acid mucopolysaccharides, composes the primary part of the cartilage, together with collagen-like protein, and is present as proteoglycan in connective tissues and in various biological membranes, giving the charge and the anisotropic structure of biological membranes, and controlling the transport of the drugs through the membrane¹⁻². The maintenance of the integrity connective tissue is, in part, dependent on the macromolecular properties of its constituent proteoglycan. Shark fin cartilage proteoglycan complexes consist of a protein core with covalently bound mucopolysaccharide chains of chondroitin sulfate and keratan sulfate. These mucopolysaccharides are important pharmacologically as a blood anticoagulant and also a rejuvenator. The anticoagulant activity increases with increasing molecular weight and is related to structural features, e.g., molecular shape and size.

For the first step, the gross structural properties of mucopolysaccharides and their neutron scattering length density, the size and shape of the isolated proteoglycan complexes in native state were determined by the small-angle neutron scattering (SANS) method in aqueous solution of different D₂O/H₂O ratio, i.e., 100%, 70%, 20% and 0%, where a unit of the ratio is mol%.

Materials and Method

The native complexes of proteoglycans were isolated from shark fin cartilage by means of cold ethanol fractionation method and gel filtration method. The molecular weight of the present sample determined by the Zimm plot with laser light scattering method was 3.7×10^6 .

Sample concentration was mainly 10.4 mg/ml and pH of the solution is kept at 7.2 with using 10 mM phosphate buffer (ionic strength is 0.02). Neutron scattering experiments were performed with SANS-U (JRR-3M) of the Japan Atomic Energy Research Institute(JAERI).

Results and Discussion

The scattering function $I(Q)$ obtained in different D_2O/H_2O ratio are shown in Fig. 1. At this concentration of the proteoglycan complexes (10.4mg/ml) the scatter of the data was relatively small and $I(Q)$ monotonously increased at the smallest Q -range.

The example of Guinier plot derived from the above $I(Q)$ is shown in Fig. 2. The Guinier plots in each cases also showed a good straight line. The radius of gyration, R_g , and the intensity extrapolated to $Q=0$, $I(0)$, were obtained from this straight line using the least square fitting method.

A contrast matching point of the complexes was estimated to be 53% using square root of $I(0)$ extrapolated intercept of the ordinate of Guinier plot, vs D_2O/H_2O ratio as shown in Fig. 3. The mean excess scattering density $\bar{\rho}$ was determined as $3.4 \times 10^{-10} \text{ cm}^{-2}$. The matching point calculated from the crystal data by assuming full H-D exchange is 55.3% for ionized chondroitin sulfate and 46.3% for ionized keratan sulfate. The 53% obtained in the present paper is, therefore, very much reasonable from the dissociation constant of carboxyl and sulfate groups.

R_g^2 is correlated with $\bar{\rho}$ as (so-called Stuhrmann plot)

$$R_g^2 = R_{gc}^2 + \alpha(1/\bar{\rho}) - \beta(1/\bar{\rho})^2$$

where R_{gc} , α and β are the radius of gyration of the particle at infinite contrast ($\bar{\rho}=0$), a radial second moment of the scattering density distribution and a displacement of the center of the scattering density distribution with respect to the center of the geometrical shape, respectively. The dependence of R_g on the solvent contrast, as shown in Fig. 4, showed that a radial second moment of the scattering density distribution was positive, indicating that the mucopolysaccharide such as chondroitin sulfate is on the surface of the molecule with a higher scattering density than that of the core protein.

The proteoglycan complex in the native state can be approximated as a model of two uniform concentric ellipsoidal shells as mentioned above. The scattering function calculated by a spherical shell model gives periodically harmonic patterns indicating unsuitable model in the present case. The comparison between the data (open circles in Fig.1) and the theoretical scattering curves shown in Fig.1 indicates that the proteoglycan complex in SANS method is approximated as the two uniform concentric ellipsoidal shell model having the axial ratio of about 3.

References

1. Sano, Y(1986) Bull. Natl. Inst. Agrobiol. Resour., 2:1-12.
2. Sano, Y(1985) Bull. Natl. Inst. Agrobiol. Resour., 1:53-62.

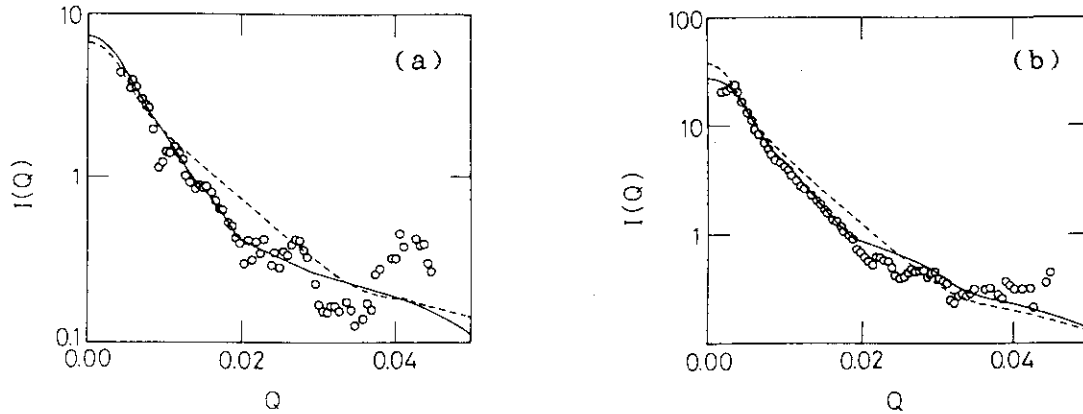


Fig. 1. Scattering functions of proteoglycan complexes (10.4mg/ml) in aqueous solution at 70%(a) and 0%(b) D_2O/H_2O ratio. The real and dotted lines show the theoretical scattering curves calculated as a model of the two uniform concentric ellipsoidal shells having the axial ratio of 3(real line) and 6(dotted line), respectively.

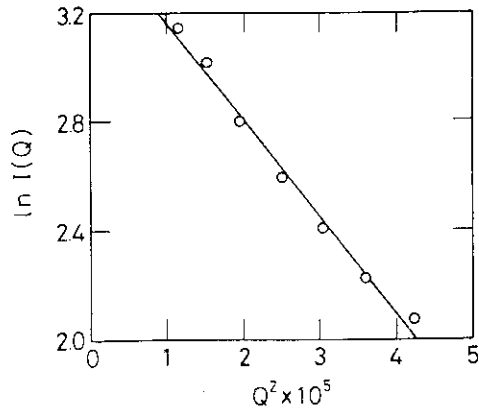


Fig. 2. Guinier plot of proteoglycan complexes (10.4mg/ml) in aqueous solution at 0% D_2O/H_2O ratio.

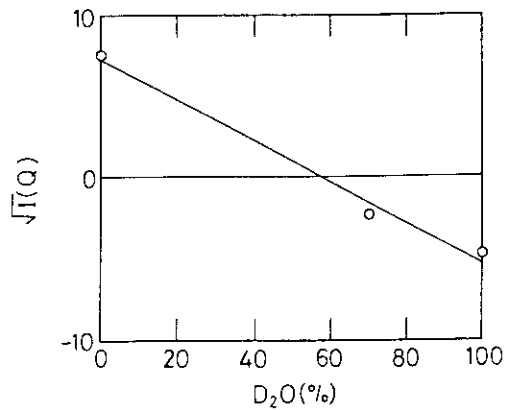


Fig. 3. Square root of $I(0)$ vs D_2O/H_2O ratio of proteoglycan complexes.

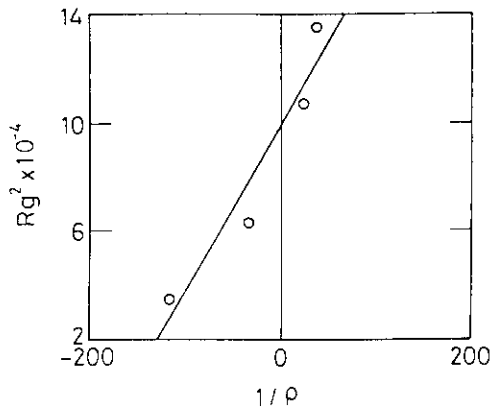


Fig. 4. Stuhrmann plot of proteoglycan complexes.

7. SMALL-ANGLE NEUTRON SCATTERING STUDY OF RECOMBINANT YEAST-DERIVED HUMAN HEPATITIS B VIRUS SURFACE ANTIGEN VACCINE PARTICLES

Y.Ito¹, M.Sato², K.Kameyama³, N.Ishikawa³ and T.Takagi²

¹Institute for Solid State Physics, the University of Tokyo, Tokyo 106 Japan

²Institute for Protein Research, Osaka University, Osaka 565 Japan

³Kanonji Institute, Research Foundation for Microbial Diseases, Osaka University, Kanonji, Kagawa, 768 Japan

SUMMARY

Synthetic human hepatitis B virus surface antigen vaccine particles were investigated by means of small-angle neutron scattering. Contrast matching point of the particle was determined at 24% D₂O content indicating most or all of the non-protein components of the particle to be either lipids or hydrocarbons from yeast. Almost uniform mixture of the antigenic proteins and lipids and hydrocarbons was inferred from the Sthurmann plot. However the protein distribution is different from that of lipids and hydrocarbons as indicated by the intensity profile difference at 40% D₂O content solution from that of other D₂O content solutions. Radius of gyration of the vaccine particle was determined as 10.5 nm, whereas the maximum particle size was 34 nm from the Patterson function calculated from intensity vs Q curves for 0 and 15% D₂O content solutions.

INTRODUCTION

Recombinant DNA human hepatitis B virus vaccine particles were obtained using yeast cells by the similar method reported by Miyanohara et al¹⁾. They contain a surface protein of 235 amino acid residues, 226 of which are encoded by the human hepatitis B virus S gene and the first 9 residues correspond to the preceding S2 gene²⁾. In addition, lipids and hydrocarbons derived from the host yeast cells are included also. The previous characterization of the vaccine particles performed by the high-performance size-exclusion chromatography and by low-angle laser light scattering revealed that the size of the vaccine particles was rather homogeneous with radius of about 36 nm, and the molar mass of the particle was 5.0×10^6 gr/mol^{2,3)}. This paper reports the first small-angle neutron scattering investigation of the human hepatitis B virus surface antigen (HBsAg) vaccine particles to reveal the vaccine internal structure using the contrast variation.

EXPERIMENTAL

The newly built small-angle neutron scattering instrument (SANS-U) at the C1-2 beam port of the JRR-3M reactor of JAERI at Tokai was used for the investigation. Neutrons with wavelength λ of 7.0 Å was used with a sample-to-detector distance of 4000 mm to cover the Q ($=4\pi\sin\theta/\lambda$) range between 0.005 and 0.01 Å⁻¹.

Because of the limited sample quantities, sample solutions containing four kinds of D₂O contents 0, 15, 40 and 100%, each HBsAg concentration (c) of about 8 mg/ml were prepared and placed in quartz cells of 1 to 3 mm pathlength, depending on the D₂O proportion. The solvent was a 5mM sodium phosphate buffer (pH 7.6) containing 0.02% gelatin. The sample cells were placed in an automatic sample changer and kept cooled at about 7°C in He gas during measurements.

Scattered neutrons were collected by a helium-filled 2-dimensional position-sensitive detector. The data were corrected for the buffer solvent background and then circularly averaged to obtain a 1-dimensional intensity profile as a function of Q .

RESULTS

Fig.1 shows the results of the measurements from 4 different D₂O content sample solutions. The intensity profile of the 40% D₂O solution, where the protein components are matched out revealing only the remaining lipids and hydrocarbon distribution in the particle appears clearly different from that of other D₂O content solutions.

A representative of the Guinier plot is shown in Fig.2 for 0% D₂O content sample solution. The square-root of the normalized forward scattering intensity $\sqrt{I(0)/c}$ when plotted as a function of the D₂O content gives nearly a straight line with the zero-crossing matching point at 24% D₂O as shown in Fig.3⁴⁾. The match point value indicates that most or all of the non-protein components of the particle are composed of either lipids or hydrocarbons from yeast in agreement with the previous results.

In Fig.4 squares of the radius of gyration (R_g) were plotted

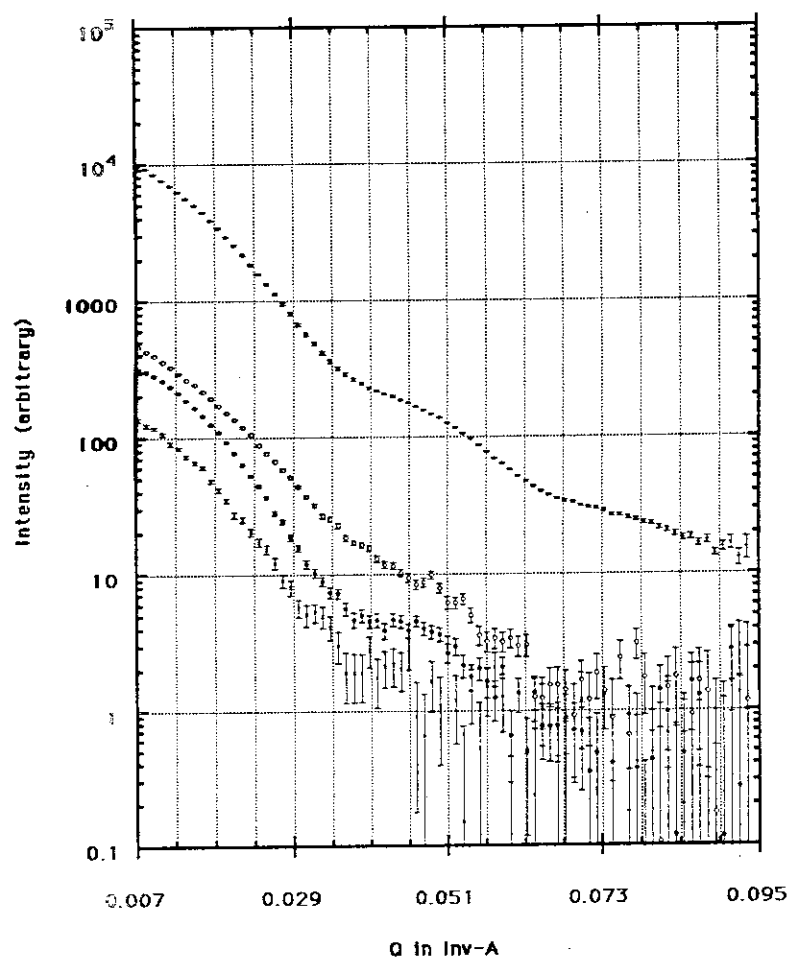


Fig.1

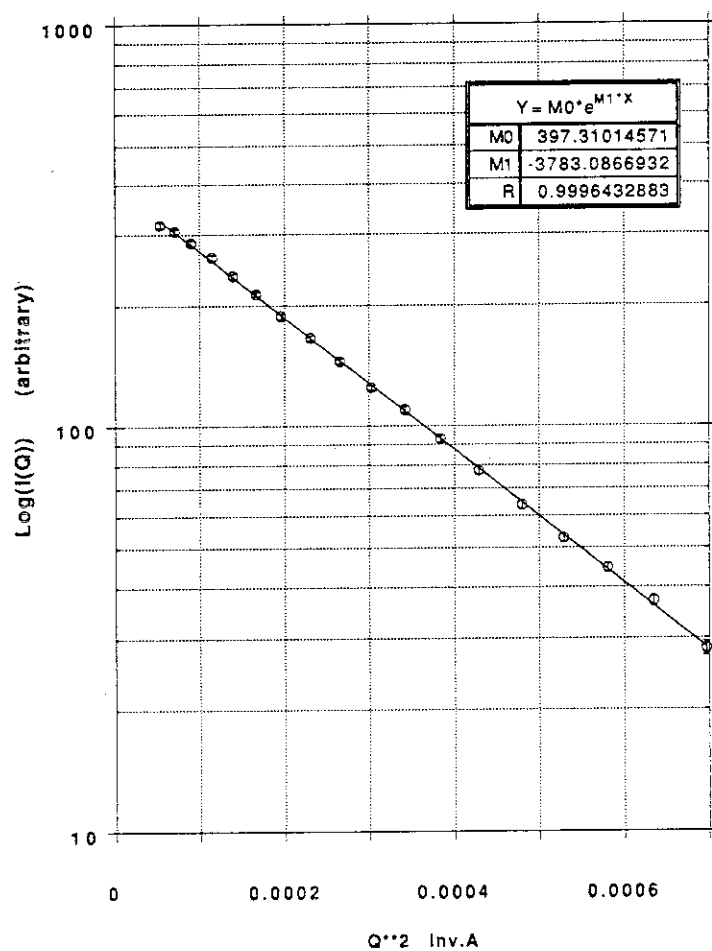


Fig.2

Guinier Plot of D0HBsAg

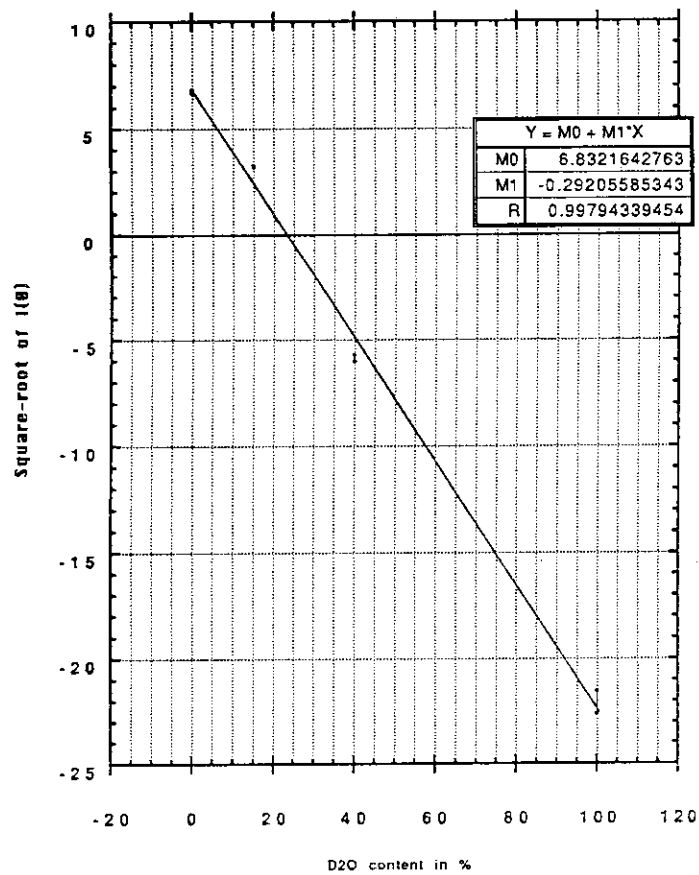


Fig.3

Contrast Variation

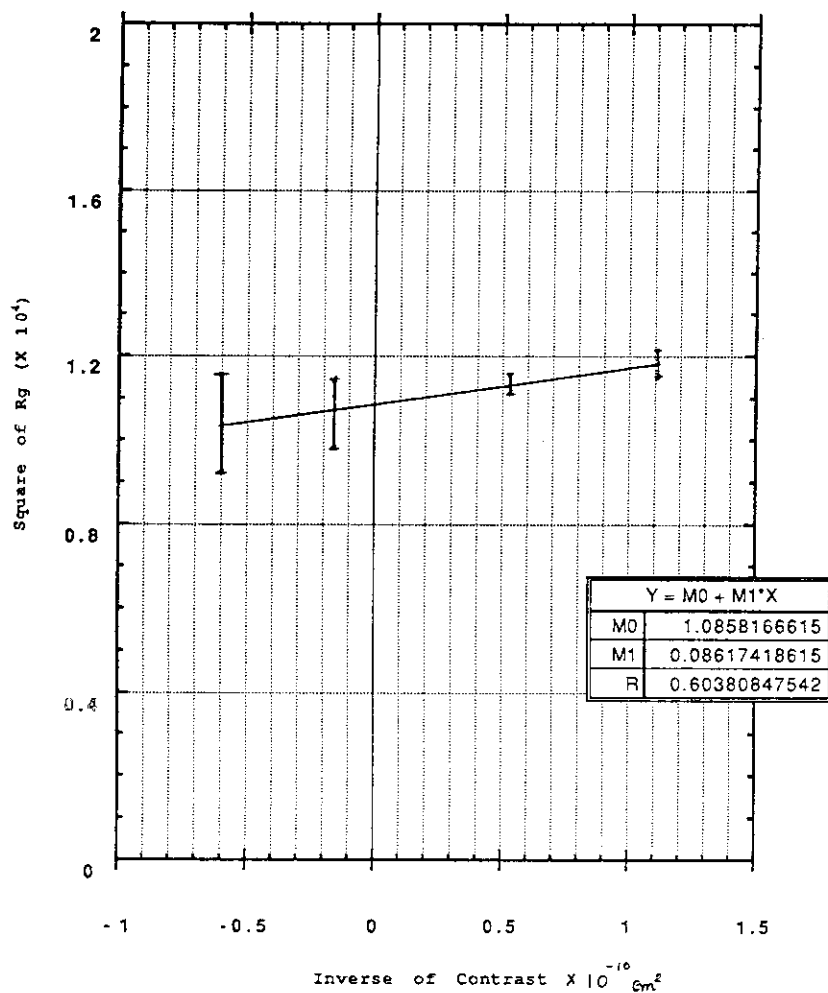


Fig.4

against the inverse of the contrast (Sthurmann plot). A slight positive slope indicates almost uniform mixture of the antigenic proteins and lipids and hydrocarbons inside the vaccine particle. R_g at an infinite contrast becomes 10.5 nm. However, Patterson function $P(r)$ calculated from intensities at 0 and 15% D_2O contents give the particle size of about 34 nm (Fig.5), which is consistent with the 36 nm diameter observed under electron microscope for these particles.

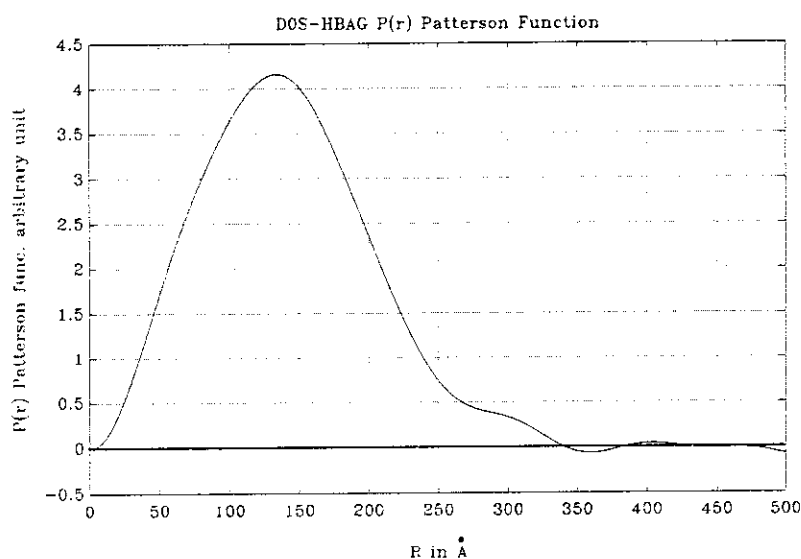


Fig.5
 $P(r)$ function

DISCUSSION

Little aggregation effect of vaccine particles was detected since no deviation from the Guinier rule was found up to the smallest observable Q of 0.007 \AA^{-1} . The 0.02% gelatin contained in the buffer seemed effective in preventing aggregation as expected.

When a sphere of uniform density has the R_g of 10.5 nm, its diameter is calculated as 27.1 nm. The maximum particle size deduced from the $P(r)$ function is 34 nm. This fact and the almost contrast-independent R_g 's of the Sthurmann plot negate such a model in which a hole or cavity is present at the vaccine particle core.

The antigenic surface protein components of HB virus are distributed differently from lipids and hydrocarbons originated from yeast cells. This was inferred from the intensity profile difference of the sample containing 40% D_2O solution and that of other D_2O content solutions. The former reflects the scattering pattern from lipids and hydrocarbons in the particle, the latter

represents scattering from both proteins and lipids and hydrocarbons in various combinations.

Further analysis of data is now under way to separate the protein distribution from that of lipids and hydrocarbons.

REFERENCES

- 1) A.Miyanohara, A.Tohe, C.Nozaki, F.Hamada, N.Ohtomo and K.Matsubara, Proc. Natl. Acad. Sci. U.S.A., **80** (1983) 1-5.
- 2) Y.Sato, Thesis(M.S., Osaka Univ.) 1990, in Japanese.
- 3) Y.Sato, N.Ishikawa and T.Takagi, J. of Chromatography **507** (1990) 25-31.
- 4) B.Jacrot, Rep. Prog. Phys. **39** (1976) 911-953.

8. INELASTIC NEUTRON SCATTERING FROM DNA AND WATER

Agui, A., Tominaga, Y. and Ikeda, S.^A
 Dept. of Phys. Ochanomizu Univ., KEK^A

Recently it has been interested in to study the dynamics of DNA double helix with hydrated water. The temperature dependence of DNA gel has been investigated by inelastic and elastic neutron scattering experiments. We performed incoherent inelastic neutron scattering experiments on DNA gel by using the crystal analyzer time-of-flight spectrometer, abbreviated as CAT, which has been installed at the spallation pulsed neutron source at KENS, in Tokai. The configuration of CAT is shown in Figure 1. In CAT spectrometer the incident neutron is scattered by the sample and the energy of the scattered neutron is fixed to 3.9 meV by a pyrolytic graphite crystal analyzer in the time-focused configuration and a cooled Beryllium filter is used to eliminate the higher order reflection of the analyzer. This spectrometer is especially effective in observing the incoherent scattering. The energy resolution of CAT is 0.3 meV around the elastic peak.

The specimen was 20 weight percent gel of DNA from calf thymus. The specimen was packed with Helium exchange gas into a sample cell and cooled by a closed cycle refrigerator. Measurements were carried out from -100 °C to 60 °C. The temperature dependence of inelastic neutron scattering spectrum is shown in Figure 2. In low temperature we can observe some peaks, but in high temperature, we cannot distinguish them because of the strong quasielastic component. We can assign 2 large peaks at 6.2 meV and at 70 meV at -100 °C. The peak at 6.2 meV shifts to the high energy side with decreasing temperature. And the peak at 70 meV shifts to the low energy side with decreasing temperature.

Figure 3 shows the temperature dependence of Raman spectra of DNA gel. We cannot see the 6.2 meV peak in these Raman spectra. On the contrary, the strong peak appears around 2 meV. Raman spectra give the fluctuation of electronic polarizability modulated by atomic motion, but neutron spectra mainly give the fluctuation of atomic motion itself. Since the neutron cross section of hydrogen atom is large, the 6.2 meV peak is related to the hydrogen motion around DNA double helix and/or the vibration of hydrogen-bonds between bases. But further data should be needed for the determination of details.

We have also measured the temperature dependence of elastic scattering. The temperature dependence of integrated intensity of the elastic component is shown in Figure 4. The value of integrated intensity decrease with increasing temperature. The rate of intensity change in high temperature is greater than that of low temperature. The break point of the curve is around -20 °C. We consider that the temperature dependence of the integrated intensity of the elastic component corresponds to the freezing process of water of hydration around DNA.

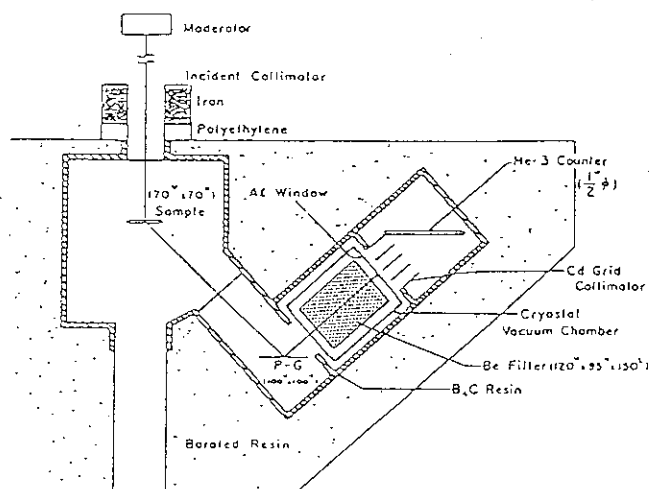


Figure 1
Configuration of CAT
(crystal analyzer TOF spectrometer)

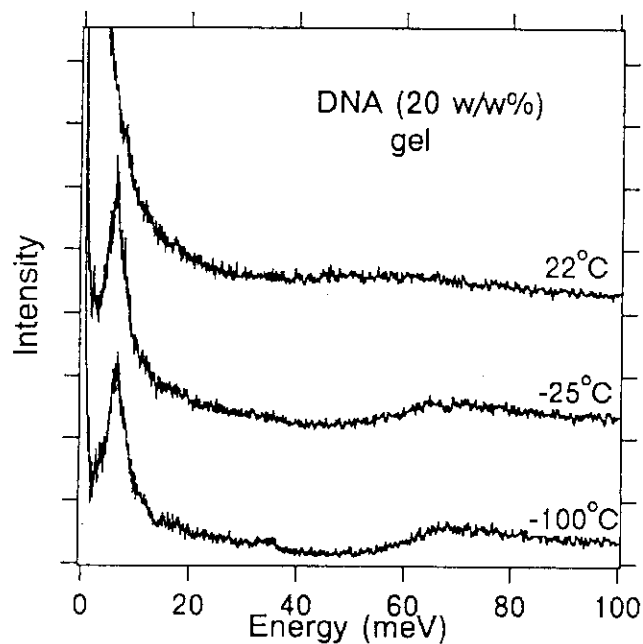


Figure 2
The temperature dependence
of inelastic neutron scattering
spectrum.

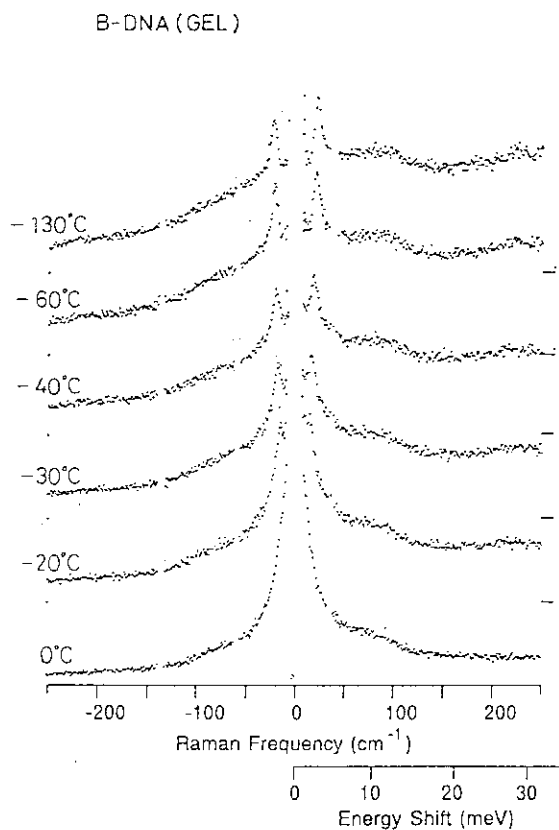


Figure 3
The temperature dependence
of Raman spectra.

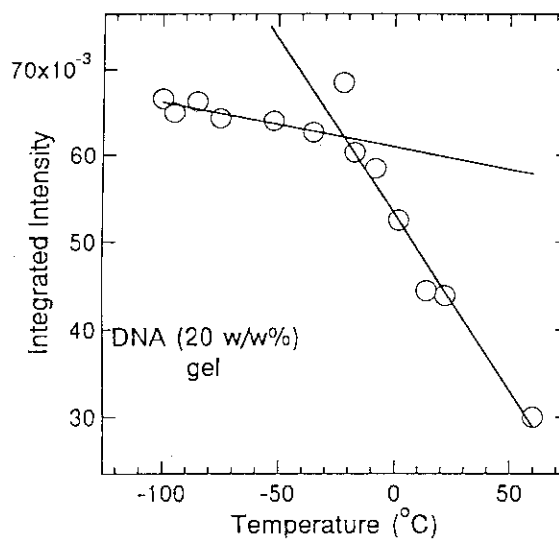


Figure 4
The temperature dependence
of integrated intensity of elastic
component.

9. NEUTRON SCATTERING IN SMALL BIOLOGICAL MOLECULES AND
HYDROGEN BONDING STUDIES AT TROMBAY AND FUTURE PLANS

K.K.Kannan, M.Ramanadham, K.R.Rao and P.S.Goyal

Solid State Physics Division, Bhabha Atomic Research Centre
Trombay, Bombay 400085, India

Introduction

An understanding of the structure of biological molecules is an essential pre-requisite for an understanding of the function of such molecules. A large number of amino acids, peptides, proteins, nucleic acids, nucleoprotein complexes like viruses, ribosomes and membranes have been under intense study by a variety of methods. Neutron diffraction and neutron small angle scattering have contributed significantly to our understanding of biological macromolecules. Due to the scattering by the nuclei neutron scattering has almost uniform scattering properties from all elements and thereby been useful in the determination of structures containing varying atomic distributions including hydrogens/deuterium and has therefore been very useful in locating hydrogen atoms and subsequently in hydrogen bond analysis.

In the Bhabha Atomic Research Centre, Trombay, Bombay, India the CIRUS reactor at 40 MW thermal power and the very recently built Dhruva reactor at 100 MW thermal power have been utilised to study amino acids, peptides, and nucleic acids by single crystal neutron diffraction. Micelles and surfactants have also been studied by small angle neutron scattering techniques at the

Cirus reactor. We review below some of the research activities at the Bhabha Atomic Research Centre.

Neutron Beam Instrumentation at Trombay

The most modern facilities for neutron research set up at Trombay are to be found in the Dhruva reactor which is a high flux reactor. Table 1 gives details of the reactor, the instruments assembled and in use around the reactor.

Dhruva is a heavy water moderated heavy water cooled natural uranium 100 MW reactor with a neutron flux of about 2×10^{14} neutron $\text{cm}^{-2} \text{S}^{-1}$. Fig.1 gives the layout of the neutron beams for experimentation. Rao (1989), Vijayaraghavan (1989) and Madhava Rao et al. (1989) have detailed the neutron instrumentation available for research at Dhruva. Dhruva has been built with a view to provide both cold and hot neutrons with facility for physics, chemistry and biology research. Monochromatic neutron beams are provided through a variety of monochromators like pyrolytic graphite, copper crystal etc., mounted in a shielding drum (Fig.2) constructed to give close approach to the reactor pile and also to remove all unwanted reactor radiation so that the experimental sample on the instrument is irradiated by monochromatic neutrons only. This brings down unnecessary background and enhances the detection efficiency. The drum assembly consists of lead shielding for gamma rays, steel, boron carbide and borated paraffin wax for slow and fast neutrons. The monochromator drum has rotatable middle drum, a stationary top shield, and a top plug in which the monochromator crystal is suspended. The monochromator crystal can be rotated by a motor and gear system to orient the crystal as required. The middle drum can also be rotated suitably.

Several instruments have been fabricated at Trombay and used with CIRUS and Dhruva reactor facilities (Fig. 2) such as neutron crystallography, magnetic diffraction, inelastic scattering, quasi-elastic scattering and small angle scattering (Table 1). The four circle neutron diffractometer has been the main workhorse for single crystal neutron diffraction analysis of peptides, amino acids and nucleic acids. The monochromator with an angular range of 10 degrees to 60 degrees is mounted on one of the axis of a two axis diffractometer. The four circle Eulerian geometry goniometer is mounted on the other axis. A microprocessor based computer is used for the control of the movement of the four circles with high precision and for data collection.

Small angle scattering has been the choice of experimentation for large assemblies of macromolecules for elucidating their size, shape and geometries. The Mark I version of SANS has been operational at CIRUS and another one is being constructed at Dhruva which will use a 1 m diameter two dimensional position sensitive detector placed at the end of a cold neutron guide tube looking into an incore cold source for shifting the neutrons to higher wavelengths.

Biomolecular Crystallography and Hydrogen Bonding

The principal motivation has been, and still is the study of hydrogen-bond interaction in crystal structures. Diffractometers ranging from a 2-D double crystal diffractometer to the present computer-controlled 3D-diffractometer, have been indigenously designed, fabricated and installed at CIRUS and Dhruva reactors at BARC. The entire range of crystallographic software from

on-line data acquisition to the analysis of results have been developed.

Earlier studies on the crystal structures of inorganic hydrates have resulted in a comprehensive analysis (Chidambaram et al. 1964) of the H-bonding properties including the lone-pair coordination of water molecule. The semi-empirical Lippincott-Schroeder potential function was modified to handle the bent O-H....O H-bonds (Chidambaram and Sikka, 1968), and later extended to N-H....O H bonds (Chidambaram et al. 1970). The applicability of direct methods to solve crystal structures from neutron data was also successfully demonstrated by Sikka (1969, 1970) and used for solving structures from Neutron diffraction data at BARC, Brookhaven National Laboratory (BNL) and elsewhere (See, for example Bernal and Watkins, 1972, Verbist et al, 1972, Frey et al, 1973 and Ramanadham et al, 1973b).

The project on the high-precision neutron studies of amino acids and small peptides was initiated during the late sixties. The aim was two-fold, viz., to obtain precise and reliable information about the stereochemistry of hydrogen atoms, and to analyse H-bonding interactions in these important biomolecules. (Fig.3). Molecular structures of L-glutamic acid HCl (Sequeira et al., 1972), L-asparagine H_2O (Ramanadham et al., 1972), L-lysine HCl $2H_2O$ (Bugayong et al. 1972), L-cysteic acid H_2O (Ramanadham et al., 1973a), L-threonine (Ramanadham et al., 1973b), L-cystine $2HCl$ (Gupta et al. 1974), glycyl-L-threonine $2H_2O$ (Sequeira et al. 1981) and DL-aspartic acid (Sequeira et al. 1989) have been successfully carried out. Most of the other amino acids and three out of the eight structures listed above have been studied at Brookhaven National Laboratory, USA (For a very recent list of references, see Chidambaram and Ramanadham, 1991).

The availability of high-precision structural data on most of the amino-acid and small peptide structures has resulted in a number of analyses on the systematics of H-bonding and other aspects pertaining to these structures (see, for example, Ramanadham, 1975, Koetzle and Lehmann, 1976, and Ramanadham and Chidambaram, 1978). Some of the most important results of the work, carried out at BARC (Ramanadham and Chidambaram, 1978) are briefly summarised here.

Average representative values were computed for various bond distances, angles, etc. For example, representative values involving the main-chain atoms, with neutral as well as ionized alpha-carboxyl groups, are shown in Fig.4. Other geometric parameters, involving hydrogen atoms were statistically analyzed to obtain mean and variance for each parameter. The experimental distribution and the best fitting Gaussian for C-C-H angles are shown in Fig.5. Standard parameters, thus generated, are of great use in generating H-atom positions in the X-ray protein structures.

The 1978 analysis also included other neutron studies containing H-bond donor and acceptor groups, similar to those found in amino acids. The geometric parameters of various H-bond types, such as $N^+-H \cdots O$, $N-H \cdots O$, $O-H \cdots O$, as well as those with Cl^- as acceptor have been analyzed. The distributions of donor-hydrogen, hydrogen-acceptor and donor-acceptor distances and the bending angles at the donor atom for 74 $N^+-H \cdots O$ and 30 $N-H \cdots O$ H-bonds are presented in Fig.6. The distribution of $N^+-H \cdots O$ and $N-H \cdots O$ H-bonds in R- Θ plane along with the equipotential curves, is shown in Fig.7. Data, presented in these two figures clearly indicate that small but significant differences exist between $N^+-H \cdots O$ and $N-H \cdots O$ bonds.

The earlier analysis was mainly aimed at obtaining systematics for each class of H-bonds, grouped in terms of donor and acceptor atoms. The emphasis was, thus on obtaining trends of behavior of various parameters, instead of looking for deviations from the observed behaviour. During this analysis (Ramanadham and Chidambaram, 1978), it was noticed that the influence of the donor and/or acceptor groups on the geometry of H-bonding, and, even the occurrence of a H-bond, was quite important. For example the H-bonding behaviour of a neutral carboxyl group is very different from that of an ionized one. Looking at only four -COOH groups and, with the help of bond length - bond valence correlations (Brown and Shannon, 1973), a plausible interpretation of these differences was given.

A recent analysis of H-bonding in biomolecules (Chidambaram and Ramanadham, 1991) has its main emphasis on analyzing the H-bonding capabilities of various oxygen-containing acceptor groups on the basis of the actual H-bonding populations and the bond length - bond valence correlations. As a result, significant numeric information for -COOH, -COO, -OH, H₂O, etc. has been obtained. Results obtained in this analysis for carboxyl groups have been used in identifying the neutral carboxyl groups in the highly refined X-ray structure of triclinic lysozyme (Ramanadham et al. 1990). The preliminary results are quite encouraging. The analysis is currently being extended to all neutron structures, obtainable from the Cambridge Crystallographic Database.

Small-Angle Neutron Scattering (SANS)

Many interesting and useful studies can be carried out on biological samples using small-angle neutron scattering. On the

face of it, the much smaller luminosity of a neutron source compared to an x-ray source, seems to weigh very much against the use of SANS. However, there are many advantages of using neutrons, some of which go a long way in compensating for the smaller luminosity (see, for example, Schmatz et al., 1974). The availability of high-flux reactors, with built-in cold neutron sources can provide a reasonably good neutron flux at higher wavelengths. Increase in the intensity of the beam can be achieved by using a large source area, and optimising the wavelength resolution. The need to use a large sample to go with the large source area is not a problem because of the low attenuation cross-section for neutrons.

An attractive feature of solution studies of biological samples using SANS is the so-called contrast matching. The average neutron scattering lengths of proteins and nucleic acids are significantly different from each other, and fall within the range of the average scattering lengths for H_2O (-0.06×10^{-12} cm) and D_2O ($+0.63 \times 10^{-12}$ cm). For studies on protein-nucleic acid complexes, such as chromatin (Baldwin et al., 1975), an appropriate mixture of H_2O and D_2O can be worked out which will selectively mask the scattering either from the protein or the nucleic acid component of the supra-molecular aggregate under investigation. During the past fifteen years or more, a number of macromolecular assemblies have been studied by SANS. (See Schoenborn, 1984 for references). Recently, the method of SANS has been used by Ebel et al (1991) in the study of halophilic glyceraldehyde 3-phosphate dehydrogenase.

A few years ago, a simple SANS instrument was built at the CIRUS reactor in Bhabha Atomic Research Centre, with a view to develop the know-how, necessary for building a comprehensive

instrument at the high-flux Dhruva reactor. In this instrument, BeO filtered neutrons are scattered by the sample and angular distribution is measured by step-scanning the detector (Desa et al, 1985). The accessible Q-range of this spectrometer is $0.02-0.8\text{\AA}^{-1}$. As an application, the effect of addition of sodium salicylate on the structure of CTAB micellar solutions has been investigated (Goyal et al, 1989). Typical SANS distributions, obtained in these experiments are shown in Fig. 8. As CTAB micelles aggregate to form elongated structures with the addition of NaSal, the peak in SANS distribution shifts to lower Q values. SANS experiments have also been carried out to study the mechanism of clouding phenomenon in micellar solution of Triton-100 (Srinivasa Rao et al, 1991a, 1991b). It was seen that, as one approaches the cloud point, the scattering at Q_0 diverges. Interaction potential between micelles at different temperatures has also been obtained.

The guide-tube laboratory associated with Dhruva reactor is shown in Fig. 9. The SANS spectrometer, as shown in the Figure will be a part of this laboratory. Once the facility is operational in the near future, studies on biomolecular assemblies, membranes etc., will be taken up.

Future Plans

For more than twenty years, neutron beams at Cirus reactor, BARC have been used very effectively in the studies on small biomolecules. The very modern and sophisticated instruments in the new Dhruva reactor, many of which are currently operational, and some in the near future, will be of great help in expanding the biomolecular research activities in Trombay. Single-crystal

neutron studies on peptides of moderate size, small base-paired oligo-nuclotides, and their complexes can provide useful data on the molecular structure, conformation and interactions for these molecules. Studies on the protein phase problem using anomalous scattering from Cd, Sm atoms, complexed with proteins in a crystal can be of great interest. SANS experiments can be carried out on a variety of biological samples, once the facility becomes operational at Dhruva reactor, Neutron spectroscopic studies (Thaper et al., 1991) to understand the dynamics of biological systems are feasible at present. Macromolecular dynamics, folding and unfolding of biopolymers using H/D exchange technique are some of the studies planned to be carried out in the near future.

Acknowledgements

Many significant contributions, made to the neutron-beam research at BARC by members of the Solid State Physics Division, on which this review is based, are gratefully acknowledged. We are grateful to Dr. R.Chidambaram, Director, BARC and Dr. B.A.Dasannacharya, Director, Solid State and Spectroscopy Group for encouragement, support and active participation in many of the projects reviewed in this article.

References

- Baldwin, J.P., Boseley, P.G., Bradbury, E.M. and Ibel, K. (1975).
Nature 253, 245.
- Bernal, I. and Watkins, S.F. (1972). Science 178, 1282.
- Brown I.D. and Shannon R.D. (1973) Acta Cryst. A29, 266.
- Bugayong, R.R., Sequeira, A and Chidambaram, R. (1972) Acta Cryst. B28, 3214.
- Chidamabram, R., Sequeira, A. and Sikka, S.K. (1964), J. Chem. Phys. 41, 3616.
- Chidambaram, R. and Sikka S.K. (1968), Chem. Phys. Lett. 2, 162.
- Chidambaram. R., Balasubramanian, R. and Ramachandran, G.N. (1970) Biochim. Biophys. Acta, 221, 182
- Chidambaram R. and Ramanadham M (1991) Physica B, 174, 300.
- Desa, J.A.E., Mazumdar, S., Sequeira, A. and Dasannacharya, B.A.
- Ebel, C. Krishnan, G., Altekari, W. and Zaccari, G. (1991). Physica B, 174, 306.
- Frey, M.N., Lehmann, M.S., Koetzle, T.F. and Hamilton, W.C. (1973). Acta Cryst. B29, 876.
- Goyal, P.S., Chakravarty, R., Dasannacharya, B.A., Desa, J.A.E.,

- Kelkar, V.K., Manohar, C., Narasimhan, S.L., Rao, K.R. and Valaulikar, B.S. (1989) *Physica B* 157, 471.
- Gupta, S.,C., Sequeira, and Chidambaram, R. (1974) *Acta Cryst.* B30, 562.
- Koetzle, T.F. and Lehmann, M.S. (1976), in "The hydrogen bond. II. structure and spectroscopy", P.Schuster, G. Zundel and C.Sandorfy (eds.), North-Holland, Amsterdam, p.457.
- Madhava Rao, L., Rao, K.R., Shukla, S.G., Vyas, H.P. and Raja Rao A S (1989). *Indian J. Pure Appl. Phys.* 27, 601.
- Ramanadham, M., Sikka, S.K. and Chidambaram, R (1972), *Acta Cryst.*, B28, 3000
- Ramanadham, M., Sikka, S.K. and Chidambaram, R. (1973a) *Acta Cryst.* B29, 1167
- Ramanadham, M. Sikka, S.K. and Chidambaram, R (1973b), *Pramana*, 1, 247
- Ramanadham, M. (1975) Ph.D. Thesis, Bombay University, India.
- Ramanadham, M. and Chidambaram R., (1978) in "Advances in Crystallography", R.Srinivasan (ed.), Oxford and IBM. New Delhi, p.81.
- Ramanadham, M. Sieker, L.C., and Jenson L.H. (1990), *Acta Cryst.* B46, 63.
- Rao, K.R. (1989). *Indian J. Pure Appl. Phys.* 27, 548

Schmatz, W., Springer, T., Schelten, J and Ibel, K. (1974). J. Appl. Cryst. 7, 96.

Schoenborn, B.P. (ed.) (1984). 'Neutrons in Biology', Plenum, New York.

Sequeira, A. Rajagopal, H. and Chidambaram, R. (1972), Acta Cryst. B28, 2514.

Sequeira, A. Ramanadham M, Rajagopal, H. and Padmanabhan, V.M. (1981) Acta Cryst. B37, 1839.

Sequeira, A., Rajagopal, H. and Ramanadham, M. (1989), C45, 906.

Sikka, S.K. (1969), Acta Cryst. A25, 539.

Sikka, S.K. (1970) Acta Cryst. A26, 662.

Srinivasa Rao, K., Goyal, P.S., Dasannacharya, B.A., Kelkar, V.K. and Manohar, C. and Menon, S.V.G. (1991). Pramana- J. Physics, 37, 311.

Srinivasa Rao, K., Goyal, P.S., Dasannacharya, B.A., Menon, S.V.G. Kelkar, V.K., Manohar, C. and Mishra, B.K. (1991) Physica B, 174, 170.

Thaper, C.L., Dasannacharya, B.A., Goyal, P.S., Chakravarthy, R. and Tomkinson, J. (1991). Physica B, 174, 251

Verbist, J.J., Lehmann, M.S., Koetzle, T.F. and Hamilton, W.C. (1972). Nature Lond. 235, 328.

Vijayaraghavan, P.R. (1989). Indian J. Pure Appl. Phys. 27, 567.

Table-1. Some salient features of Dhruva Reactor and the neutron beam experiments

Type	natural uranium, heavy water moderated, heavy water cooled and heavy water reflected reactor	
Maximum Reactor Power	100 MW (thermal)	
Neutron Flux	Maximum available neutron flux (Westcott-cell average)	1.36×10^{14} neutrons $\text{cm}^{-2} \text{s}^{-1}$
	Maximum thermal neutron flux expected	1.8×10^{14} neutrons $\text{cm}^{-2} \text{s}^{-1}$
(a) Spectrometers		
Profile Analysis Powder Diffractometer (PAD)		S.K.Paranjpe
Single Crystal Diffractometer (SCD)		A.Sequeira
Triple Axis Spectrometer (TAS)		P.R.Vijayaraghavan and S.L.Chaplot
Polarised Neutron Analysis Spectrometer (PNAS)		L. Madhav Rao
Hi-Q Diffractometer (HQD)		R.Chakravorthy
Filter Dectecor Spectrometer (FDS) Mark-1		P.R.Vijayaraghavan
Small Angle Spectrometer (SAS)		P.S.Goyal
Medium Resolution Inelastic Spectrometer (MRIS)		R.Mukhopadhyay and S.K.Paranjpe
Neutron Interferometer (NIN)		V.C.Rakhecha and A.G.Wagh
Spin Echo based Spectrometer (SES)		S.L.Chaplot

* Dhruva experimental facilities are a National Facility, and are also available to users outside BARC on application to Head, Solid State Physics Division, BARC, Bombay 400085, INDIA.

Figure Captions

- Fig. 1 General layout of neutron beams at Dhruva reactor
- Fig. 2 Neutron scattering instruments at Dhruva reactor.
- Fig. 3 ORTEP-II stereoscopic picture of glycyl-L-threonine
(Sequeira et al. 1981)
- Fig. 4 Average distances and angles for the main-chain atoms in amino acids (reproduced from Ramanadham and Chidambaram, 1978)
- Fig. 5 Distribution of C-C-H angles in amino acid structures (reproduced from Ramanadham and Chidambaram, 1978)
- Fig. 6 Distribution of H-bond parameters for 74 $N^+-H \cdots O$ and 30 $N-H \cdots O$ hydrogen bonds (reproduced from Ramanadham and Chidambaram, 1978)
- Fig. 7 Distribution of $N^+-H \cdots O$ and $N-H \cdots O$ H bonds in the R-O plane, along with the equi potential contours of H-bond energy (reproduced from Ramanadham and Chidambaram, 1978).
- Fig. 8 SANS distributions from CTAB/NaSal micellar solutions
- Fig. 9 Planned layout of the guide-tube laboratory adjacent to Dhruva Reactor Hall.

NEUTRON BEAM LAYOUT AT DHRUVA

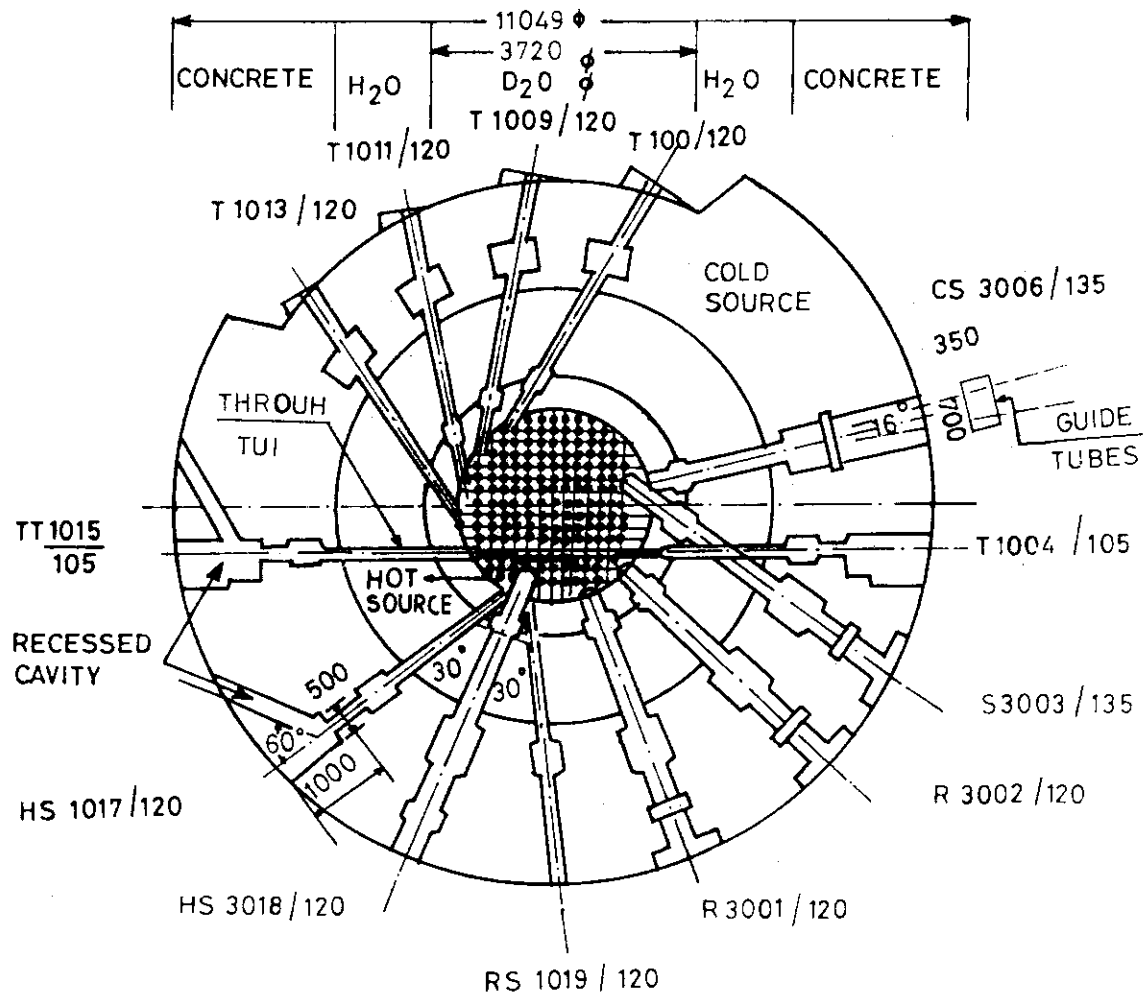
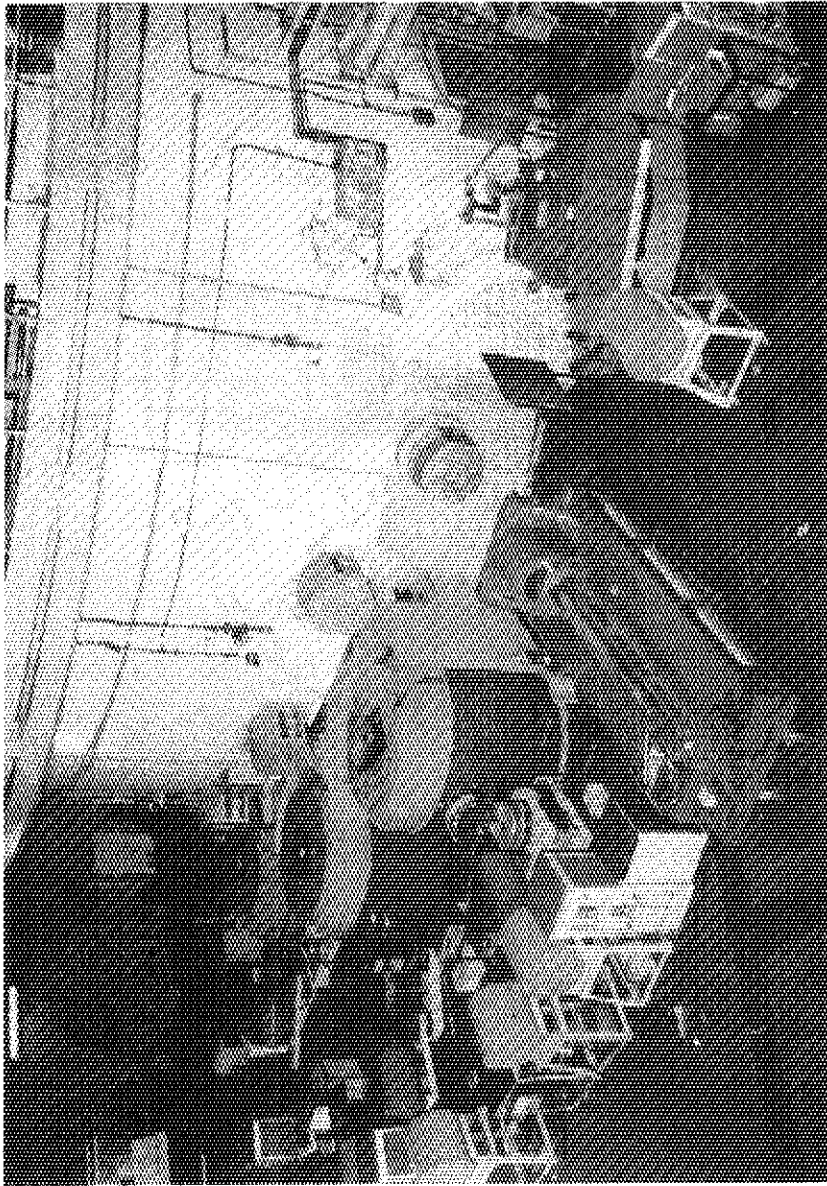


Figure 1



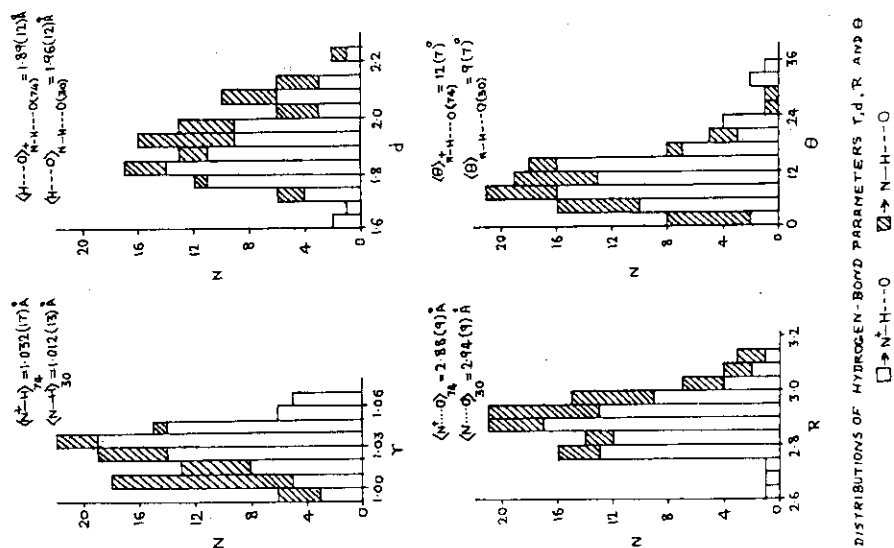
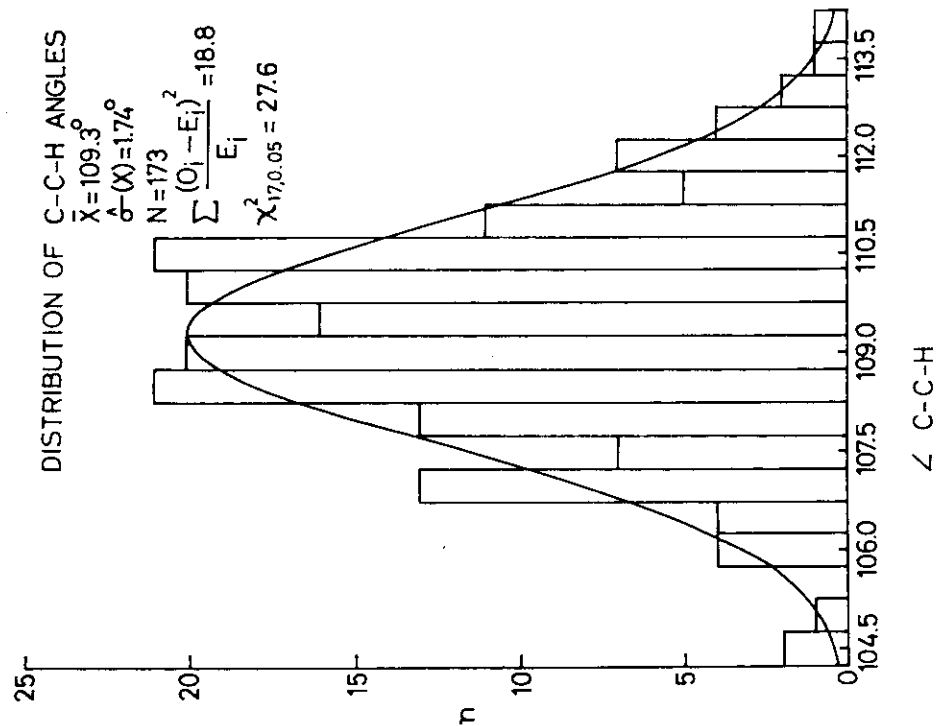
Neutron spectrometers at Dhruva

Figure 2

(A)

(B)

— 57 —



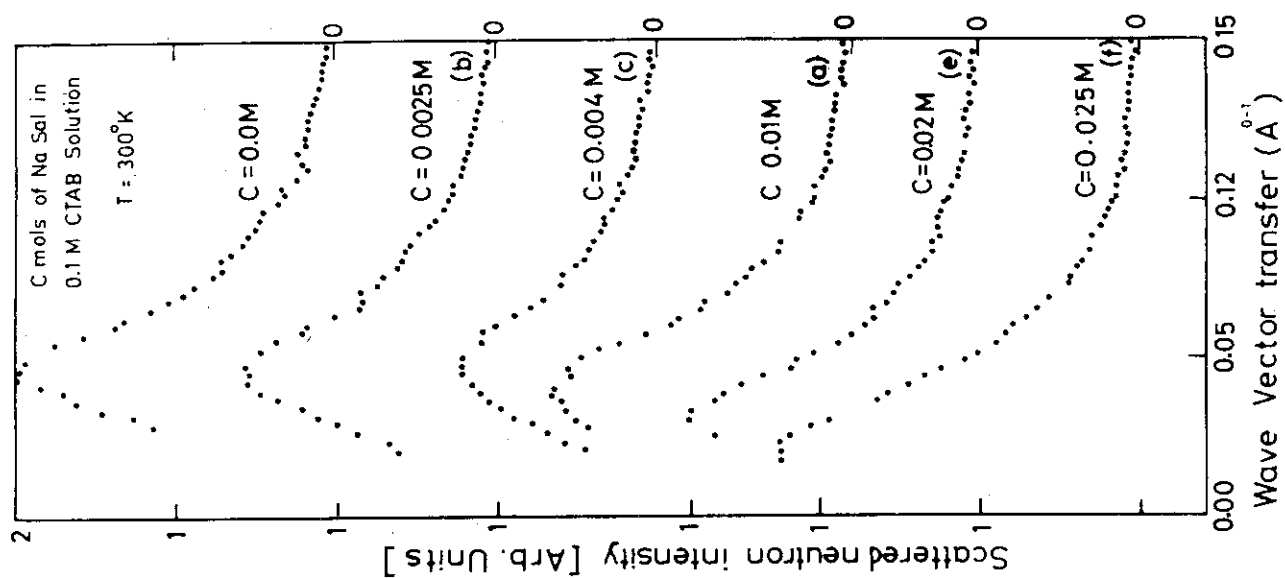


Figure 8

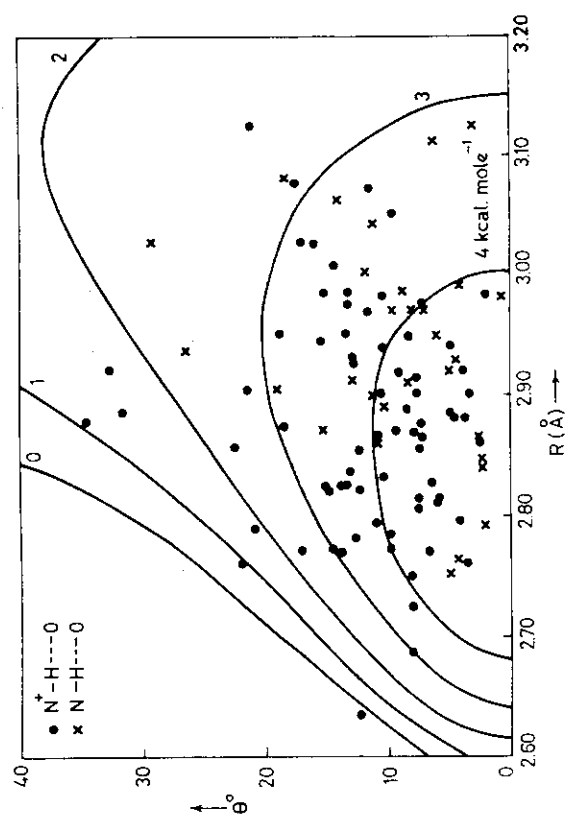


Figure 7

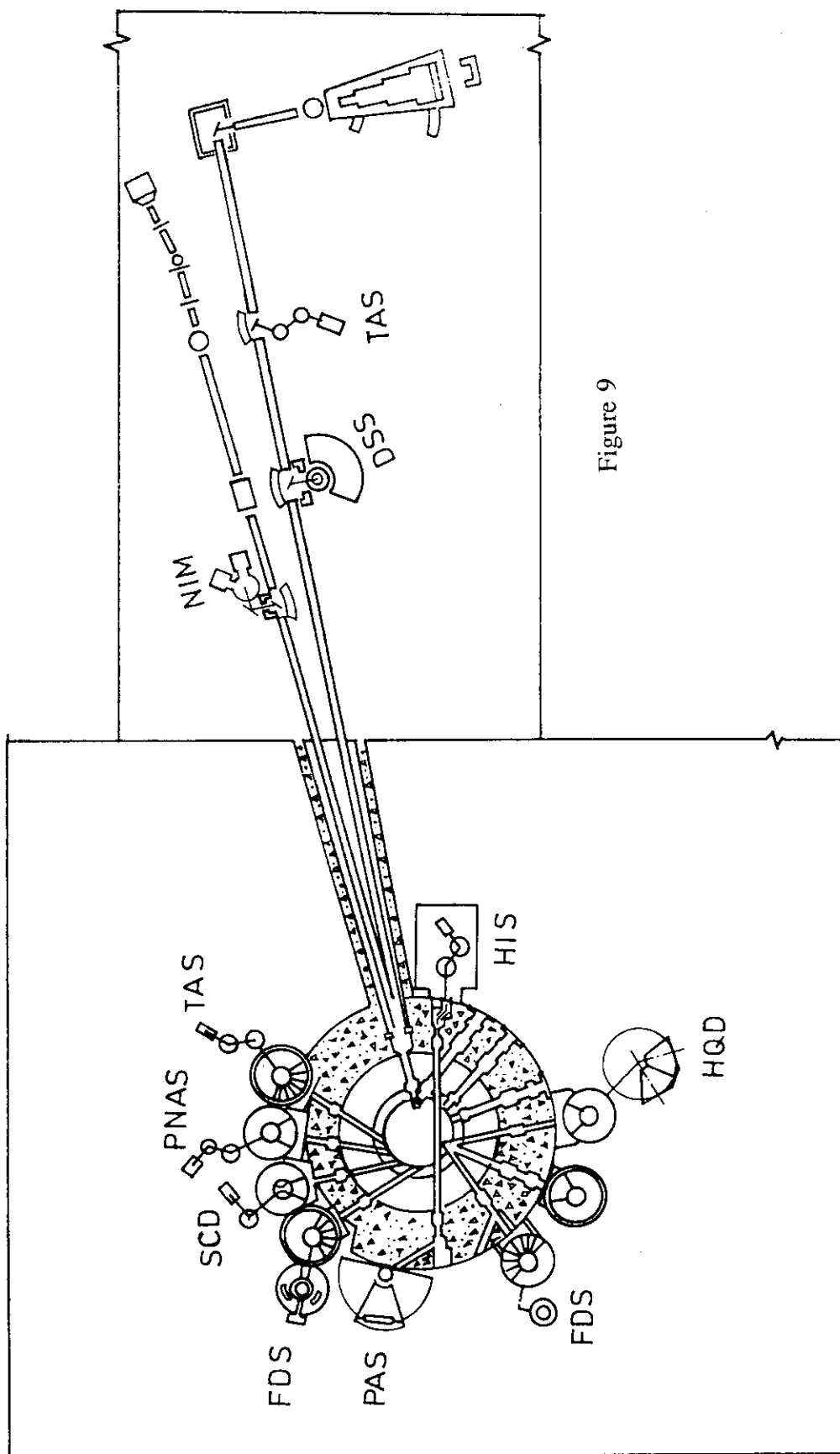


Figure 9

10. A LARGE SINGLE CRYSTAL OF THE TETRAGONAL FORM OF LYSOZYME CAN BE GROWN IN A CONCENTRATION GRADIENT OF NiCl_2

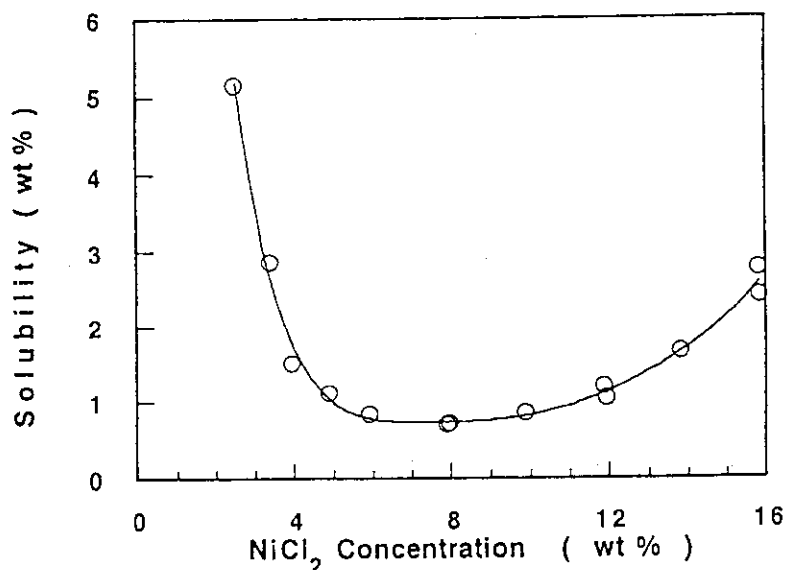
ATAKA, M. and KATSURA, T.,
Res. Inst. Polym. Text., Tsukuba 305 Japan

Protein structure analysis by neutron diffraction requires a single crystal of a size of 3 - 5 mm. We have found that the tetragonal form crystal of hen egg-white lysozyme, rarely reported so far to exceed 1 mm, reproducibly reaches 4 mm within 10 d when grown in a concentration gradient of NiCl_2 .

Powders of NiCl_2 (1 g) were put into the bottom of a vertically held test tube of 100 mm in length at 23°C, upon which an aqueous solution of lysozyme (50 mg/ml and pH 4.6) was carefully applied. The salt dissolved within a few hours and started to diffuse upwards. The salt concentration at various heights could be evaluated by the green color of the nickel ion. A concentration gradient of NiCl_2 between >20 and 0 wt% was maintained over more than 10 days in the tube. Lysozyme crystals started to grow only in a narrow region of 21 - 50 mm from the bottom, which corresponded to 5 - 15 wt% NiCl_2 . One or two crystals reproducibly reached 4 - 4.5 mm at the height of about 35 mm after 10 d.

In order to understand why the crystal growth occurred only in an intermediate concentration range of the salt, the solubility of lysozyme was measured in batches of different salt concentrations by a method reported earlier [Ataka & Asai: J. Cryst. Growth 90, 86 (1988)]. Interestingly, as shown below, the solubility as a function of salt concentration had a minimum at 8 wt% NiCl_2 .

When the salt concentration gradient was present, the crystals grew only in the part corresponding to this solubility minimum. Crystals did not grow both in the more concentrated and in the less concentrated regions. Since crystal growth was inhibited in these regions, protein molecules were continuously supplied from those parts to the limited number of the crystals that had started growing, thus helping them grow efficiently to an unexpectedly large size.



11. SMALL ANGLE NEUTRON SCATTERING STUDY OF THE INITIAL STAGE OF LYSOZYME CRYSTALLIZATION PROCESS.

MINEZAKI.Y, TANAKA.I, NIIMURA.N,
ATAKA.M^{*1}, KATSURA.T^{*1}

Laboratory of Nuclear Science, Tohoku University, Sendai, Japan

^{*1} Research Institute for Polymers and Textiles, Tsukuba, Japan

ABSTRACT

Despite the enormous amount of information obtained from atomic resolution crystal data, the difficulties encountered in growing crystals preclude structural X-ray studies for the majority of known isolated proteins. The protein crystal growth process can be studied by electron microscopy and by light scattering, and recently Ataka & Asai¹⁾ have discussed the kinetics on lysozyme crystal growth.

We have conducted small angle neutron scattering (SANS) experiments on the time evolution from the initial stages to the visible size of crystallization of hen egg-white lysozyme. SANS from several kinds of solutions have been carried out. One example of solutions where single crystals of lysozyme grow for a day, is that the concentration of lysozyme and NaCl is 20 mg/ml and 0.51M, respectively, pH is 4.6 and the temperature is 18 C, and the SANS result showed the distinctive change of time evolution. On the other hand, another example of solutions, where single crystal never grows, did not show any change of SANS of time evolution at all.

And we have also conducted the experiments under various unsaturated condition. From this experiment, we found that even under unsaturated conditions, aggregation of lysozyme was found to be started, against another data from light-scattering experiments.

INTRODUCTION

On the molecular biology, the determination of the three-dimensional structures of biological macromolecules, i.e. proteins, nucleic acids, etc. is the key to elucidate the mystery of life. Among the three major techniques, X-ray crystallography, nuclear magnetic resonance, and electron microscopy or electron diffraction (and very recently, also neutron crystallography), crystallography has been the main and the most useful tool for this purpose. In the field of the crystallography, many progresses in techniques, sources, etc. have been developed during the last decade. But even now, the crystallization

process is the most mysterious and unknown, and the bottle-neck for crystallography. Recently the work to know it has started all over the world using many methods. We have also started to know the first stage of crystallization process of lysozyme using SANS method.

EXPERIMENTAL

We have carried out SANS experiments using two kinds of instruments. One is the SANS-U located at the C1-2 beam port of the JRR-3M of JAERI. Incident neutron wavelength is 7.0Å. And sample-to-detector distance is 4000 mm to cover the Q range between 0.005 \AA^{-1} and 0.1 \AA^{-1} , and also used 12000 mm to cover the Q range between 0.002 \AA^{-1} and 0.03 \AA^{-1} . The other is WIT at KENS in Tokai. The covered Q range used for this experiment is between 0.055 \AA^{-1} to 0.144 \AA^{-1} .

Lysozyme was purchased from Seikagaku Kogyo Corp.

The time-evolution of the crystallization has been observed in a quartz sample cell (4mm in thick) in D₂O buffer at every 15 minutes for one day. The lysozyme concentration is 60 mg/ml, the one of NaCl is 3.0 wt%, pD is 4.6, and the temperature is 18°C. Under this condition the crystal grows for a day. As a reference, the unsaturated conditions, such as the lysozyme concentration is 20 mg/ml and others are the completely same as before, are adapted. Under this condition, the crystal never grows.

The effect of NaCl to the crystallization process has been studied by changing the NaCl concentration in the solution from 0 wt% to 3.0 wt%, under the concentration of which the lysozyme solution becomes supersaturated. Lysozyme concentration is 20 mg/ml, pD is 4.6, temperature is 18°C, and NaCl concentration is selected as 0, 0.12, 0.3, 0.6, 1.2, 1.8, 2.4 and 3.0 wt%.

RESULTS

(Time-evolution)

Fig.1 & 2 show the time dependence of the scattered neutrons detected on the total area of the detectors. Fig.1 shows the result under the saturated condition where the crystal grows, and Fig.2 shows the one under the unsaturated condition where the crystal doesn't grow. By the comparison of these two graphs, we can declare that the lysozyme crystallization process has been really observed.

Fig.3 shows the time-evolution of $I(q)$ which is obtained under the saturated condition. $I(q)$'s at every 15 minutes in the first two hours are displayed on this graph. The result described by the squared dot in the lowest is the one of the only lysozyme solution without NaCl. As soon as NaCl is added in that solution, $I(q)$ suddenly changed to the result

described by $I(q)$ [1]. Fig. 3 indicates that $I(q)$ changes dramatically as the time elapses. Especially during the first 3 hours, $I(q)$ was unstable, and after that till 15 hours, $I(q)$ became stable. After 16 hours, $I(q)$ decreased with time.

Fig.4 shows the time evolution of the integrated value of $I(q)$ at the q -region from 0.02 \AA^{-1} to 0.09 \AA^{-1} obtained from Fig.3. The fact mentioned above could be seen more clearly.

We have tried to carry out the Guinier plot and to extract $I(0)$, the extrapolation value to $Q=0$, and the radius of gyration R_g though the system is multi-dispersive. Fig.5 and Fig.6 show the time evolution of $I(0)$, and of R_g , respectively. Squared dots, closed circles and closed squares describe the results obtained from the data in the q region of $0.076 \text{ \AA}^{-1} < q < 0.09 \text{ \AA}^{-1}$, $0.05 \text{ \AA}^{-1} < q < 0.064 \text{ \AA}^{-1}$ and $0.015 \text{ \AA}^{-1} < q < 0.038 \text{ \AA}^{-1}$, respectively. Fig.5 and Fig.6 indicate that as far as the q -range considered, the number and the size of aggregated lysozyme clusters might be constant and stable between 200 minutes and 900 minutes.

(Change of NaCl concentration)

Fig.7 shows the change of $I(q)$ with the various NaCl concentrations. As the NaCl concentration increases, $I(q)$ increases gradually and the peak shifts toward the low Q . One interpretation is that aggregation of lysozyme occurs even under the unsaturated condition when NaCl is added, and the other one is that the interparticle interaction decreases as the NaCl concentration increases. In any interpretation, this fact is very interesting and important to understand the lysozyme crystallization process.

Fig.8 shows the Guinier plot of the data at the higher q -region. The $I(0)$ and R_g obtained from it are shown in Fig.9 & 10, respectively. Both $I(0)$ and R_g increase with the increase the NaCl concentration in this q -region.

DISCUSSION

The effort to know the crystallization process of protein has been just started at everywhere since only a few years ago by using several method. Direct observation of the crystallization process in the microscopic level is very important, and for that the SANS experiment might be superior to other method, especially the small angle X-ray scattering (SAXS) experiment. The reasons are as follows: (1) It takes one day or so to complete the protein crystallization, and if X-ray is used, radiation damage might occur during the measurement for one day. (2) The sample thickness is less than 1mm for the SAXS, and the surface effect of the cell cannot be neglected. (3) The addition of the salt such as NaCl is necessary for the protein crystallization, and this affects the absorpton of X-rays fatally.

We have started the preliminary observation of the initial stage of the crystallization process of lysozyme by using the SANS experiment. Fortunately we could get two results as follows; (1) We could follow early stage of lysozyme crystallization process, and (2) we could discover that the transition from the unsaturated state to the saturated one might look like continuous, and even under the unsaturated condition the aggregation of lysozyme might occur.

We could not put the clear line between our results of $I(q)$ under the saturated or unsaturated states. We must have an important question. What is the difference between the saturated and unsaturated states in the microscopic level? The answer will give us the solution to understand the microscopic mechanism of the crystallization process.

REFERENCE

- 1) M. Ataka & M. Asai; Biophys. J. 58 (1990) 807~811

'92/06 Lyso. time-evolution

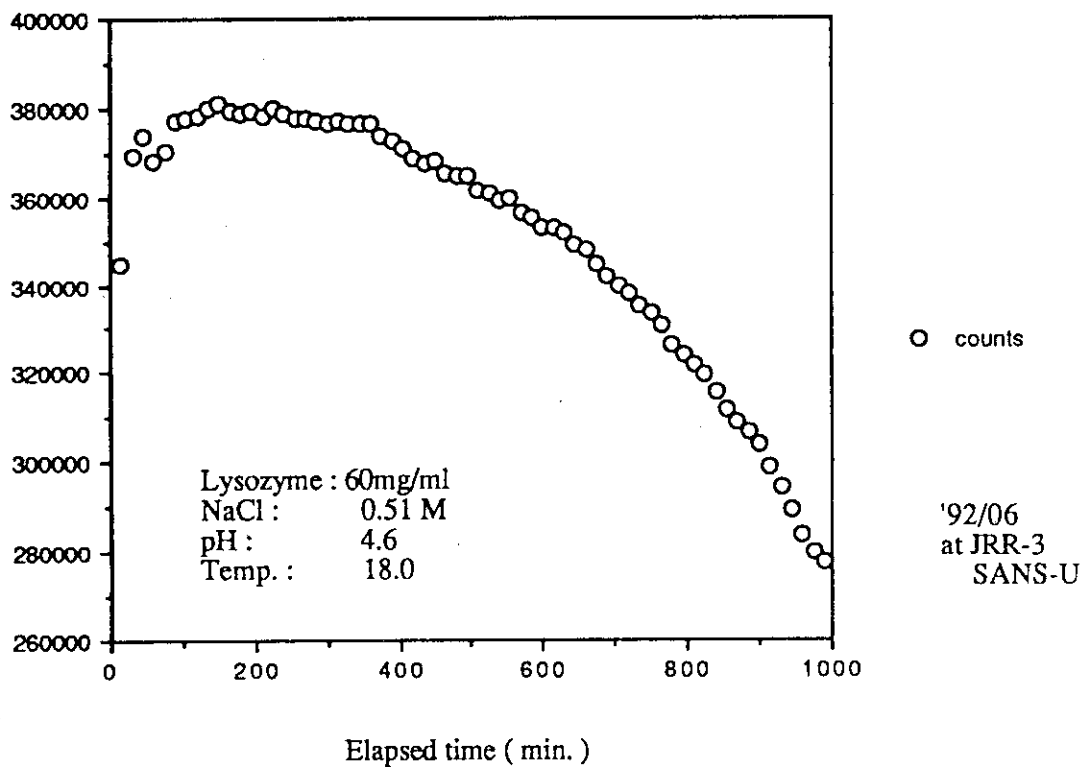


Figure 1

'92/06 Lyso. time-evolution

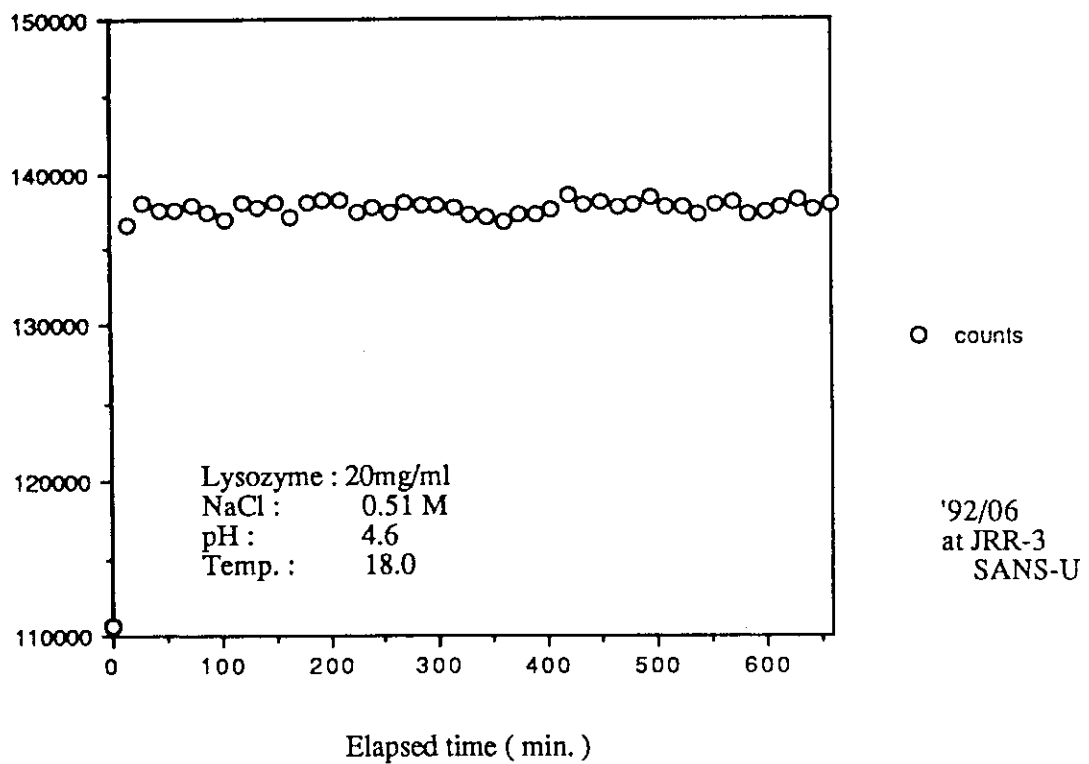


Figure 2

'92/06 Lyso.time-evolution

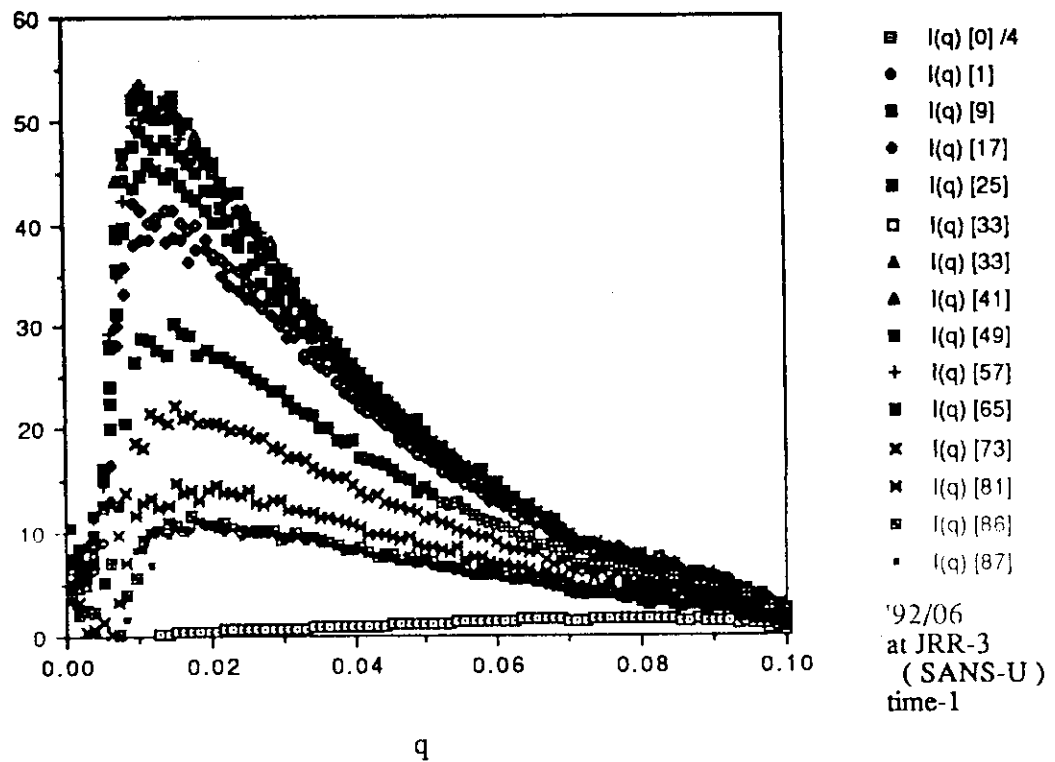


Figure 3

'92/06 Lyso. time-evolution

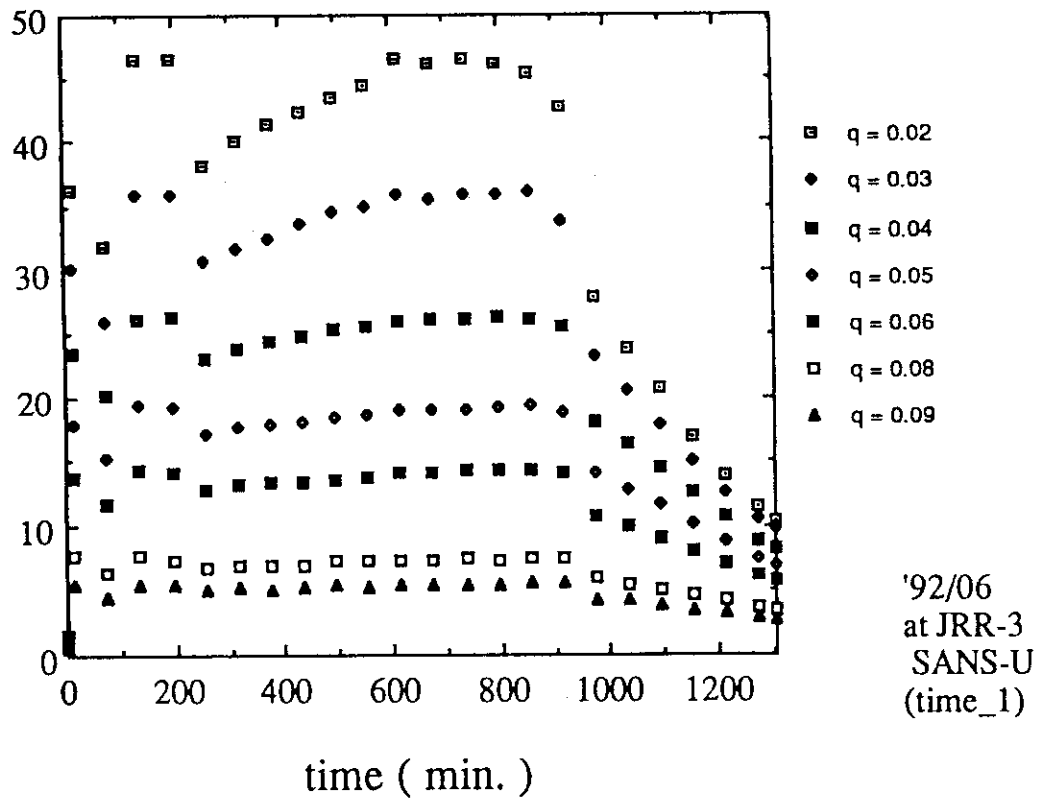
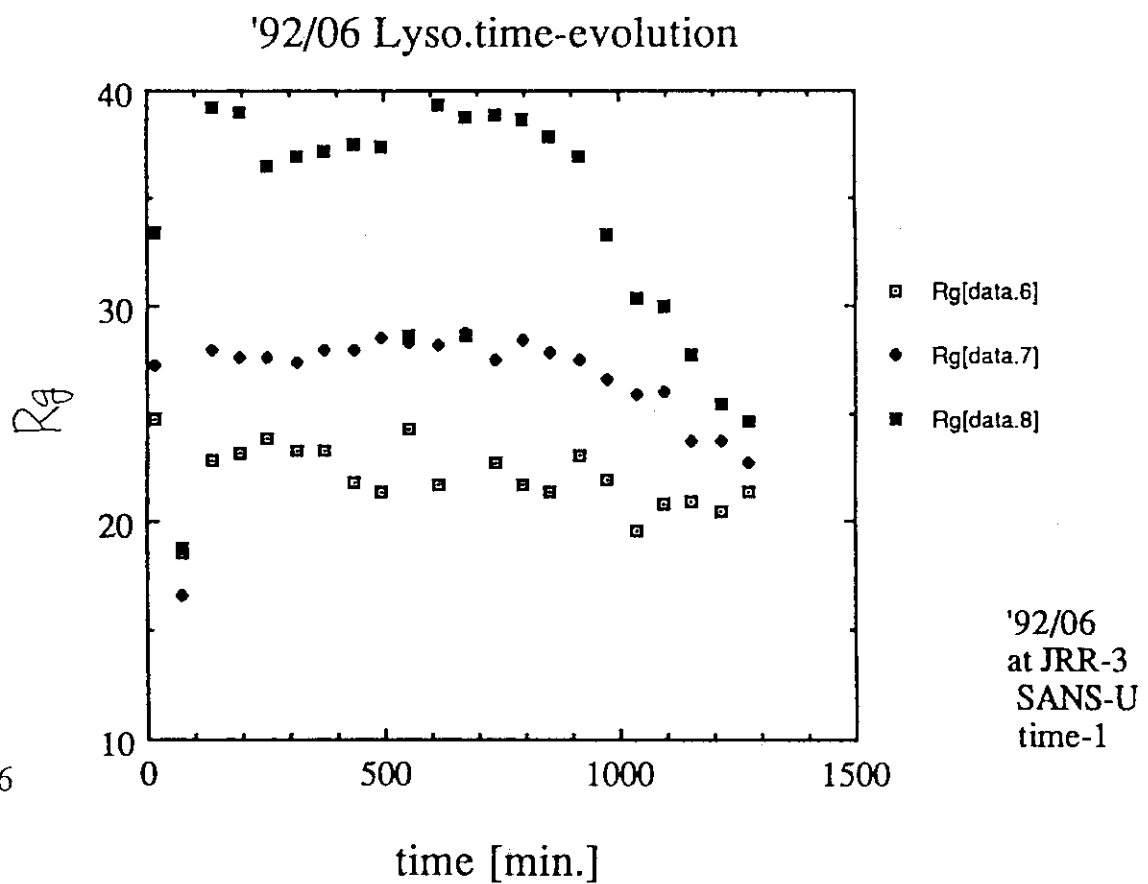
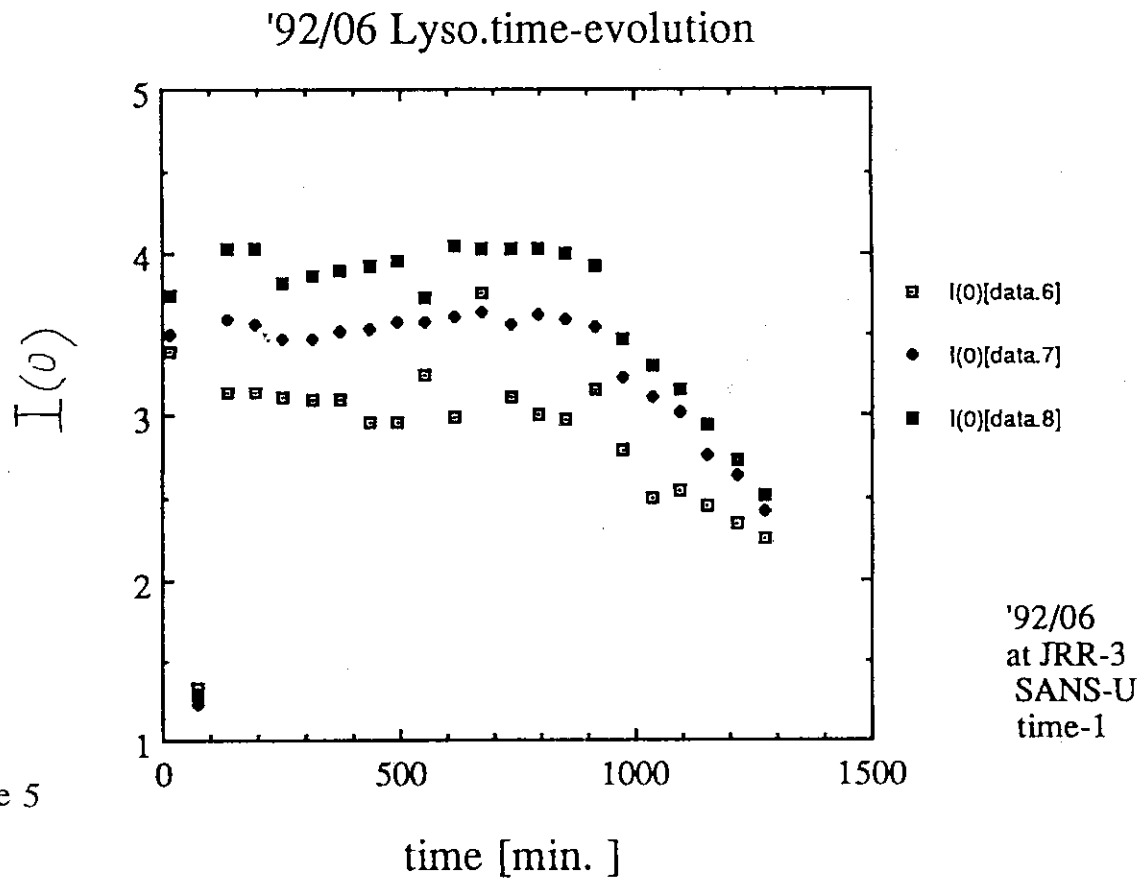


Figure 4



'92/07 Lyso.-NaCl change

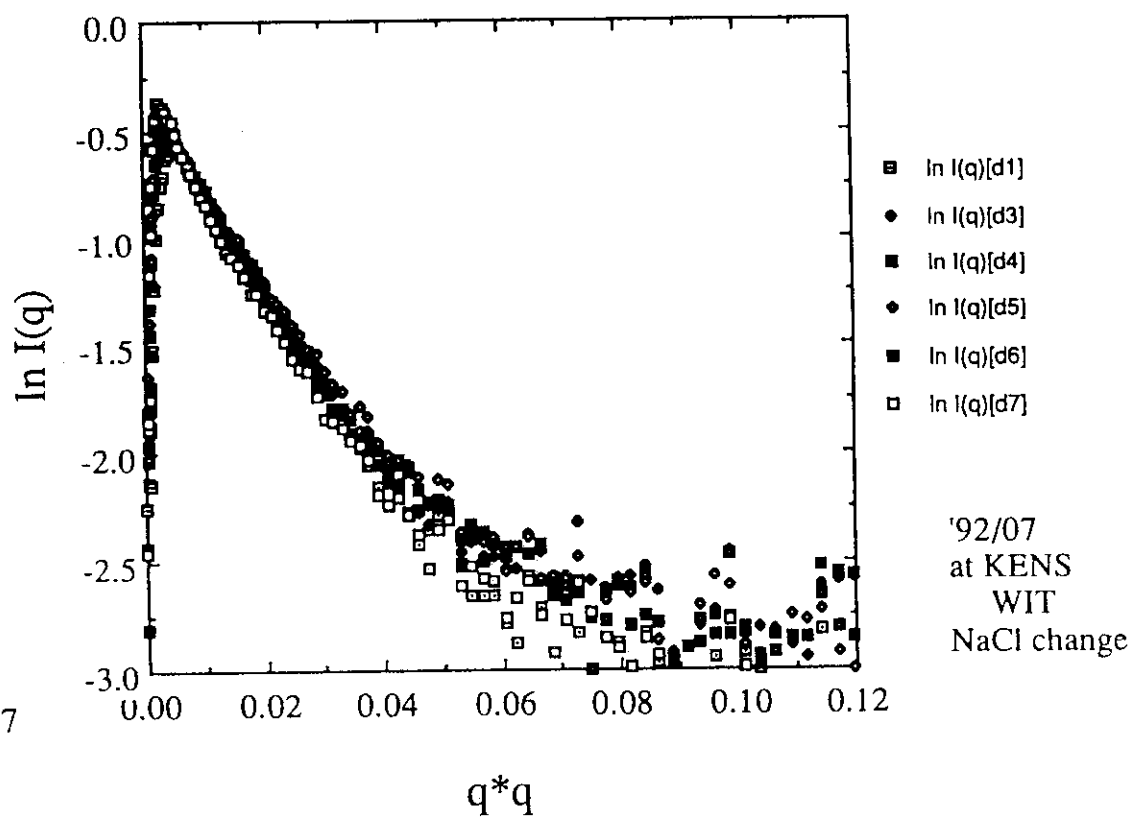


Figure 7

Lyso. NaCl change

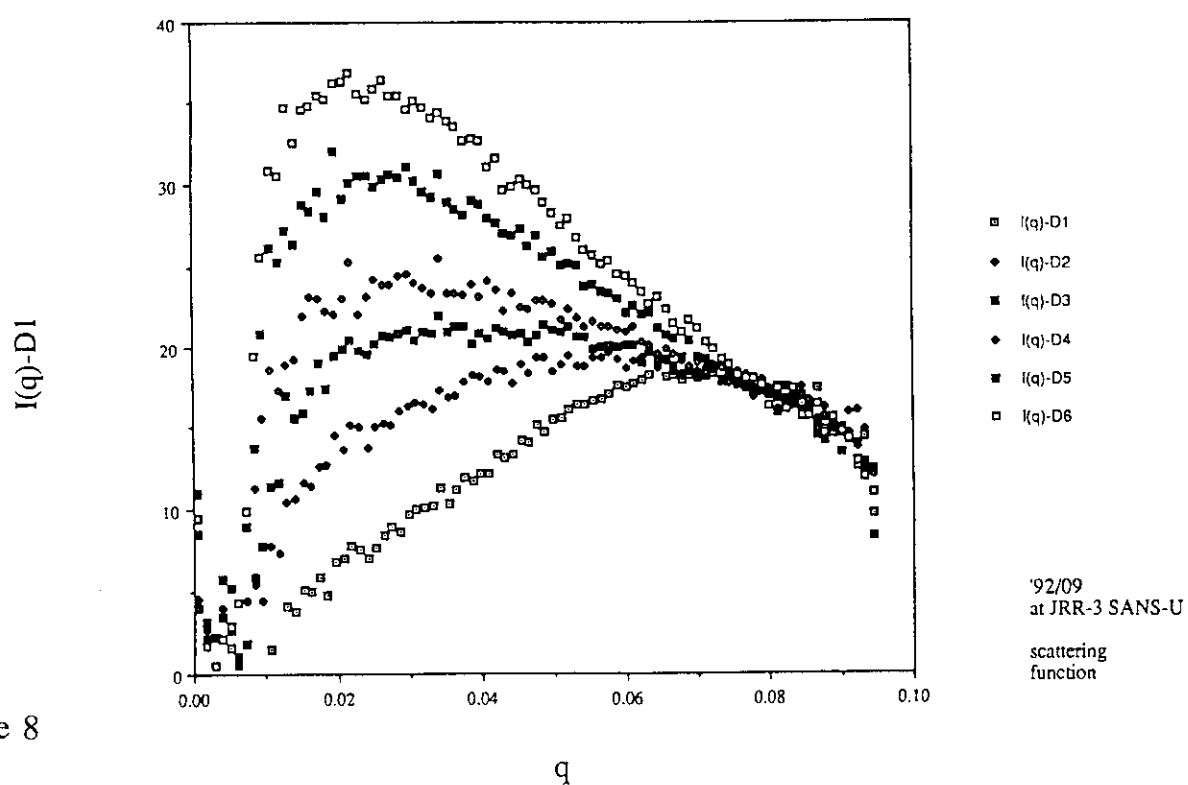
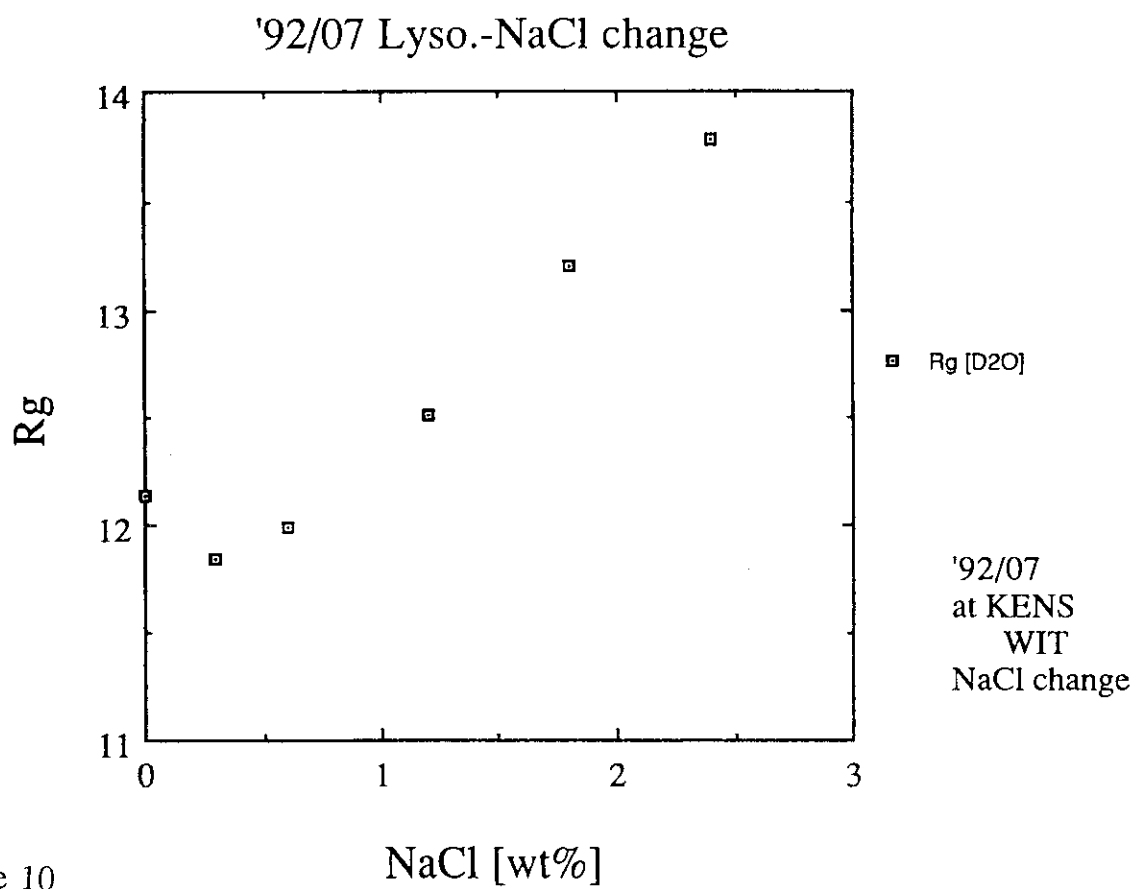
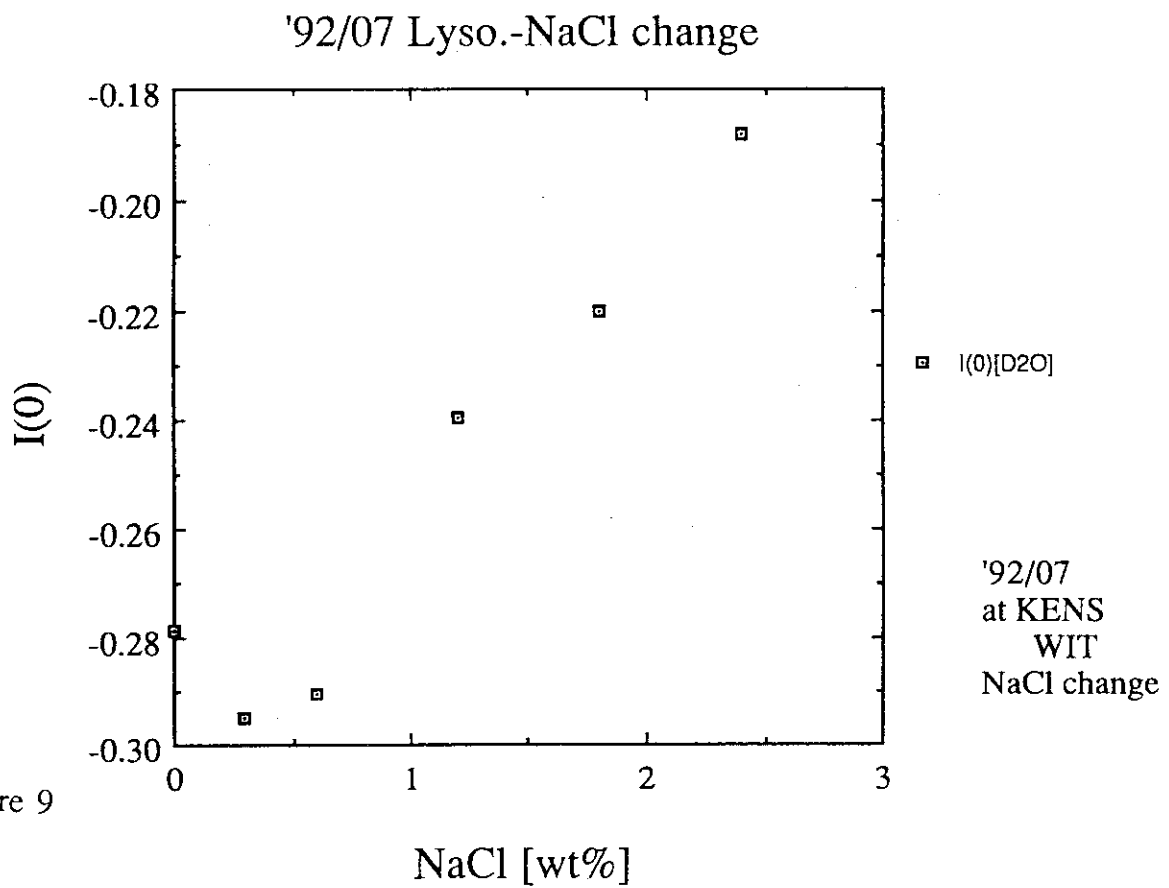


Figure 8



12. NEUTRON DIFFRACTION CAMERA USING A THERMO-LUMINO SHEET.

HIDAKA, M. . MORISAKO, T

Department of Physics, Kyushu University, Fukuoka, Japan

NISHI, M

The Institute for Solid State Physics, The University of
Tokyo, Tokyo, Japan

Although some kinds of proportional detectors have been developed for a neutron diffraction to observe two dimensional reciprocal space at the same time, it is well known that a film method is often very convenient. Usually, a $\text{Li}^6\text{F} + \text{ZnP}(\text{Ag})$ sheet and a X-ray film are used as a scintillator and its detector, respectively, for the neutron diffraction camera method.

At the present work, we have been developing a new detector system of the neutron diffraction camera. The system is mainly based on a thermal luminescence effect. The thermo-lumino sheet (TLS) is made of the thermal luminosity being fine powders of $(\text{BaSO}_4; \text{Er, Cl}) + (^{10}\text{B}$ -chemical compound). First, the compound detects cold- and thermal- neutron beams by a (n, α) reaction and the BaSO_4 system is second transported to the excited energy-level by the emitted α - particles quickly. Therefore, it is considered that there are some localized areas having the excited energy-level in the thermo-lumino sheet, as the neutron beams passing through. During the thermal treatment of heating up to about 250°C , the excited BaSO_4 system emits the luminescence of about 370nm.

TLS is remarkably good at neutron absorption efficiency and quite stable against lighting, drift of temperature and humidity, and fading.

TLS also has an excellent linearity to the neutron flux density, and its dynamic range is more than 6 places.

After gathering the recorded vision image, TLS can be used cyclically by an annealer which eliminates the recorded image data.

TLS is inserted into the heating unit of TLS reader and inflicted thermal excitation from the unit.

Then two dimensioned thermal luminescences, being directly proportional to the stored energies, are detected and amplified by an imaging intensifier and converted by a CCD camera to electrical signals (vision image data).

A Computerized vision system can handle the signals and analyze vision image.

At the present, we will report the new instrumental system of the thermo-lumino detector and its applications to the neutron diffraction camera, which were carried out at JRR-3.

13. LOW RESOLUTION NEUTRON CRYSTALLOGRAPHY OF LARGE MACROMOLECULAR ASSEMBLIES

**Peter A. Timmins
ILL,
156X,
38042 Grenoble Cedex 09,
France**

Introduction

It is widely accepted that the preeminent technique for the determination of the structure of biological macromolecules is X-ray crystallography. For the solution of structures at near atomic resolution it has for many years been the only technique although recently a number of structures of low molecular weight (< 25000) have been solved by NMR. A handful of structures has also been investigated at high resolution by neutron crystallography but in these cases the X-ray structure was already known and neutrons were used to obtain complementary information on the positions of important protons in the macromolecule or on the surrounding water molecules. Despite the success of the X-ray technique there exist, however, a number of cases, in particular of large macromolecular assemblies, where high resolution information cannot be obtained for at least part of the structure even though highly diffracting crystals exist. It is often one particular chemical component or part of a molecule that cannot be seen with X-rays. This is usually due to the fact that these components are at least partially disordered in the crystal. Some examples are the nucleic acid in spherical viruses, the DNA in nucleosome core particles, the lipid in lipoproteins and detergent in crystals of detergent solubilised membrane proteins.

How can neutrons help?

The atomic scattering lengths for neutrons are very different from those for X-rays, and in particular are unrelated to the atomic mass. The most important difference is for hydrogen where the normal isotope ^1H , has a negative scattering length whereas deuterium, ^2H (D), has a positive scattering length as have all other atoms commonly found in biological macromolecules. The consequence of this is that different molecular species (protein, nucleic acid, lipids) have different scattering length densities due in large part to their different hydrogen contents. In low

resolution studies the contrast which produces scattering is that between the macromolecule and its aqueous environment. Because of the difference in scattering length density between hydrogen and deuterium this contrast may be altered by the replacement of deuterium for hydrogen either in the water or in the macromolecule. This is the contrast variation method that is well known in neutron small angle scattering. Crystals of biological macromolecules invariably contain substantial amounts of water (25 - 75%) and the same technique may therefore be applied with the advantages associated with crystal studies rather than solution studies, ie, the molecules all have the same orientation giving much more reliable information and they diffract in phase giving a much stronger signal for a given volume of sample.

A secondary reason for which neutrons are of such use in low resolution studies is the relative ease, compared with X-rays, of measuring diffraction from very large lattices. This is due primarily to the availability of cold neutron beams of wavelength 4 - 10 Å. It is particularly important in such studies to measure the maximum number of diffracted intensities to the largest possible d-spacings.

Instrumentation

Classical neutron diffractometers are not capable of resolving reflections from crystals of cell dimensions greater than $\sim 100\text{\AA}$ and only then with severely compromised flux. The first experiments in low resolution macromolecular crystallography with neutrons (Finch et al., 1982) were therefore carried out on the small angle instrument D17 at the ILL, Grenoble. The basic characteristics of this instrument, long wavelength, two-dimensional multidetector, long crystal to detector distance proved to be satisfactory for such experiments and therefore a dedicated instrument, DB21, was built as a joint venture between ILL and the European Molecular Biology Laboratory (EMBL). Table 1 shows the details of the instrument which, because it is adapted to the size of normal macromolecular crystals ($\sim 1 - 2\text{ mm}$), has dimensions similar to an X-ray diffractometer. It is possible to measure diffraction data from crystals with unit cell dimensions up to 1000\AA to a minimum d-spacing of about 12\AA . There are plans to extend this resolution limit to 5\AA by installation of a new monochromator (C. Wilkinson, private communication).

Samples and Data Collection

It is a widely held belief that neutron crystallography of biological macromolecules requires exceptionally large crystals. This belief has arisen from the experience of the requirements for high resolution diffraction. For low resolution diffraction it is possible to use crystals similar to those used for high resolution x-ray crystallography i.e. $< 1\text{ mm}^3$. This is possible for two major reasons:

(i) At 12Å resolution the molecular transform of a macromolecule is very strong as the contrast is derived from the difference in scattering length density between the macromolecule and the surrounding solvent, whereas at atomic resolution it is between the atoms and surrounding vacuum.

(ii) The use of cold neutrons leads to an increased reflectivity and hence greater integrated intensity per reflection compared with shorter wavelengths.

It is usual for a contrast variation series to collect data from crystals containing at least 4 different H₂O/D₂O ratios. These are prepared by soaking the crystals for a period of weeks in the appropriate mixture to ensure the exchange of all labile protons. A small number of labile protons in the interior of the macromolecule will probably exchange on only a very long time scale of months to years. Data are then collected by step scanning the crystal about the ω - (or ϕ -) axis of the diffractometer until a unique data set is obtained. Depending on the symmetry of the crystal this may require several orientations of the crystal. Typical data collection times are 3 -15 days per crystal depending on the contrast, crystal volume, space group etc.

Table 1 DB21 Instrument Details

Beam	H15 cold neutron guide
Monochromator	Potassium intercalated graphite
Wavelength	7.56Å
Wavelength spread	2%
Maximum flux at sample position	$1.7 \times 10^6 \text{ n cm}^{-2}\text{s}^{-1}$
Maximum horizontal divergence	0.030 rad
Maximum vertical divergence	0.025 rad
Maximum beam size	2 mm diameter
Detector:	two-dimensional PSD (Anger camera type) 200 x 200 mm ²
Resolution	1.8 x 1.8 mm ²
Efficiency	~80%
Angular setting	$-45^\circ < 2\Theta_D < +20^\circ$
Sample detector distance	165 - 500 mm
Background	Beam off: 7 cps
	Beam on, no sample, Ar atmosphere:
	28 cps

The crystallographic phase problem

The variation of the crystallographic structure factor as a function of contrast can be expressed as:

$$\bar{F}(h, X) = \bar{F}(h, 0) + X\bar{F}(h)_{HD} \quad \dots\dots\dots(1)$$

where h is the reciprocal lattice point
 X is the mole fraction of $[D_2O]/[D_2O]+[H_2O]$ in the crystal
 $\bar{F}(h)_{HD}$ is the vector difference between the structure factor in H_2O and that in D_2O .

Multiplying by the complex conjugate we obtain the diffracted intensity:

$$I(h, X) = F(h, 0)^2 + 2X \cos \phi F(h, 0) F_{HD}(h) + X^2 F_{HD}^2(h) \quad \dots(2)$$

where ϕ is the phase angle between $\bar{F}(h, 0)$ and $\bar{F}(h)_{HD}$.

This relationship has several important consequences for low resolution crystallography including the possibility of scaling together data from different contrasts and the interpolation of missing data (Roth et al., 1984). In terms of structure solution it is of fundamental importance as it means that the phase difference, ϕ , between any two contrasts, of a reflection (h), may be determined except for the sign (\pm), if the amplitudes at 3 contrasts are known. Therefore if the structure is known at any one contrast then the phases at that contrast may be calculated and then determined at any other contrast except for knowledge of the sign. In the particular case of centrosymmetric reflections where $\phi = 0$ or π then there is of course no ambiguity and the phase may be calculated at any contrast (Roth, 1987).

In most studies carried out to date the structure of one component of the macromolecular complex has been determined by X-rays or could be modeled from other information. Hence structure factors calculated from the known part of the structure at a contrast where the other component is visible provide starting phases for the determination of the structure at any contrast. This is illustrated in Fig. 1 which demonstrates the vector relationships between structure factors at four different contrasts. The two triangles bounded by F_0 , F_{HD} and F_{100} are the two possible relationships which can be constructed through knowledge of the structure factor amplitudes alone following eqn. 1, and corresponding to the two possible signs of ϕ .

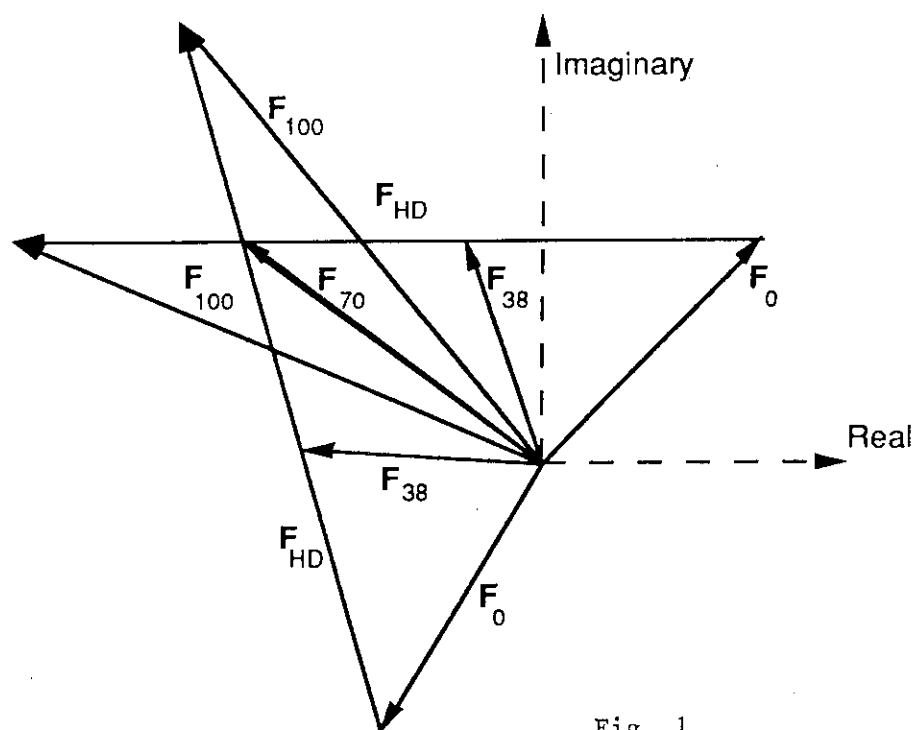


Fig. 1

This particular figure illustrates the case of, for example, a hypothetical protein/RNA complex where data would be measured at 38% D₂O where the protein is invisible, 70% D₂O where the RNA is invisible and two other contrasts, 0 and 100% D₂O. In this case we imagine that the protein structure is known and that the RNA structure is to be determined. We may therefore calculate the phase of the structure factor in 70% D₂O and thus determine the orientation of the phase triangle with just the ambiguity of sign corresponding to the two triangles shown. This is very closely analogous to the situation in X-ray protein crystallography of single isomorphous replacement. Once this (ambiguous) phase has been determined then the ambiguity may be resolved and an approach to the true phase may be made using a number of constraints such as the invariability of the known part of the structure, solvent flattening or non-crystallographic symmetry averaging (Roth, 1992).

Some examples

Tomato Bushy Stunt Virus

This is an icosahedral plant virus whose structure has determined by X-ray crystallography (Olson et al., 1983). The high resolution structure however was unable to locate some 25% of the protein and none of the nucleic acid. Neutron crystallographic maps from crystals soaked in 38% and 70% D₂O have localised the RNA and missing protein and enabled details of the protein-nucleic acid interactions

to be elucidated (Timmins, 1988, P.A. Timmins, D. Wild, J. Witz, manuscript in preparation.). Fig 2 shows a portion of the neutron scattering map in 70% D₂O. The outer shell of protein corresponds to that seen in the X-ray maps but the inner density and particularly the 3 lobes of density closely associated at the 3-fold symmetry axis were invisible, most probably because of disorder. The RNA is located in the space between the two protein layers and is only visible in the map from 38% D₂O (not shown).

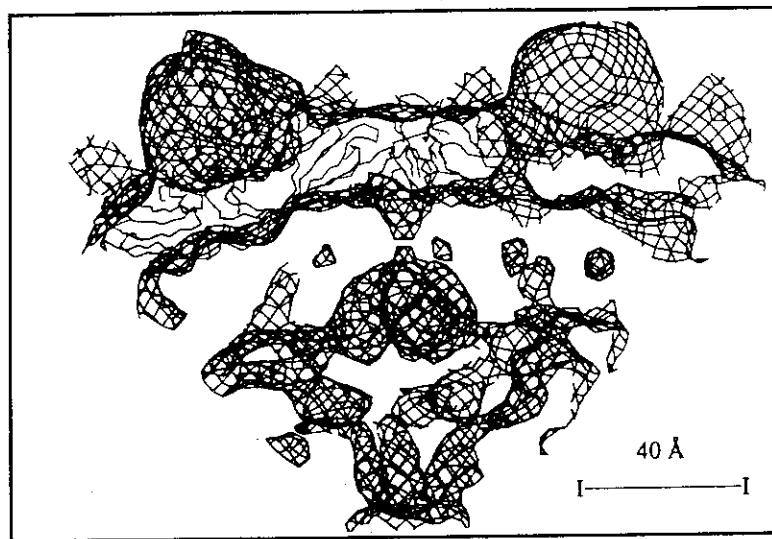


Fig. 2. Tomato Bushy Stunt Virus neutron scattering density map in 70% D₂O. The polypeptide chain trace from the X-ray model is visible in the outer shell of density whereas the inner density shows the protein visible only by neutron scattering.

Lipovitellin

Lipovitellin is a lipoprotein found in the oocytes of egg-laying animals where it sometimes forms *in vivo* two-dimensional crystals. The structure was solved using standard X-ray crystallographic techniques (Raag et al, 1988) but in this study they were unable to locate any of the bound lipid which was known to comprise some 15% of the molecular mass. Neutron crystallographic data were measured to 12 Å resolution from crystals soaked in 5 different H₂O/D₂O mixtures. From these data sets were interpolated the structure factors for the molecule in 10% D₂O at which contrast the lipid scattering is minimised. Phases calculated from the known protein structure were applied to the measured amplitudes and this constituted a starting point for determination of the phases at contrasts where the lipid should be visible. These starting phases were refined using the known protein structure, the known proportion of lipid in the complex and solvent flattening. The neutron scattering density map at 40% D₂O, where the lipid is visible and the protein invisible, is shown in Fig. 3

(Timmins et al., 1992). The contours representing scattering density are in white. Superimposed on the density map is the trace (in grey) of the polypeptide chain as determined by X-rays. We see clearly that the lipid is located as a condensed phase in a cavity of the protein, possibly in the form of a bilayer.

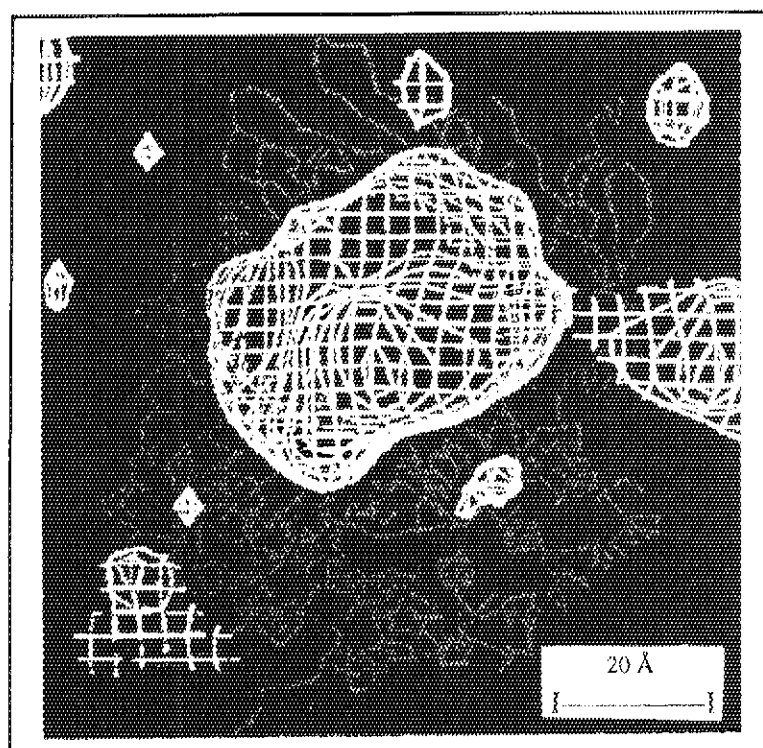


Fig. 3. Lipovitellin neutron scattering density in 40% D₂O, representing the lipid, superimposed on the polypeptide chain trace from X-ray crystallographic studies.

Conclusions and future prospects

Low resolution neutron crystallography has already shown its power as a technique complementary to X-ray diffraction. In the future we can expect more sophisticated applications of the technique exploiting for example specific deuteration. Ever larger molecular complexes are being crystallised, for example the ribosome. The resolution of these structures presents an enormous challenge to X-ray crystallography. If these and other particles such as multi-enzyme complexes can be reconstituted with single deuterated proteins then neutron crystallography will play an important role in defining sub-unit boundaries and interactions between more or less ordered parts of the complex. In order to solve these structures by neutrons then new methods of phasing, independent of the X-ray structure, may have to be developed.

First steps in the development of such direct methods are already being taken to interpret data from crystalline ribosomes (Roth, 1992, Eisenstein et al., 1991).

References

- Finch, J.T., Lewit-Bentley, A., Bentley, G.A., Roth, M. and Timmins, P.A. (1980)
Phil. Trans. R. Soc. Lond. **B290**, 635-638
- Olson, A.J., Bricogne, G. & Harrison, S.C. (1983) *J. Mol. Biol.*, **17**, 61-93.
- Raag R., Appelt K., Xuong N. H., Banaszak, L.J. *J. Mol. Biol.*, **200**, 553 (1988)
- Roth, M. (1987) *Acta Cryst.* **A43**, 780-787
- Roth, M., Lewit-Bentley, A. and Bentley, G.A. (1984) *J. Appl. Cryst.* **17**, 77-84.
- Roth, M. (1992), in *Crystallographic Computing 5*, D.M. Moras, A.D. Podjarny, J.C. Thierry, Eds. (Oxford Univ. Press, Oxford)
- Timmins, P.A. (1988) *Makromol. Chem., Makromol. Symp.*, **15**, 311-321.
- Timmins, P.A., Poliks, B. and Banaszak, L. (1992) *Science*, **257**, 652-655.
- Eisenstein, M., Sharon, R., Berkovitch-Yellin, Z., Gewitz, H.S., Weinstein, S., Pebay-Peyroula, E., Roth, M. and Yonath, A. (1991) *Biochimie*, **73**, 879-886.

14. DIFFRACTOMETER FOR NEUTRON CRYSTALLOGRAPHY IN BIOLOGY-JAPANESE PROJECT.

Nobuo NIIMURA

**Laboratory of Nuclear Science, Tohoku University, Mikamine
1-2, Taihaku-ku, Sendai, 982, Japan**

§ 1. Introduction

The x-ray diffraction of single crystals has supplied knowledge about the atomic structure of proteins, viruses, t-RNA and DNA. Since the structure- function relationship of proteins is dominated by the behavior of hydrogen atoms, it is important to know the structural information of hydrogen atoms. However, it is difficult for X-ray crystallography in biology to give the structural information of hydrogen atoms.

On the other hand, neutron diffraction provides an experimental method of directly locating hydrogen atoms. So, we have had a project to construct the dedicated diffractometer for the neutron crystallography in biology at JRR-3M in JAERI(Japan Atomic Energy Research Institute) . This paper reports the tentative and general view of the project.

§ 2. Advantages and Disadvantages of Neutron Diffraction

Several distinctive advantages of neutron diffraction are summarized as follows: Neutron diffraction can locate light atoms such as hydrogen and deuterium. Since the scattering length of hydrogen is different with that of deuterium, hydrogen and deuterium could be distinguished, and this is useful to study H/D exchange, contrast variation with different D₂O/H₂O mother liquid, and so on. Nitrogen, with its greater scattering length, can be distinguished from carbon and from oxygen. The crystals are not damaged by neutrons as they are by x-rays. The higher-angle data should be more easily observable for neutrons than for x-rays.

The most serious disadvantage of neutron diffraction is the low flux of neutrons irradiated on the sample specimen. The diffraction intensity is written as

$$I \propto I_0 \cdot V \cdot A / (v_0)^2$$

where I , I_0 , V , A and v_0 are diffraction intensity, incident neutron intensity, the volume of the sample specimen, detector area and the volume of the unit cell, respectively. Normally the unit cell dimension of

the protein crystal is about ten times larger than that of the most of inorganic materials. Because of this term, diffracted intensity from the protein crystal is weakened to the 10^{-5} - 10^{-6} compared with that of the most of inorganic materials.

§ 3. General concept and view of the diffractometer

In order to overcome the intensity problem, three items should be considered carefully. Those are (1) how to get a large single crystal, (2) how to get intense neutron flux on a sample position, and (3) how to get a genuine detector system.

(1) A large single crystal.

It could be said that the neutron flux at JRR-3M is about one half of that at BNL(Brookhaven National Laboratory) and about one fifth of that of ILL(Institute of Laue-Langevin), and the usual volumes of the protein single crystal used at BNL and ILL are 1 mm^3 and 3 mm^3 , respectively. If the diffractometer of the same performance as the one of BNL or ILL is available in JRR-3M, the sample of 5 mm^3 in volume is necessary, in principle. To get such a large single crystal is a hard job, but not impossible. Recently Ataka *et al.* have developed the method to grow a lysozyme single crystal of more than 200 mm^3 in volume easily¹⁾. Fortunately, Dr. Ataka will join our project and he will continue developing the method and try to apply it for the other proteins.

(2) Intense neutron flux.

In order to get intense neutron flux on a sample position at the inelastic neutron scattering instrument, it is a normal way to adopt the focussing monochromator as far as the Q-resolution is tolerable. However, in the single crystal diffractometry, such a focussing monochromator method is not applied so far because the Q-resolution is rather serious in this case.

We would like to develop a new type of a focusing monochromator even in the case of the single crystal diffractometry. In this method, a monochromator is composed of several different kinds and pieces of crystal and is curved as refracted neutrons of **different kinds of wavelength** are focused onto the sample. Neutrons of each wavelength could be enough **collimated** if the conditions as a monochromator of each piece of crystal such as the size, mosaicity and so on are sufficiently arranged. Because of the multi-wavelength, the neutron flux irradiated onto the sample should be increased, although the diffraction pattern becomes more complicated. The special data acquisition procedure should be developed in order to realize this method.

(3) A detector system.

In order to enlarge the solid angle subtended by a sample, the plural area detectors are equipped. At the first stage the conventional gas-filled proportional detector should be utilized as the area detector.

At the same time more genuine detector, as an example, an imaging plate for neutrons which is common to X-ray diffractometry should be developed.

The general performances are summarized in the Table.

Table

beam tube
1G-A
monochromater
Graphite (002),
Silicon (311),
Copper(002)
Germanium(311)
monochromater Bragg angle
$2\theta=32, 44$
intensity at the sample position
$10^6-10^7 \text{ n cm}^{-2} \text{ s}^{-1}$
maximum beam size at sample
10mm x 10mm
incident wavelength
$\lambda=0.9-2.5 \text{ \AA}$
detector type
ORDERA MODEL 2250N (x3; tentatively)
detector resolution
2mm x 2mm
sample to detector distance
60cm-100cm
observable d range
$0.52 \text{ \AA} < d < 9.4 \text{ \AA}$

Reference

- 1) M.Ataka & T.Katsura, *In this Proceedings*:

15. QUAST LAUE NEUTRON PROTEIN CRYSTALLOGRAPHY

The major problem in neutron protein crystallography is the low flux of present neutron sources. The collection of a data set using a conventional rotation technique and a 2D detector takes many weeks. One way to increase the flux at the sample is to increase the wavelength bandwidth. The conventional technique using a standard monochromator like Cu or Be has a typical bandwidth of 1%. A multilayer monochromator (1) can however be tailored to give bandwidth up to 25% or even larger. In this case the diffraction geometry is such that the reflection in diffraction condition is 'scanned' by the $\Delta\lambda$ and not by rotating the reciprocal lattice point through the Ewald sphere (2). Wavelength bandwidth of 10% satisfy this condition. It is important to tailor the bandwidth to the size needed by the extend of the reciprocal lattice 'point' to minimize background. The intensity of the reflection is proportional to the $\Delta\lambda_r$ that just covers the width of the reciprocal 'point' while the background is proportional to the full wavelength spread $\Delta\lambda$ that hits the crystal. The conventional Laue technique is not suitable since it increases the background by the ratio of $\Delta\lambda/\Delta\lambda_r$, a ratio that can easily reach multiples of 10. In neutron protein crystallography the background is a problem since it is significantly higher than the equivalent x-ray case due to the large incoherent background contribution of H atoms. Some preliminary tests with a large myoglobin crystal and a double multilayer monochromator with a bandwidth of 10% and a d spacing of 70Å have been carried out at the H3B spectrometer at the HFBR (BNL) and demonstrated that a minimal gain of 5x can be achieved by this technique. The integration of such reflections has to be performed in 3 dimensions (x,y,w) with x and y being detector coordinates and w the rotation of the crystal.

1) Saxena, A. and Schoenborn, B.P., Material Science Forum 27/28,313-318,1988

2) Schoenborn, B.P. Acta Cryst. A39,315-321,1983

Benno P. Schoenborn (516) 282-3421

New data collection technique using a partial laue method;
decreases data collection time for neutron protein crystallography.

16. NEUTRON SCATTERING FACILITIES AT JRR-3M

Satoru Funahashi

Department of Physics

Japan Atomic Energy Research Institute

Neutron scattering research in Japan was started in 1962 when JRR-2 started to operate at JAERI. Soon after that, JRR-3 started up, too. Both reactors were 10 MW but JRR-2 was more favorable for neutron scattering because of its higher flux than JRR-3 due to the highly enriched uranium fuel used there while natural or slightly enriched uranium fuel was used at JRR-3. Most of the neutron scattering experiments in JAERI had been performed at JRR-2 until 1990 and JRR-2 is still continuing to operate. On the other hand, JRR-3 was shutdown in 1983 to be replaced with an upgraded reactor to meet the growing demand of thermal neutrons in Japan. The construction of the new reactor was started in 1985. The whole reactor body of the old JRR-3 including the biological shielding weighing 2,150 tons in total was cut in one block out of the place where it had been and was carried out of the reactor building. It is now kept in a basement under the new guide hall.

The new 20MW reactor called JRR-3M was built at the place where the old JRR-3 existed. The main characteristics of JRR-3M are described in Table I. Since the start up of the JRR-3M in 1990, the reactor is running regularly as planned and most of the neutron scattering experiments in

JAERI have been done at this reactor because at JRR-3M the neutron flux is about five times as high as; the number of beam ports is about three times as many as; and the operating time is about twice as long as, respectively, compared with JRR-2. Figure 1 shows the lay out of the neutron scattering instruments at JRR-3M. The flux at the monochromator position of the instruments in the reactor room is about $3 \times 10^9 \text{ n/cm}^2/\text{s}$ with open inpile collimator and those at the end of the thermal and the cold guides are about $2 \times 10^8 \text{ n/cm}^2/\text{s}$.

Table II shows list of the neutron beam instruments at JRR-3M and Fig.2 shows the classification of them. Obviously triple axis spectrometers are the major instruments at JRR-3M. From the view point of biology, two small angle scattering machines in the list are available. In addition, a four circle diffractometer with two-dimensional neutron detectors dedicated to biology has been proposed by Niimura. Since most of the beam ports, however, have been already occupied, it is considered for the diffractometer to share the beam of the high resolution powder diffractometer(HRPD) unless this change causes significant loss of flux at HRPD. The HRPD which is equipped with sixty-four sets of six minutes collimator and detector system is one of the most crowded and the most productive instruments at JRR-3M. If the loss at the HRPD should be too large other possibility at thermal guide will be sought. The four-circle diffractometer will be constructed in a year or two.

Table I JRR-3M (Main Features)

Reactor Type	Light water cooled and modulated swimming pool reactor with heavy water tank.		
Thermal power	20MW		
Core size	60cm diameter \times 75cm height		
Fuel	UAl _x (20% enriched uranium)		
Flux	2×10^{14} n/cm ² /s		
Beam tubes	7 horizontal tubes in the reactor hall 2 horizontal tubes for neutron guides		
Cold source	Liquid hydrogen		
Neutron guides	Thermal guides	($\lambda^*=0.2$ nm)	2×20 cm ² \times 2
	Cold guides	($\lambda^*=0.4$ nm)	2×12 cm ² \times 2
		($\lambda^*=0.6$ nm)	2×20 cm ² \times 1
Irradiation	17 vertical irradiation holes		
Operation	4 weeks \times 7 or 8 cycles/year		

Table II Neutron Beam Facilities at JRR-3M

Facility	Total number	Reactor room	Guide hall	
Triple Axis Spectrometers	8	4	4	3 for polarized n
Diffractometers	3	1	2	HRPD, DA, 4-circle
Small Angle Scattering	2		2	10-10m, 16-16m
Neutron Interferometer	2	1	1	
Neutron Camera and Video	3	1	2	Topography etc.
Special Polarized Machines	2		2	NSM, Spin-Echo
TOF Spectrometer	1		1	Focusing TOF
Non-scattering Machines	3	1	2	Radiography, Ultra-cold, Prompt gamma

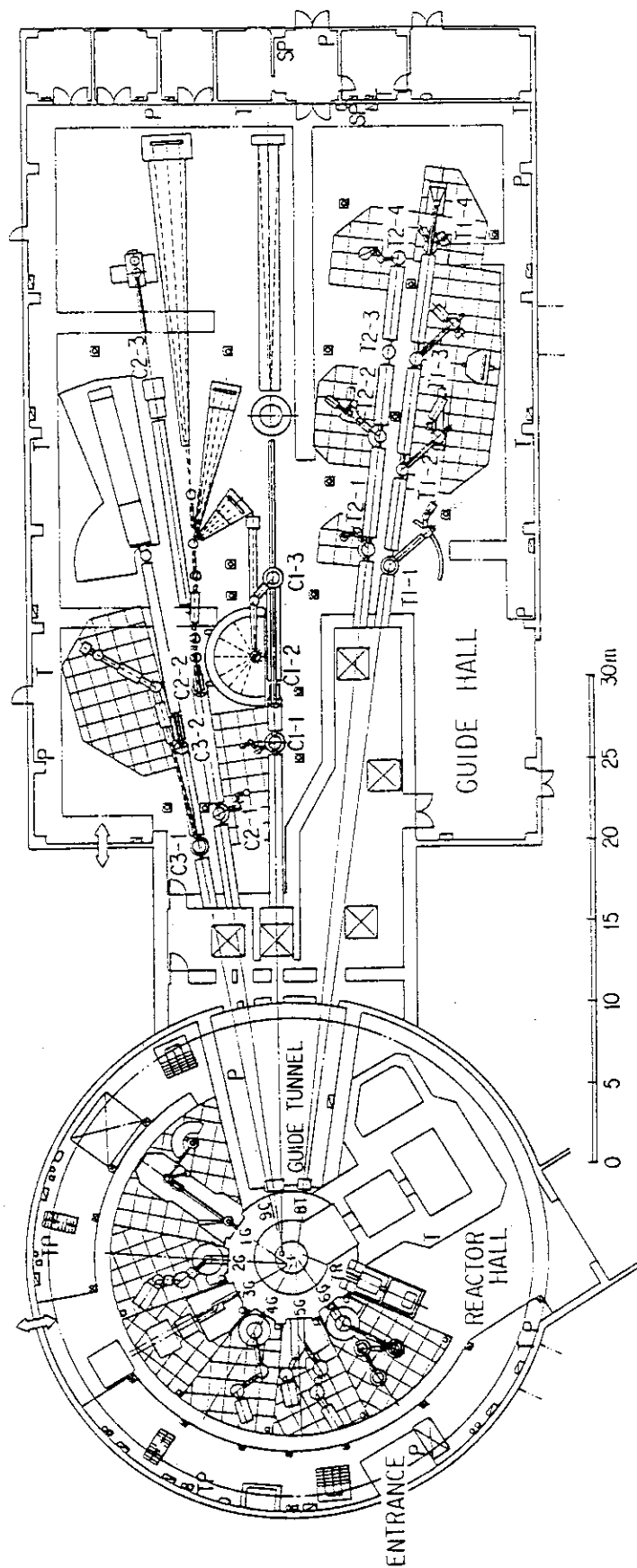


FIG.1 NEUTRON RESEARCH FACILITIES AT THE NEW JRR-3

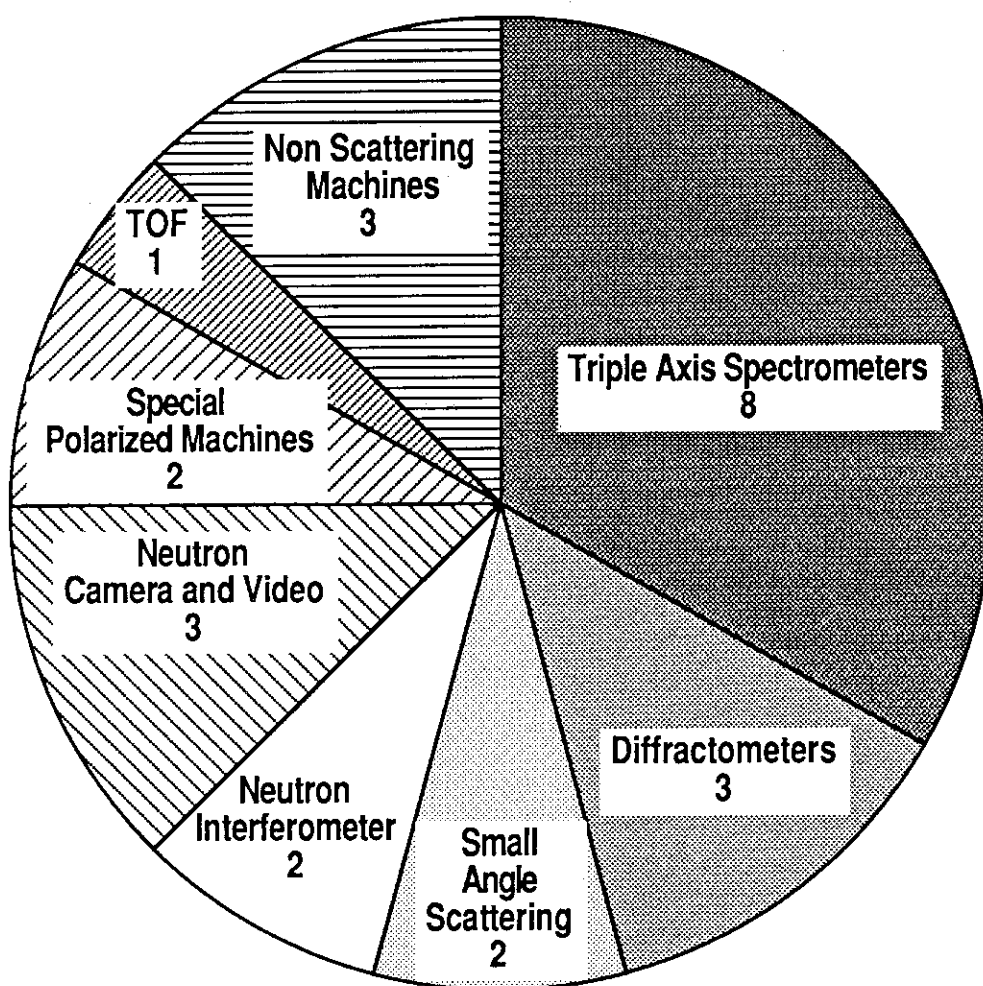


Fig.2. Neutron Beam Facilities at JRR-3M

APPENDIX

(Record of the Workshop "Neutrons in Biology")

Program

Organizing Committee

List of Participants

Photography

Program of

NEUTRONS IN BIOLOGY

5 SEPTEMBER 1992

9:00-9:05	Opening Address
-----------	-----------------

Y.Ito

(Current Status Reports on Neutrons in Biology and Related Instruments at each Facilities)

Chair Person: Y.Ito

9:05- 9:20	BNL	B.P.Schoenborn
9:20- 9:35	ILL	G.Zaccai
9:35- 9:50	GKSS	H.B.Stuhrmann
9:50-10:05	HMI	N.A.Dencher
10:05-10:20	KENS	M.Furusaka
10:20-10:35	JAERI	S.Funahashi

(Coffee Break: 10:35-10:45)

(Contributed Lectures)

Chair Person :S.Yabuki

10:45-11:00 SMALL-ANGLE NEUTRON SCATTERING INSTRUMENT AT
THE KYOTO UNIVERSITY REACTOR
SUGIYAMA,M., UEHARA,S. , MAEDA,Y.

11:00-11:15 POLARIZED NEUTRON SMALL-ANGLE SCATTERING IN BIOLOGY.
STUHRMANN, H.B.

11:15-11:30 SMALL-ANGLE NEUTRON AND X-RAY SCATTERING OF INSECT LIOPHORINS.
KATAGIRI,C., ITO,Y. AND SATO,M.

11:30-11:45 THE STRUCTURE OF GELSOLINE-PIP₂ COMPLEX AS STUDIED BY
SMALL ANGLE NEUTRON SCATTERING
ITO, T., FUKUSHIMA, J., MINEZAKI, Y., TANAKA, I., NIIMURA, N.,
HAYASHI, K.

11:45-12:00 SMALL-ANGLE NEUTRON SCATTERING STUDIES OF
PROTEOGLYCAN FROM SHARK FIN CARTILAGE.
SANO,Y., NIIMURA,N., TANAKA,I.

12:00-12:15 SMALL-ANGLE NEUTRON SCATTERING STUDY OF
RECOMBINANT YEAST-DERIVED HUMAN HEPATITIS B VIRUS
SURFACE ANTIGEN VACCINE PARTICLES
ITO,Y., SATO,M., KAMEYAMA,K., ISHIKAWA,N., TAKAGI,T.

12:15-12:30 INELASTIC NEUTRON SCATTERING FROM DNA AND WATER.
AGUIA, TOMINAGA, Y., IKEDA, S.

(Lunch & Photography: 12:30-13:30)

(Contributed Lectures)

Chair Person :M.Sato

- 13:30-13:45 NEUTRON SCATTERING IN SMALL BIOLOGICAL MOLECULES
AND HYDROGEN BONDING AT TROMBAY AND FUTURE PLANS
KANNAN,K.K.
- 13:45-14:00 A LARGE SINGLE CRYSTAL OF THE TETRAGONAL FORM OF
LYSOZYME CAN BE GROWN IN A CONCENTRATION GRADIENT
OF NiCl_2 .
ATAKA,M., KATSURA,T.
- 14:00-14:15 SMALL-ANGLE NEUTRON SCATTERING STUDY OF THE INITIAL
STAGE OF LYSOZYME CRYSTALLIZATION PROCESS.
MINEZAKI,Y., TANAKA,I., NIIMURA,N., ATAKA,M., KATSURA,T.

(Current Status and/or Future Perspective in Neutron Crystallography in
Biology)

Chair Person: M.Sato

- 14:15-14:30 NEUTRON DIFFRACTION CAMERA USING A THERMO-LUMINO
SHEET
HIDAKA,M., MORISAKO,T., NISHI,M
- 14:30-14:45 LOW RESOLUTION NEUTRON CRYSTALLOGRAPHY OF LARGE
MACROMOLECULAR ASSEMBLIES
TIMMINS,P
- 14:45-15:00 DIFFRACTOMETER FOR NEUTRON CRYSTALLOGRAPHY IN
BIOLOGY :PROJECT
NIIMURA,N.
- 15:00-15:15 QUASI LAUE NEUTRON PROTEIN CRYSTALLOGRAPHY
SCHOENBORN,B.P.
- 15:15-15:20 Closing Address N.Niimura

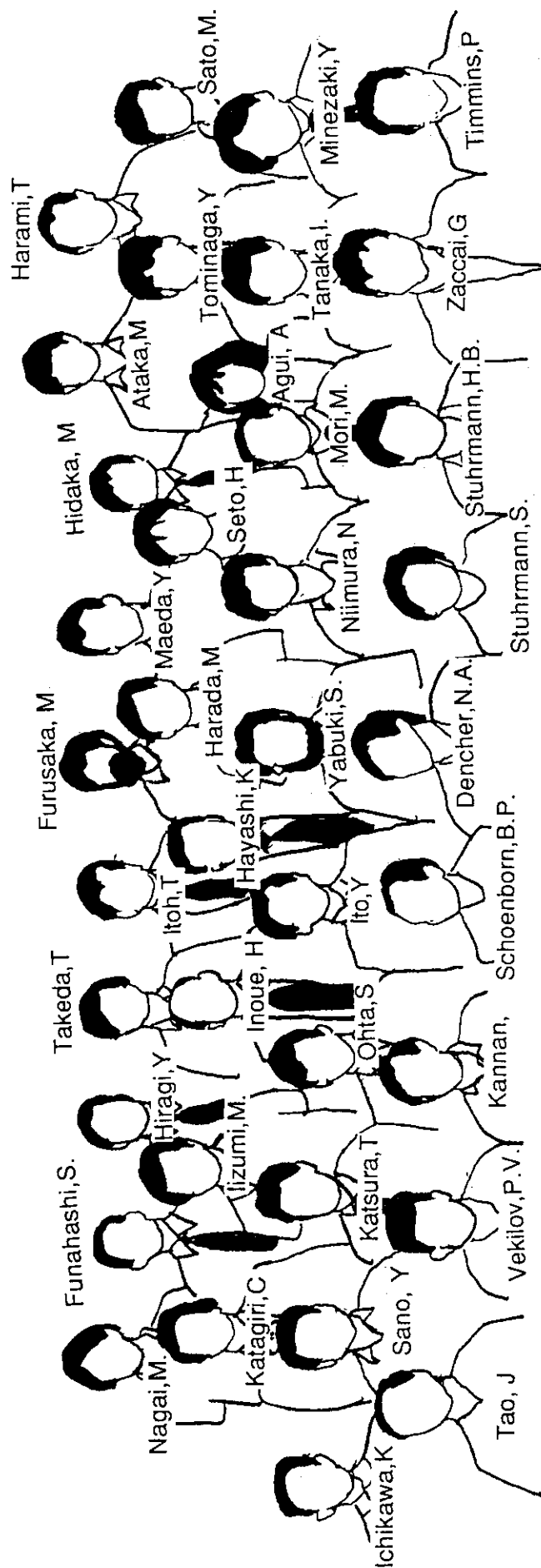
Organizing Committee

Chairman	Y. Ito (Univ. Tokyo)
Co-Chairman	S. Funahashi (JAERI)
Secretary	N. Niimura (Tohoku Univ.)
Programme	I. Tanaka (Hokkaido Univ.)
	Y. Maeda (Kyoto Univ.)
	K. Miki (Tokyo Inst. Tech.)
	M. Sato (Osaka Univ.)
	S. Yabuki(Gunma Univ.)

Participants List

Name	Affiliation
Agui, A	Ochanomizu Univ.
Ataka, M	Res. Inst. Polymers & Textiles, Tsukuba
Dencher, N.A.	Hahn-Meitner-Inst., Germany
Fujita, I.	Hitachi Life Co., Ltd.
Funahashi, S.	Japan Atomic Energy Res. Inst.
Furusaka, M	KENS
Gorai, S.	Daishin Industrial Co., Ltd.
Gorai, Y.	Goken Industrial Ltd.
Haginiwa, T.	Nissho Electricity Ltd.
Harada, M	Jichi Med.Sch.
Harami, T	Japan Atomic Energy Res. Inst.
Hashimoto, Y.	Johsoh Maintenance Ltd.
Hayashi, K	Ibaraki Univ.
Hidaka, M	Kyushu Univ.
Hiragi, Y	Kyoto Univ.
Ichikawa, K	Hokkaido Univ.
Iiyama, T.	Mayor of Hitachi city
Iizumi, M.	Japan Atomic Energy Res. Inst.
Ikeda, S.	KENS
Inoue, H	Shimazu Corp.
Ito, Y	Univ. of Tokyo
Itoh, T	Kyoto Univ.
Kannan, K.K.	Bhabha Atomic Res. Ctr., India
Kashimura, M.	Kankyo Giken Co., Ltd.
Katsura, T	Res. Inst. Polymers & Textiles, Tsukuba
Katagiri, C	Hokkaido Univ.
Kawamura, Y	Univ. of Tokyo
Kobayashi, H	Hiroshima Univ.
Kobayashi, S.	Hitachi Civil Engineering Co., Ltd
Kurabayashi, K.	Kurabayashi Administrative Law Office
Maeda, Y.	Kyoto Univ.
Minezaki, Y	Tohoku Univ.
Mori, M.	Aloka Co., Ltd
Nagai, M.	Hiroshima Univ.
Namekawa, H.	Hitachi Civil Engineering Co., Ltd.

Niimura, N	Tohoku Univ.
Ohta, S	Jichi Med.Sch.
Sagara, Y.	Shinsen Industrial Ltd.
Sano, Y	Ntl. Food Res. Inst., Tsukuba
Sato, M.	Osaka Univ.
Schoenborn, B.P.	Brookhaven Ntl. Lab., USA
Stuhrmann, H.B.	GKSS, Germany
Stuhrmann, S.	Germany
Seto, H	Hiroshima Univ.
Sugihara, M.	Daishin Industrial Co., Ltd.
Suzuki, K.	Suzuki Co., Ltd.
Takeda, T	Hiroshima Univ.
Tanaka, I.	Tohoku Univ.
Tao, J	PF, KEK
Timmins, P	Inst. Laue-Langevin, France
Tominaga, Y	Ochanomizu Univ.
Uchiyama, H.	Member of Hitachi city assembly
Uchiyama, T.	Misaki Iron Industrial Ltd.
Vekilov, P.V.	Hungary
Yabuki, S.	Gunma Univ.
Zaccai, G	Inst. Laue-Langevin, France





BSR92 Satellite Meeting "Neutrons in Biology" 4/5 Sep, 1992 IN SUNPIA HITACHI